Universidade de Aveiro
2009
Departamento de Electrónica, Telecomunicações e Informática

Nuno Rafael Mendonça Lourenço

Sistemas de Comunicação com Luz Visível: Emissor/Receptor

Communication Systems Using Visible Light: Emitter/Receiver

Universidade de Aveiro
2009
Departamento de Electrónica, Telecomunicações e Informática

Nuno Rafael Mendonça Lourenço

Sistemas de Comunicação com Luz Visível: Emissor/Receptor

Communication Systems Using Visible Light: Emitter/Receiver

Dissertação apresentada à Universidade de Aveiro para cumprimento dos requisitos necessários à obtenção do grau de Mestre em Engenharia Electrónica e Telecomunicações, realizada sob a orientação científica do Doutor Dinis Gomes de Magalhães dos Santos, Professor Catedrático do Departamento de Electrónica, Telecomunicações e Informática da Universidade de Aveiro e do Doutor Luis Filipe Mesquita Nero Moreira Alves, Professor Auxiliar do Departamento de Electrónica, Telecomunicações e Informática da Universidade de Aveiro

o júri

presidente

Professor Doutor Rui Luis Andrade Aguiar
Professor Associado do Departamento de Electrónica, Telecomunicações e Informática da Universidade de Aveiro

Professora Doutora Guiomar Gaspar de Andrade Evans
Professora Auxiliar do Departamento de Física da Faculdade de Ciências da Universidade de Lisboa

Professor Doutor Dinis Gomes de Magalhães dos Santos
Professor Catedrático do Departamento de Electrónica, Telecomunicações e Informática da Universidade de Aveiro

Professor Doutor Luis Filipe Mesquita Nero Moreira Alves
Professor Auxiliar do Departamento de Electrónica, Telecomunicações e Informática da Universidade de Aveiro

agradecimentos

Nunca tão pequena secção conseguiria conter todas as menções e agradecimentos a todos os que, directa ou indirectamente, contribuíram para a realização deste trabalho. No entanto, e não menosprezando qualquer tipo de contribuição, pretendo desta forma apresentar as minhas menções e agradecimentos aos que, de uma forma mais directa, contribuíram para a realização deste trabalho:

Em primeiro lugar aos meus orientadores, o Professor Doutor Dinis Gomes de Magalhães dos Santos e o Professor Doutor Luis Filipe Mesquita Nero Moreira Alves, pela oportunidade apresentada e pela confiança que depositaram em mim. A constante discussão e orientação científica foram uma bússola preciosa para levar este trabalho a bom porto.

Aos colegas do Laboratório de Circuitos e Sistemas Integrados pelo bom ambiente de trabalho. Em particular, ao Mestre Navin Kumar pelas imensamente proveitosas partilhas de conhecimento e pela oportunidade de participar num trabalho reconhecido.

Ao Instituto de Telecomunicações de Aveiro e ao Departamento de Electrónica, Telecomunicações e Informática da Universidade de Aveiro, pelos meios disponibilizados. De uma forma especial, aos técnicos Paulo Gonçalves e Paulo Martins pela paciência e pelos conhecimentos transmitidos na construção de circuitos impressos.

A todos os professores que me incentivaram o gosto pelo conhecimento, em especial na área da electrónica.

Aos meus pais, Lurdes Mendonça e Rafael Lourenço, pelo incondicional apoio e pela fé depositada em mim. Mesmo a custo de um imenso sacrifício pessoal, sempre me proporcionaram as condições necessárias para perseguir o sonho e a realização pessoal. De igual forma, à minha irmã Fátima Lourenço pela motivação, pelo exemplo e pela paciência demonstrada, mesmo nas fases mais difíceis.

À minha família e amigos mais próximos, que de mil e uma maneiras estiveram presentes e me ajudaram durante este percurso. Em especial, aos meus tios Miguel e Lúcia por todo o carinho e apoio, e à dona Fernanda e ao Sr. Elísio por me acolherem de braços abertos.

Aos eternos colegas Hugo, Paulo Cerqueira e Paulo Sérgio, que animaram e enriqueceram de variadas formas o percurso académico. Também, aos colegas e amigos com quem partilhei o Bloco 13.

À *Makoto Kan*, pelo ambiente de respeito, disciplina e acima de tudo amizade, em especial ao Sensei Jorge Vieira… *OSS!*

Finalmente à Ana, a minha fonte de inspiração e motivação. Por todo o seu apoio, por todo o carinho, pela imensa paciência e acima de tudo, por todo o seu amor.

A todos, muito obrigado!

palavras-chave

Luz visível, Emissor, Receptor, Díodos emissores de luz, Fotodíodos, Projecto de sistema, Resposta ganho/fase, VIDAS.

resumo

A presente dissertação aborda o design de um transdutor optoelectrónico para um sistema de comunicações sem fios que utiliza a luz visível como meio de transmissão. Estes sistemas tiram partido dos conhecimentos tecnológicos existentes sobre sistemas de comunicações sem fios utilizando o espectro dos infravermelhos, e da recente introdução em massa de díodos emissores de luz de elevado brilho em diversas aplicações de iluminação.

O trabalho apresentado foi desenvolvido dentro do projecto VIDAS, tendo em conta os respectivos cenários de aplicação propostos. Este projecto visa aumentar a segurança rodoviária através da introdução de sistemas de comunicação com luz visível, para estabelecer ligações veículo-a-veículo e/ou veículo-a-semáforo. Através destas ligações, poderão ser antecipadamente fornecidos diversos avisos de segurança aos condutores.

O estudo do transdutor proposto, começa com uma introdução ao conceito e evolução dos sistemas de comunicação com luz visível. Segue-se uma apresentação do canal de transmissão, na qual são definidos os modelos de emissor, receptor e propagação. São também discutidas as diversas fontes de ruído óptico e suas influências na aplicação pretendida. A restante análise é dividida em dois dispositivos principais, o emissor e o receptor ópticos.

Sobre o emissor, são apresentados os principais blocos funcionais, seguidos de uma exposição das características de diversos díodos emissores de luz e da análise de diferentes topologias de receptor. Para a topologia mais viável de ser implementada, são apresentados diversos resultados de simulação do circuito electrónico.

Do lado do receptor, de forma análoga, são apresentados os diferentes blocos funcionais e as características de diversos fotodíodos. No entanto a experiência do grupo de trabalho levou à escolha de uma topologia de receptor mais específica. Desta, fazem parte diversos módulos, cuja análise e resultados de simulação dos respectivos circuitos electrónicos são apresentados.

De forma a avaliar a performance dos dispositivos propostos, foram efectuados diversos ensaios e respectivas medições. Estes resultados permitiram obter informações sobre o comportamento da componente óptica do sistema. Deste conjunto de informações, diferentes considerações sobre a performance de módulos individuais e do transdutor são apresentadas. Estas permitem concluir sobre a viabilidade do transdutor optoelectrónico num cenário de aplicação real.

keywords

Visible light, Emitter, Receiver, Light emitting diodes, Photodiodes, System design, Gain/phase response, VIDAS.

abstract

This dissertation addresses the design of an optoelectronic transceiver for a wireless communication system, using visible light as the transmission medium. These systems take advantage from the available technological expertise on wireless communication systems using the infrared spectrum, along with the recent massive introduction of high brightness light emitting diodes in several lighting applications.

The present work was developed within the scope of project VIDAS, regarding the proposed application scenarios. This project aims at increasing road traffic safety by introducing visible light communication systems to establish vehicle-to-vehicle and vehicle-to-traffic light communications. Through these connections, early safety warnings can be provided to drivers.

The study of the proposed transceiver begins with an introduction to the concept and evolution of visible light communication systems. This is followed by the presentation of the transmission channel, in which the emitter, receiver and transmission models are defined. Also, the sources and influences of the various optical noise sources are discussed. The remaining analysis is divided between the two major devices, the optical emitter and receiver.

From the emitter, the main building blocks are presented, followed by an exposition of several light emitting diodes characteristics and the analysis of diverse receiver topologies. In the case of the most viable topology for implementation, several simulation results of the respective electronic circuit are presented.

On the receiver, the main building blocks and the characteristics of several photodiodes are presented in a similar fashion. However, the workgroup experience led to the choice of a specific receiver topology. This is made up of several modules, whose analysis and simulation results for the electronic circuits are presented.

In order to evaluate the performance of the proposed devices, several tests and measurements were made. These results also provided information on the system's optical component behavior. From this assortment of information, different considerations on the performance of the individual modules, as well as the transceiver are presented. They allow for a conclusion on the viability of the optoelectronic transceiver in a real application scenario.

Dedicatória

Para a Ana… por tudo.

Para os meus pais, Lurdes e Rafael… pela oportunidade.

Para a minha irmã, Fátima… pelo exemplo.

…e para toda a família e amigos que ao longo dos anos me apoiou e ajudou nesta caminhada académica.

Contents

List of Tables

List of Figures

Acronyms

A

AC – Alternating Current
ADAS – Advanced Driver Assistance System
AlGaAs – Aluminum Gallium Arsenide
AlInGaP – Aluminum Gallium Indium Phosphide

D

DC – Direct Current

F

FET – Field-Effect Transistor
FOV – Field-Of-View
FPGA – Field-Programmable Gate Array

G

GaAsP – Gallium Arsenide Phosphide
GBW – Gain-BandWidth product
GPS – Global Positioning System

H

HB-LED – High Brightness - Light Emitting Diode
HID – High-Intensity Discharge
HP – Hewlett Packard
hpa – half-power angle

I

IC – Integrated Circuit
IEEE – Institute of Electrical and Electronics Engineers
InGaN – Indium Gallium Nitride
IR – InfraRed
ITS – Intelligent Transportation System

L

LED – Light Emitting Diode
LOS – Line-Of-Sight

M

MFB – Multiple FeedBack

N

NRZ – Non Return to Zero

O

OOK – On-Off Keying

P

PCB – Printed Circuit Board
PDA – Personal Digital Assistant
PIN – Positive-Intrinsic-Negative
PLC – Power Line Communications
PWM – Pulse-Width Modulation

R

RF – Radio Frequency
RGB – Red, Green and Blue

S

Si – Silicon
SMD – Surface Mount Device
SNR – Signal-to-Noise Ratio

T

TFFC – Thin Film Flip Chip

U

UHP – Ultra-High-Performance

V

VIDAS – VIsible light communications for advanced Driver Assistance Systems

VLC – Visible Light Communication

Chapter I

Introduction

Visible Light Communication (VLC) is a recent technique in the field of wireless communications. As the name implies, light in the visible range of the electromagnetic spectrum is used as the communication medium for data transmission. Although it might seem a revolutionary idea, history has several examples of usage of this medium. Ancient tribes used smoke signals, and there is even the record of Graham Bell's *photophone* [Bel81], an attempt for transmitting information through visible light.

In 1978, Gfeller proposed "Wireless In-House Data Communication via Diffuse Infrared Radiation" [Gfe79], this way laying the stepping-stone to the usage of the optical spectrum in modern wireless data transmission. Although infrared (IR) wavelengths were proposed for both directed and non-directed communications, many of the knowledge and studies done in this area can easily be adapted and re-used for VLC. The used wavelengths are fairly close, which makes propagation models, noise sources and even system design easily adaptable.

The current work focuses on the design of the front-end electronics for a visible light emitter and receiver. For this purpose, the workgroup background and expertise in areas such as wireless IR, VLC and electronic system design were essential in deciding the path to follow.

The current chapter presents the main motivations of this project for researching VLC technologies. The objectives are explained, and a brief description of the dissertation is presented.

I.i Background

The present dissertation *"Communication Systems using Visible Light: Emitter/Receiver"* is inserted in the area of conceptual investigation for mobile wireless communications using visible light as a transmission medium. In this area of investigation the current work is part of project VIDAS (VIsible light communications for advanced Driver Assistance Systems) (PTDC/EEA-TEL/75217/2006) [VIDweb] currently being developed in the Integrated Systems and Circuits laboratory at the Institute of Telecommunications of Aveiro.

Within the compass of this project several studies, which serve as background to the present dissertation, have been performed by the workgroup. In the project report entitled "*Projecto Luz Comunicante*" referred as [Per07], an initial analysis to the proposed VLC system, along with experimental characterization of several light emitting diodes (LED's) was performed. In the published article "*Visible Light Communication Systems Conception and VIDAS*" referred as [Kum08], the state-of-the-art of VLC systems and other VIDAS related research issues were addressed. More recently, a study entitled "*Design and Analysis of the Basic Parameters for Traffic Information Transmission Using VLC*", referred as [Kum09], was also published, including a deeper system analysis with model description and parameter optimization.

I.ii Motivation

Modern society is highly dependent on information technologies, especially on mobile and wireless products and applications. The evolution of the personal computer towards mobility and portability was essential for this evolution. Devices such as notebooks, personal digital assistants (PDA's) and cell phones have become part of people daily lives. By changing work habits throughout the world, they played an important role in boosting the growth of wireless communications networks, with some of the most known standards defined by the Institute of Electrical and Electronics Engineers (IEEE) under project 802.11 [802web].

From an early start, wireless radio-frequency (RF) technologies achieved commercial domination in detriment of wireless optical technologies which use the IR spectrum. Although they offer major advantages such as high bandwidth or implementation simplicity, IR based technologies still have some drawbacks, mainly regarding user safety when handling high power signals. IR radiation makes chemical bonds resonate which corresponds to an increase of energy in molecules. This increase is perceived as heat and can have harmful consequences in humans. Even for a moderate amount of IR radiated energy, prolonged exposure over the years can lead to a gradual

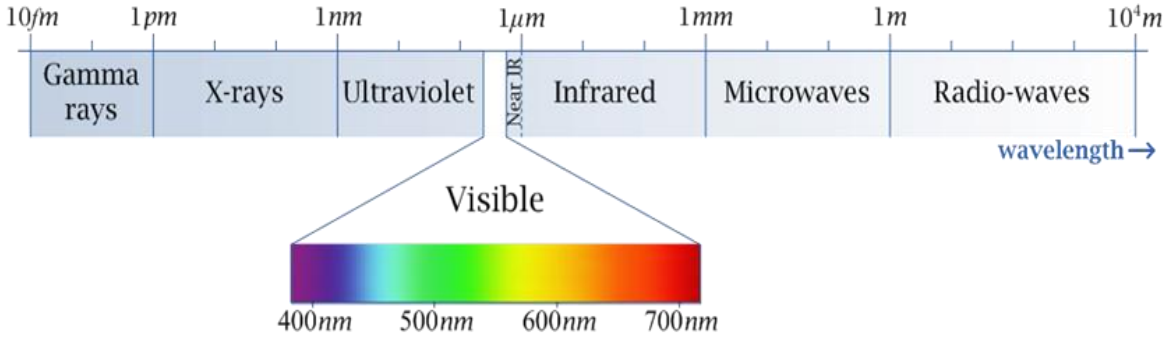

Figure 1: The electromagnetic spectrum

opacity of the eye lens, also known as cataracts. These power limitations seriously affect the available data rates and communication ranges, nevertheless optical wireless communications are still highly desirable, and where IR showed its major flaws, VLC presents itself as a viable solution. Visible light also encompasses a relatively wide range of the electromagnetic spectrum, with the advantage of being un-licensed, allowing, at least in theory, larger bandwidth to be explored than in radio based systems. It is safe to humans and does not cause any interference with RF based electronics.

Figure 1 shows a portion of the electromagnetic spectrum. Although the IR range contains wavelengths from around 750nm to 1mm, the actual interval used for data communication is the near-IR which includes wavelengths from 780 to 950nm. Visible light lies in the range of 380 to 750nm. These two ranges are very similar, which means that most of the advantages of wireless IR systems are also present in VLC systems, and light behavior will be similar. Therefore, the research for techniques and models of communication systems using the visible range of the electromagnetic spectrum appears as a viable alternative. Such models and techniques can easily be adapted from the extended studies already available on IR communication systems.

In order to become practical, thus standing a chance of becoming a leading technology, VLC systems will need to take into account several drawbacks. Probably the most important is the need to coexist, and not be affected by, existing lighting systems, while not interfering, or being interfered by, current radio based wireless technologies. This could hardly be achieved by using conventional light sources, such as incandescent or fluorescent lights, the alternative lies on solid state lighting. LED's present a number of advantages over conventional light sources that makes them the ideal component for VLC systems, with the most important being the fact that any LED is a semiconductor, and therefore as an inherent fast switching ability. Along other advantages are also high energy conversion efficiency, larger lifetime, humidity tolerance and an overall low maintenance cost.

By reaching performances easily comparable to conventional light sources, the new high-brightness light emitting diodes (HB-LED's) have reached new lighting markets and can be found in applications as diverse as indoor and outdoor general lighting, large size advertising boards, interior and exterior automotive lighting or traffic semaphores, also known as traffic lights. All of these applications are also different possibilities for a VLC system, with the final two being determinant to the implementation of VIDAS.

For long, road traffic safety has been a major concern for the authorities, with the European Union setting challenging targets for its improvement until the year 2010. Currently, several projects that aim to improve road traffic safety, such as AIDE-IP, PREVENT-IP or SAFESPOT-IP, are being supported by the European Union. Also, the daytime running lights proposal, which intends for motor vehicles to travel with their lights turned on at all times, has been opened for discussion and is expected to be implemented in the close future [VIDweb]. With this background, and taking advantage from the increasing usage of HB-LED's, in traffic lights and vehicle external lighting, the VIDAS project was introduced.

Presenting itself as a complement to the existing advanced driver assistance system (ADAS), VIDAS proposed the usage of outdoor illumination to increase road traffic safety. This is to be achieved by studying VLC as a possible solution for implementing a communications system for vehicle-to-vehicle and/or vehicle-to-traffic lights, as represented in figure 2. This way, early warnings regarding collision avoidance, intersection information, speed control, along with others, can be provided to drivers, thus helping reduce road traffic accidents and fatalities. Another possibility of VIDAS is the optimization of traffic flow by establishing an interactive navigation support system, using traffic lights as information broadcasters [VIDweb].

Figure 2: VIDAS Application examples

I.iii Objectives

The main objective presented for this dissertation, was to study and develop an optoelectronic transceiver for a VLC application, specifically for the VIDAS project. The tasks proposed in order to achieve this objective were:

- Study and understand the concepts of VLC;
- Study and research transceiver devices (LED's and photodiodes) for the desired application;
- Design and prototype a VLC emitter and receiver;
- Characterize the developed prototypes;
- Characterize the optoelectronic transceiver.

I.iv Dissertation structure

The current dissertation is divided into six chapters. The current chapter starts with a small introduction on VLC and follows, in subsection I.i, with the background that led to the work developed. Subsection I.ii gives a more insightful look on the motivations for developing this study, followed by its primary objectives in subsection I.iii. A summary on the structure of this text is given in this subsection, followed in I.v with a description of original work produced.

Chapter II is divided into four subsections. It is dedicated to introducing the concept of wireless communication systems using visible light, and starts in subsection II.i by presenting the history of VLC. In order to further explain the dissemination of HB-LED's subsection II.ii shows the new trends in lighting systems, followed by some VLC application examples in subsection II.iii. The transmission channel is also analyzed in this chapter, in subsection II.iv. It is divided into four parts, in which the emission, reception and line-of-sight propagation models are presented, along with an analysis of the most important noise sources and its influences on the VLC system.

Chapter III is fully dedicated to the analysis of the VLC emitter design. It starts in subsection III.i with a description on the receiver main building blocks. In subsection III.ii, the characteristics of several researched LED's, that could be used in VLC, are presented and discussed. The final subsection, III.iii, is divided into three groups of implementation topologies. In the first group, of alternating current topologies, the implementation schemes of some configurations are presented and discussed. In the group of HB-LED driver topologies, the concept of using this type of already built devices to implement a VLC emitter is discussed. Finally a discrete transistor topology is analyzed, by presenting simulation results and some practical considerations.

In a similar way, chapter IV is dedicated to the analysis of the VLC receiver, and is also divided into three subsections. Starting in IV.i a description of the main building blocks is presented. The research results on several photodiodes for VLC and their most important characteristics are presented in subsection IV.ii. The final subsection, IV.iii, presents the analysis of the different modules of the receiver. Simulation results and considerations are made for the preamplifier, the filter and the voltage amplifier.

Chapter V is a chapter dedicated to presenting the experimental results of the implemented devices. Starting in subsection V.i, the design guidelines followed in the development of the several prototypes built is presented. In subsection V.ii the setup measurements used to obtain the experimental results are presented, and in subsection V.iii, the respective experimental results for the optical emitter, optical receiver and optoelectronic transceiver are shown and discussed.

In chapter VI, the conclusions reached during the execution of this dissertation are presented. Several considerations on the obtained results and guidelines followed are made, as well as indications for future improvements to the developed devices.

I.v Original work

During the execution of the work presented in this dissertation the article entitled "*Visible Light Communication Systems Conception and VIDAS*" was submitted to the Institute of Electronics and Telecommunications Engineers Technical Review (IETE Technical Review), to be published. The article addressed several research issues and ideas related with VLC and project VIDAS, which were being explored at that time. Namely, the state-of-the-art of VLC systems, implementation issues in indoor and outdoor scenarios, possible applications and system design. With most of the credit going to the author, Mr. Navin Kumar, I was given the opportunity to collaborate by writing about some of the implementation aspects of a wireless USB application, especially the emitter and receiver design. Recently the article was awarded with the IETE – Gowri Memorial Award (2009) for the best paper on topic of general interest.

Chapter II

Wireless communication systems using visible light

"I have heard articulate speech by sunlight!
I have heard a ray of the sun laugh and cough and sing! "
Alexander Graham Bell, in a letter to his father

Communication systems have become the backbone of our *"information society"*. From the beginning, RF-based systems dominated the wireless applications world, but eventually began to reach a saturation point. This made alternatives highly desirable, leading to the introduction of IR wireless technologies [Gfe79]. Although presenting several benefits over RF, IR never became a mainstream technology. However, optical wireless technologies are still highly desirable, and with the affirmation of HB-LED's as the lighting technology for the future, visible light spectrum became a viable alternative [Pan02, Cra95]. HB-LED's have reached, among others, automotive lighting and traffic light applications, thus making the usage of VLC in ADAS a possibility, of which VIDAS is an example. It becomes necessary to define specific emission, propagation and reception models, as well as to analyze the influence of different noise sources [Tav99, Kum08, Kum09].

This chapter begins with an introduction to the history of VLC in subsection II.i. LED applications and advantages are presented in subsection II.ii, followed by the application possibilities for VLC systems in subsection II.iii. The line-of-sight model of the

optical link is presented in subsection II.iv, with emission, propagation and reception models analysis. The noise sources that affect this application are also presented.

II.i The history of VLC

The importance of communication systems in today's society hardly needs to be emphasized. Every day, information, economical, financial, transportation and other important systems depend on the fast and reliable access to information. People need it to be everywhere, easily and quickly available. This has been made possible through the evolution of portable devices and the arrival of wireless communications.

Modern wireless communications have been dominated by RF-based technologies. They are used on a daily basis in things such as cell-phone communications, computer wireless networks (Wi-Fi), global positioning systems (GPS), etc. But despite their widespread use, RF-based technologies present considerable limitations. With the frequency range for RF wireless systems being strictly regulated, it is not always possible to obtain licenses to implement new communication networks. Also, radio signals travel freely, with obvious consequences on information security. And in some cases, data encryption can be resource demanding on a secured wireless network. Another problem occurs when trying to use RF-based positioning systems like GPS. Not only its precision is limited, but it is also practically impossible to use inside a building, especially in basements or underground parking lots. Therefore, it becomes highly desirable to find alternatives to RF wireless systems.

IR wireless technologies were presented as an alternative for the RF based systems [Gfe79], offering several benefits in bandwidth, implementation simplicity and data security, among others [Kah97]. However, they never became a mainstream technology. Constraints to the levels of radiated energy, regarding user health, seriously limited the data rates or communication ranges of commercially available devices. However, optical wireless technologies still play an important role in future developments.

Some of the earliest references to a communication system using visible light come from ancient tribes, which used smoke signals to convey information, or from the ancient Greeks, who used their polished shields to transmit messages by reflecting sunlight. But the first reference to conceptual investigation and prototype building of a VLC system comes from the father of the telephone, Alexander Graham Bell. On the 3rd of June of 1880, Alexander Graham Bell and his assistant Charles Tainter succeeded in transmitting the world's first wireless telephone message over a distance of 213 meters. Their design used the sunlight as source, which was modulated through the vibration of a reflecting

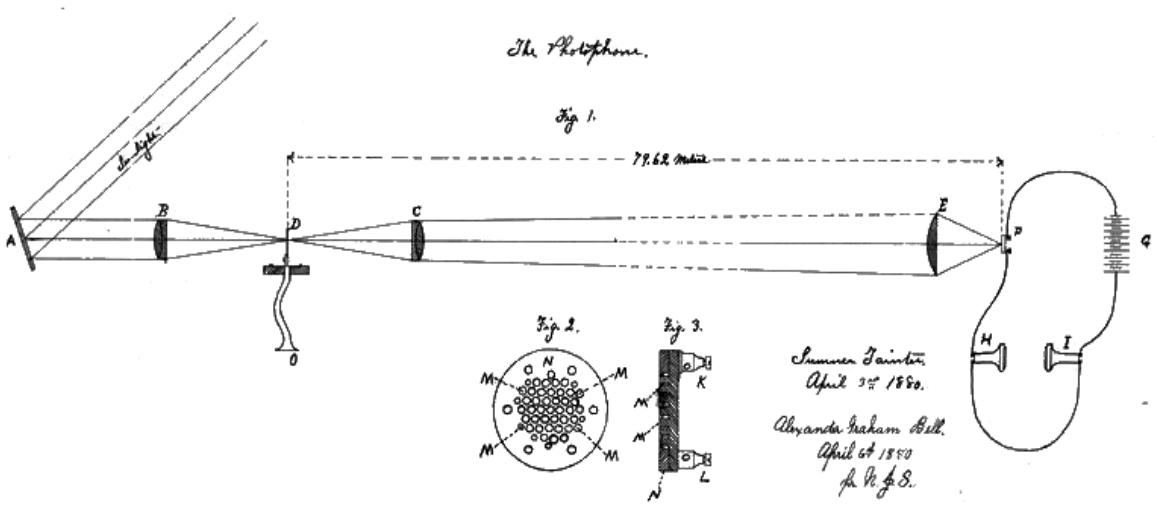

Figure 3: The *photophone* - drawing by Alexander G. Bell and Charles Tainter [Bel80]

mirror and then captured in a parabolic mirror with photoconductive selenium cells at the focal point [Bel81, Hra05]. A drawing of the design is presented in figure 3.

In spite of this early discovery, VLC was overtaken by the advances in both wired and RF communications, with the help of great names like Hertz, Bell, Edison and Marconi along with many others. However, history has several major breakthroughs on record in the area of VLC. In the mid-1920's, Oleg Vladimirovich Losev, who worked as a technician in several radio laboratories in the former Soviet Union, observed light emission from zinc oxide and silicon carbide crystal rectifier diodes, when a current was passed through them. These were used in radio receivers. Losev realized the potential in his discovery and invented the first LED. Further, on December 31st 1929 he wrote:

"The proposed invention uses the known phenomenon of luminescence of a carborundum detector and consists of the use of such a detector in an optical relay for the purpose of fast telegraphic and telephone communication, transmission of images and other applications when a light luminescence contact point is used as the light source connected directly to a circuit of modulated current.".

With this plan of thought, Losev could have started the revolution of optical communications, but he died young and unrecognized [Zhe07]. It was only in 1962 that Nick Holonyak Jr. created the first practical red LED, after inventing a method to synthesize Gallium Arsenide Phosphide (GaAsP) crystals, which exhibited wavelengths in the visible spectrum [Perr03]. In the following years the efficiency of red LED's increased significantly, and the first commercially available LED's were presented by Monsanto and Hewlett Packard (HP) in the late 1960's. These devices exhibited very low efficiency, about 0,1 lumens of output flux per watt of input electrical power. They were mainly used as indicators in indoor applications. In 1968 another technological breakthrough occurred

with the addition of nitrogen which led to the first orange and yellow LED's, and in the early 1980's the arrival of red Aluminum Gallium Arsenide (AlGaAs) devices, with efficiencies of the order of 2 to 10 lumens per watt (lm/w), the LED's reached new markets, such as the automotive taillights, or outdoor moving message boards. In 1990, P. Kuo and his co-workers presented their new yellow Aluminum Gallium Indium Phosphide (AlInGaP) LED's with performances comparable to the best red AlGaAs devices, and the color range of high brightness was almost complete [Cra95]. Blue was the missing color but, in 1992, Shuji Nakamura presented the first blue HB-LED. He was somewhat isolated from the mainstream of industrial research. When the industry had already dismissed the Indium Gallium Nitride (InGaN) alloy, he persevered and took one of the most important steps into the revolution of solid-state lighting. Given that blue LED's are the base for white light HB-LED's [Rio07]. With the growing evolution in optics, semiconductor devices and materials science, LED technologies have been growing in an exponential way. Since the 1960's LED's have doubled their light output and power efficiency every 36 months. This behavior became known as *"Haitz's Law"* [Hai99] and it is shown in figure 4. These numbers confirm the penetration of LED's into the market of lighting systems, not only in automotive applications, but also in city outdoor lighting, home indoor lighting, etc.

Another important foundation to VLC was the IR wireless communications systems presented by Gfeller in [Gfe79]. Although IR never became a complete alternative to RF in wireless communication systems, it presents itself as a complementary technology with several advantages. The used spectral interval of 780 to 950nm permits the use of a virtually unlimited bandwidth that is unregulated worldwide; IR emitters and

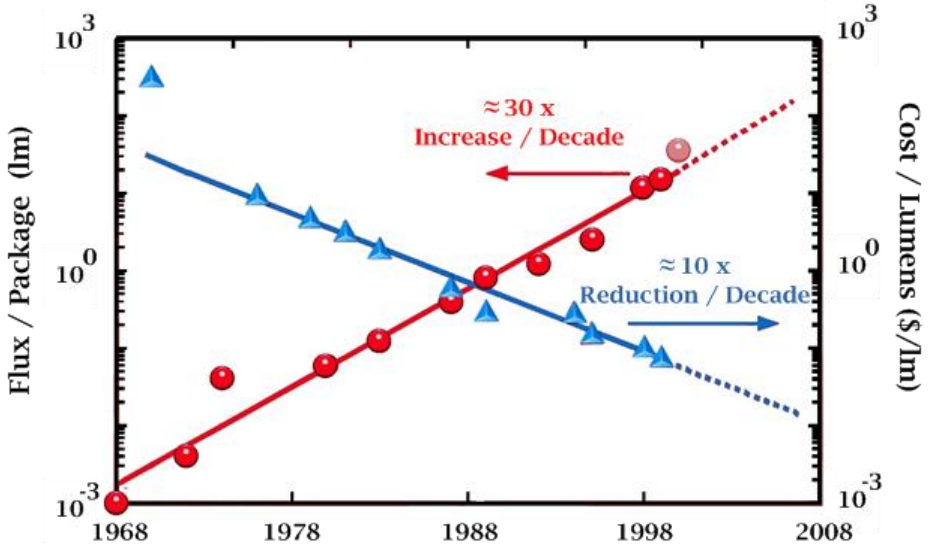

Figure 4: The evolution of performance and cost for commercially available red LED's [Hai99]
(The data was compiled by R. Haitz from HP historical records)

detectors capable of high-speed operations are available at low cost; data transmission can be confined with an opaque obstacle, thus reducing interference between links and ensures data security from outside access; if intensity modulation and direct detection are used, the smaller wavelengths combined with a large-area, square-law detector leads to efficient spatial diversity that prevents multipath fading. This factor allows the usage of much simpler designs than those used by RF, which is frequently subject to large fluctuations in signal amplitude and phase. However, in a free space optics communication channel, restrictions to these considerations need to be applied, especially on the available bandwidth.

Due to the advances in the field of solid-state lighting, HB-LED's have become available in all color ranges. White HB-LED's present themselves as the future of both indoor and outdoor lighting scenarios. By joining the penetration of HB-LED's in our daily lives, and the knowledge available on IR wireless communications, VLC presents itself as a promising technology for the future of wireless communications. It is a ubiquitous technology, generating no interference to human life or existing electronic devices. Unlike RF systems, VLC can be used in hospitals, space stations and other electromagnetic interference sensible locations. Applications such as visible light communication for audio systems [Pan99], information broadcasting using LED traffic lights [Aka01, Kum08, Kum09] and integration of VLC with power-line communications (PLC) [Kom03], are examples of the capabilities of VLC. One of the most important steps towards standardization was made with the establishment of the Visible Light Communications Consortium, a group of mostly Japanese based companies that agreed on sharing information towards the development of this new technology [VLweb]. Another signal of the importance of VLC was the creation of the task group seven (TG7) under the IEEE 802.15 working group for wireless personal areas networks [IEweb].

II.ii New trends in lighting systems

Visible light LED's have had a huge development since their days of simple indicators. The main reason for this was the great increase in efficiency and the decrease in production cost [Kra07]. In figure 5 is presented a chart on the evolution of luminance values of LED's and a comparison with some of the effective luminance values of conventional light sources: tube fluorescent, automotive halogen, automotive Xenon high-intensity discharge (HID), and ultra-high-performance (UHP) discharge lamp used for projection. LED values are color-coded to the correspondent wavelengths, and white LED's with the Thin Film Flip Chip (TFFC) technology from LUMILEDS are marked as triangles. On the right of the image are the ranges required for several applications [Kra07].

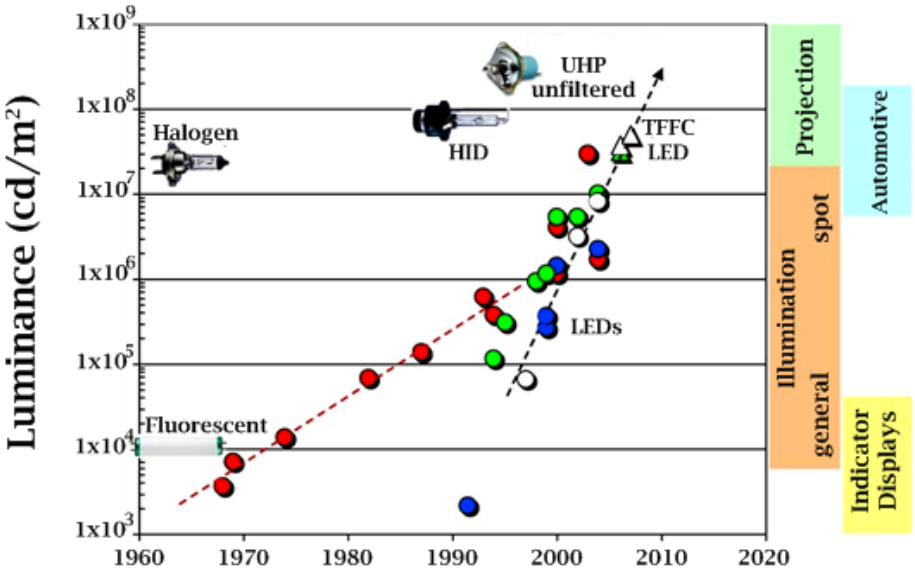

Figure 5: Luminance of several light sources [Kra07]

Table 1: Efficiency and lifetime of conventional and semiconductor white light sources [Hai99]

Lamp Type	Efficiency [lm/W]	Lifetime [h]
100W Incandescent	15	1 000
135W Long Life Incandescent	12	5 000
300W Halogen	24	3 000
50W Compact Halogen	12	2 500
11W Compact Fluorescent	50	10 000
30W Fluorescent	80	20 000
White LED (Year 2000)	20	100 000
White LED (Year 2002)	30	100 000
White LED (Year 2005)	40	100 000
White LED (Year 2010)	50	100 000

(LED's efficiency values as projected in [Hai99])

In table 1 the typical efficiency and lifetime values of common white light sources, are shown, as along with the predicted values for white light LED's around the year 2000 [Hai99]. Although the values are an optimistic prediction for white light LED's, actual Luxeon Rebel LED's achieve values of 100lm/W, and a lifetime of 50.000 hours with 70% lumen maintenance, when driven with a current of 700mA. And the state-of-the-art Luxeon K2 LED's can achieve over 200lm/w, and a lifetime of 50.000 hours with 70% lumen maintenance, when driven with a current of 1A.

In the United States of America, about a third of the electrical power is spent in lighting applications, with incandescent and fluorescent lamps being the most usual devices encountered. With power-efficiency and cost-reduction as the main concerns, white-light LED's become a perfect solution for future lighting scenarios. LED's, unlike conventional light sources, provide direct conversion of electrical energy into light, meaning that most of the energy is used for lighting and not dissipated through heating.

They are also much more robust devices, with higher tolerance to humidity, lower heat generation and longer lifetimes, thus the cost of replacement is dramatically reduced. The size of the LED's is also a great advantage. However, it has the adverse effect of concentrating heat, especially on HB-LED's, but this can be offset by dissipating heat through the fixture. Also, current packaging technologies open an array of heat dissipation possibilities, making the design of LED lighting systems easier as time passes. Arguably, LED's are also much more aesthetically pleasing [Kra02, Kra07, Shu05]

A major application for colored LED's is traffic light substitution. The increased seeing distance achieved with today's HB-LED's makes these devices easy to adapt. Color conversion is straightforward, without the necessity for a colored lens, thus simplifying the design. Also, on an outdoor scenario, white light LED's can easily be adapted to street lighting, with a better light distribution, the same is valid for indoor lighting. Special Red, Green and Blue (RGB) LED's are also used in outdoor billboards and giant screens with remarkable performance. In all of these applications, using LED's means lower power consumption, leading to less greenhouse gas emissions due to electrical power production in fossil-fuel burning power plants.

II.iii VLC application examples

All the new applications for HB-LED's have made possible to implement VLC systems in different scenarios. In figure 6 some of the outdoor scenarios are illustrated. All the vehicles, traffic lights and billboard use HB-LED's and are equipped with VLC systems. On the bottom left corner a bus passes through an intersection transmitting its

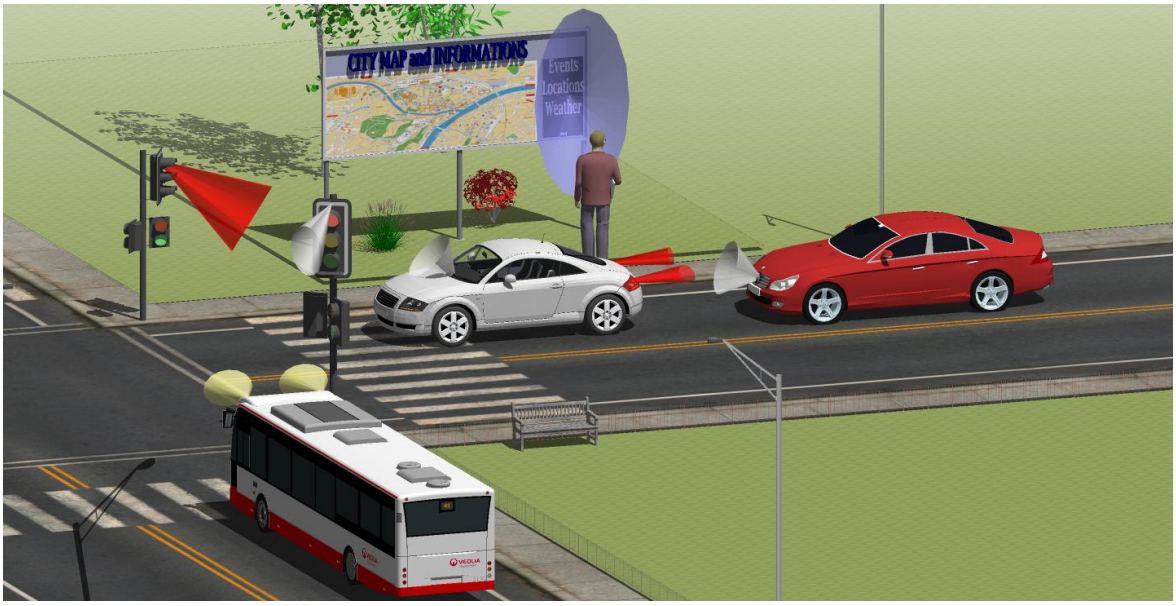

Figure 6: Outdoor VLC application examples

identification to a receiver mounted on the traffic light, this information is then relayed to a control station where a supervisor can verify the bus location or even if it is on schedule, without having to resource to an RF based GPS system. This is a clear example of an Intelligent Transportation System (ITS), which can also be used in automated tollbooths in similarity to what happens with the Portuguese system "Via-Verde". In the centre of the figure the white vehicle is receiving information from the traffic light, this information could be related to traffic conditions ahead, GPS location, etc. Also in the white car, the taillight is sending information to the vehicle behind it, transmitting that it has stopped so, even if the driver of the red vehicle fails to use the brakes, the onboard computer will stop the red car automatically. This is an example of an ADAS, which can be easily implemented through VLC. These are the type of applications that project VIDAS is trying to develop. One final application is shown in the background, a person can point a VLC equipped portable device to a billboard and automatically receive relevant information from it, such as a map or even advertisement. Not shown on the figure is the possibility of using the street lighting system as access points, creating a global network throughout a city, for sharing relevant local information.

In an indoor scenario VLC applications are mostly focused to network access. In figure 7 is presented an example of an office network using HB-LED's lighting with VLC and a PLC modem, similar to what is discussed in [Kom03]. The cones in the ceiling represent an approximation to the emission radiation patterns (bright-yellow) and the receiver field-of-view (grey), in the case of the terminals (laptops, desktops and PDA's), given the proximity of emitter and receiver, a single cone is drawn (dark-yellow). In such a scenario it is possible to see a laptop and a personal computer accessing the network through either inbuilt or USB adapters. VLC networks are contained inside opaque walls

Figure 7: Indoor VLC application examples

and the usage of a PLC modem, as shown in the right of the figure, allows the usage of the already implemented electric cables as a mainframe to interconnect different rooms. Also if each emitter is referenced to the respective GPS coordinates it allows the usage of GPS inside buildings with higher resolution and precision then the current RF based ones.

In conclusion, with the increasing usage of HB-LED's, the implementation of VLC systems can be adapted to almost any scenario. The Visible Light Communications Consortium and the IEEE 802.15 Task-Group 7 have published information on such applications. As examples are a location-information system from a traffic signal developed by "The Nippon Signal Co., Ltd" and a merchandise information delivery system, in which an intelligent shopping cart displays information about a product or promotions available at a specific area in a supermarket, developed by "NEC" and "Matsushita Electric Works" [Har08].

II.iv The transmission channel

In the current work the transmission channel is defined as the physical space included between the optical emitter and the optical receiver. Its analysis can be broken down into the analysis of three distinct parts, the emitter radiation pattern, the optical signal propagation model and the receiver optical characteristics. Given the similarity of the transmission medium used in VLC and IR systems, the knowledge acquired from the vast research in IR systems can be adapted to VLC. In a recently published paper Kumar describes the VIDAS application scenario and presents a Line-of-Sight (LOS) model for signal propagation [Kum09]. This work along with [Val95] and [Tav99] are the basis references used in the analysis of the transmission channel.

II.iv.i Emission

The basic emitter is constituted by a visible light source modulated to transmit data. Given the specificity of the project, such emitter is based in HB-LED's which can be individually modeled by a Lambertian radiation pattern having rotational symmetry. Usually in traffic lights, each signal (red, yellow and green) consists of a tight packaging of multiple LED's, resulting in a radiation pattern equal to the superposition of the individual components, but given the close arrangement of the LED's a simple Lambertian distribution is assumed for simplification purposes, therefore the radiation pattern is:

$$R_E(\varphi, m) = \frac{m+1}{2\pi} \cdot P_E \cdot cos^m(\varphi) \text{ , with } \varphi \in [-\pi/2\,;\pi/2\,], \qquad \textbf{(eq. 1)}$$

where P_E is the transmitted power, φ is the direction angle relatively to the emitter's normal, and m is the mode number of the radiation lobe which specifies the directionality of the source and it is given by:

$$m = -\frac{ln(2)}{ln\,(cos(hpa))}. \qquad \textbf{(eq. 2)}$$

In equation 1, the coefficient $(m+1)/(2\,\pi)$ is a normalizing factor which ensures that integrating $R_E(\varphi, m)$ over the surface of a hemisphere results in the source power (P_E), usually supplied in the device's datasheet. From equation 2, the directivity of the emitter is related to the half-power-angle (hpa), which represents the viewing angle at which 50% of the radiant energy is contained, in a plane that contains the lobe's maximum value, also known as half-power beam-width. This value is usually supplied by LED manufacturers. A mode number of m = 1 (hpa = 60º) corresponds to an ideal Lambertian source. Figure 8 shows a polar plot of the normalized radiation patterns of Lambertian LED's ($cos^m(\varphi)$) for directivity values of m = [1,3,10], which corresponds to hpa values of 60º, 35,5º and 21,1º respectively.

To complete the model it is also necessary to specify the position and orientation of the light emitter, relatively to the system's origin. Position is defined by the geometric coordinates (x_E, y_E) and orientation is given by the elevation angle (ϕ_E). The emitter can be then defined through:

$$E = \{P_E, hpa, (x_E, y_E), \phi_E\}. \qquad \textbf{(eq. 3)}$$

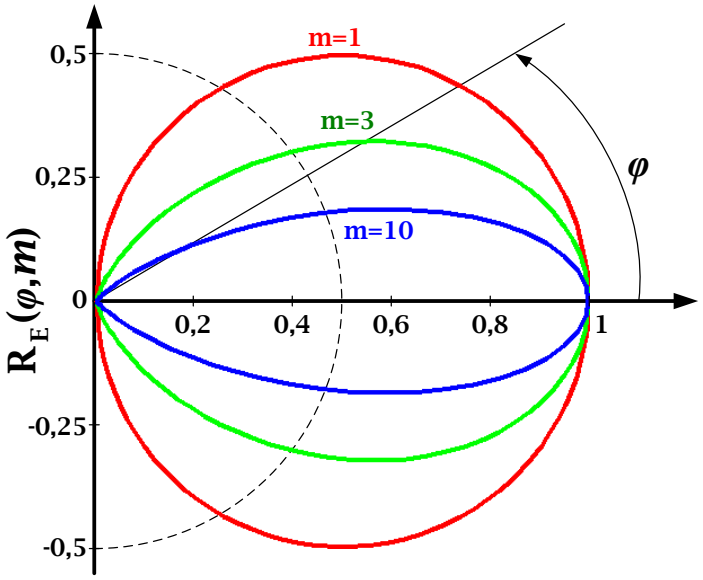

Figure 8: Normalized Lambertian radiation patterns for ***m*** = [1, 3, 10]

II.iv.i Reception

Signal reception is done using a PIN photodiode. This converts the optical signal into an electrical current which is further enhanced by a front-end amplifier. A typical receiver model is represented in figure 9. Its key parameters are the field-of-view (FOV) and the effective signal collection area (A_{eff}), which are related by:

$$A_{eff}(\sigma) = \begin{cases} A_d \cdot cos(\sigma) & ; |\sigma| < FOV \\ 0 & ; |\sigma| \geq FOV \end{cases}, \quad \textbf{(eq. 4)}$$

where A_d is the physical area of the detector and σ the angle between the receiver's axis and the direction of the incident light.

The FOV represents the maximum value of σ for which the receiver can still detect light. In a single cell receiver with a photodiode characterized by a FOV of $\pi/2$, the receiver is said to have a complete field-of-view, decreasing this value can be used to improve the detection capabilities by cutting off unwanted reflections and noise.

Similar to the emission model, the reception model will only be complete by defining the position and orientation of the receiver relatively to the system's origin. Position is defined by the geometric coordinates (x_R, y_R) and orientation is given by the incident angle (σ_R), resulting in:

$$R = \{A_d, FOV, (x_R, y_R), \sigma_R\}. \quad \textbf{(eq. 5)}$$

At this stage, optical filtering should also be considered. As will be further explained in subsection II.iv.i, a PIN photodiode has a spectral sensitivity that includes a large part of the near-IR spectrum. Given that there are several noise sources that not only affect the visible light spectrum, but also the IR spectrum. If a simple IR cut-off filter is used, the effect of such noise sources can be significantly reduced. From [Mor96], the

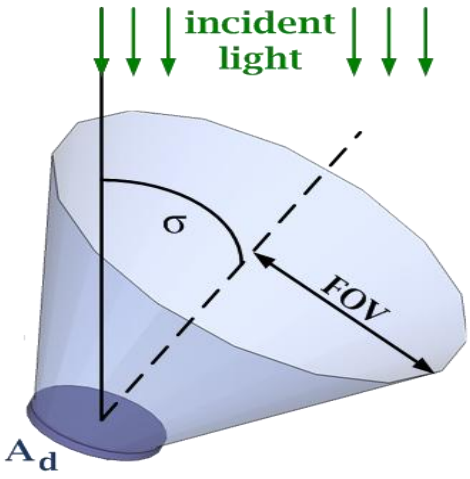

Figure 9: Receiver model

transmission coefficient of an optical filter can be broken down to several components, but for now it will be defined as T_{filter}. So, the receiver model with optical filter is now defined by:

$$R = \{A_d, FOV, (x_R, y_R), \sigma_R, T_{filter}\}. \quad \textbf{(eq. 6)}$$

II.iv.ii Line-Of-Sight propagation model

The LOS propagation model requires that the emitter has an unobstructed view to the receiver. This model is often used to describe optical wireless communication systems, namely IR connections. It helps explain the behavior of optical signals. Although the following text will address the VIDAS application, the presented model can be applied to any other optical wireless communication system that uses LOS to establish a connection between emitter and receiver.

The VIDAS application relies mostly on the LOS propagation model. The system setup is presented in figure 10. The emitter, a traffic light consisting of an array of HB-LED's is placed at a given height (h) aligned with the traffic lane with a vertical inclination of ϕ, maintaining a direct link between the emitter and the receiver. The

Table 2: LOS propagation model parameters

Parameter	Symbol
Distance between receiver and emitter	d
Distance in the ground plane	x
Height of the traffic light	h
Service area	$[U_{min}, U_{max}]$
Angle of irradiance	φ
Vertical inclination of the receiver	$0° \leq \theta \leq 90°$
FOV of the receiver	$0° \leq FOV \leq 90°$
Angle of incidence	σ

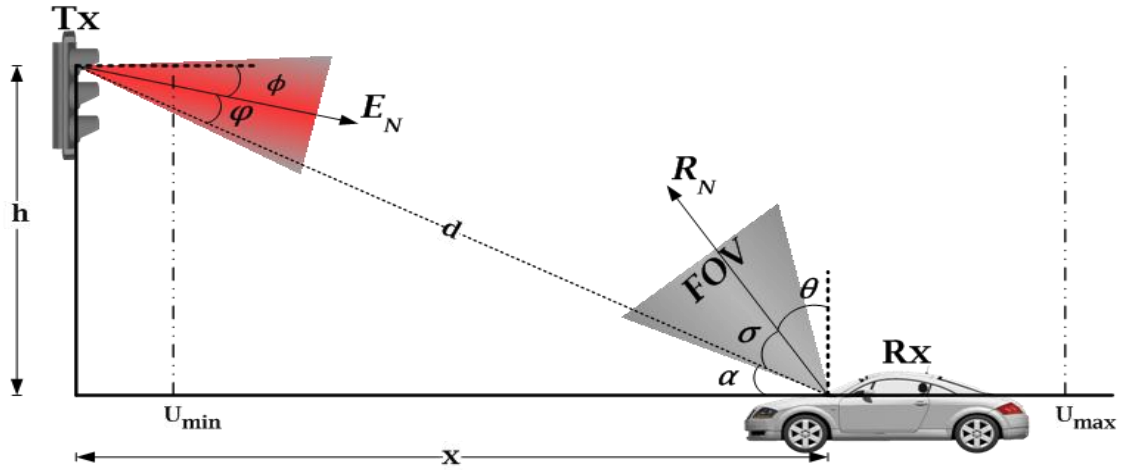

Figure 10: LOS propagation model for VIDAS application

vehicle with a built-in receiver moves towards the emitter with a certain speed on the ground plane, the receiver is mounted with a vertical inclination of θ. The interval between U_{min} and U_{max} is the range for possible communication (service area), with U_{min} being the nearest point to the traffic light, and U_{max} the starting point from where data transmission starts. For quick reference, table 2 contains the system parameters used.

In this configuration, the incident power collected in the photodiode at the receiver front-end depends on the transmitted power, on the geometry between the traffic light and the vehicle, on the channel attenuation and on the receiver model. The LOS model can be adapted from wireless IR studies, Kahn and Barry in [Kah97] presented a model in which the intensity of the received signal is given by:

$$I = P_E(t) \cdot \frac{m+1}{2\pi} \cdot \frac{cos^m(\varphi)}{d^2} \cdot A_d \cdot cos(\sigma) \cdot \partial\left(t - \frac{d}{c}\right). \quad \textbf{(eq. 7)}$$

The term $\partial\left(t - \frac{d}{c}\right)$ represents the delay due to channel propagation, and equation 7 can be written as a function of (x, σ, h, ϕ) with simple trigonometry manipulation. From the right angle triangle:

$$d = \sqrt{(x^2 + h^2)}\,, \quad \textbf{(eq. 8)}$$

$$\sigma = \frac{\pi}{2} - \alpha - \theta \text{ , and} \quad \textbf{(eq. 9)}$$

$$\alpha = tan^{-1}(h/x)\,. \quad \textbf{(eq. 10)}$$

Substituting equation 10 in 9, gives:

$$\sigma = \frac{\pi}{2} - \theta - tan^{-1}(h/x). \quad \textbf{(eq. 11)}$$

Finally the angle of irradiance can be represented as:

$$\varphi = tan^{-1}(h/x) - \phi\,. \quad \textbf{(eq. 12)}$$

This way, considering a normalized emitted power, equation 7 can be written in the format:

$$Hn(x, \theta, h, \phi) = \frac{m+1}{2\pi} \cdot \left(\frac{cos^m(\pi/2 - tan^{-1}(x/h) - \phi) \cdot cos(tan^{-1}(x/h) - \phi)}{h^2 + x^2}\right). \quad \textbf{(eq. 13)}$$

This result is available in [Kum09] with further analysis into the optimization of the system parameters. Although it falls out of the scope of this dissertation, it is still a valuable reference for the design of the front-end electronics for VIDAS, or any similar VLC systems.

II.iv.i Noise sources

Noise sources are an important challenge to overcome towards the feasibility of VLC systems. In figure 11, spectral power densities of natural and artificial light sources are compared against the spectral sensitivity of typical silicon (Si) photodiodes. Although there are usually sources of external electromagnetic interference in both the emitter and receiver, mainly due to other electronics devices and the power supply grid, their contributions are small and the effects can easily be minimized by recurring to correct shielding of the front-end electronics and filtering of the power supplies. The major contributions of noise are present in the receiver's photodiode. These are: thermal noise; shot noise; and optical excess noise.

Thermal noise is associated with the photodiode's polarizing resistor, and is considered a white noise source with small spectral density. As for shot noise, natural and artificial light sources create a steady background irradiance which causes quantum noise due to the random nature of the photo-detection process. The steady background irradiance induces a constant current on the receiver's photodiode, usually known by photocurrent. Sunlight's radiant intensity presents slow variations and can be considered stationary, the induced photocurrent is represented by I_{Ndc}, but radiant intensity produced by artificial light sources presents a periodic component. In the case of incandescent lamps and fluorescent lamps with conventional ballast, the electric noise spectrum shows harmonics in multiples of the double of the power grid's frequency. The electrical noise spectrum of fluorescent lamps with electronic ballasts shows harmonics in multiples of the power grid's frequency and in multiples of the ballast's switching frequency. Also, fluorescent lamps emit a burst of pulses in each period with short length and random starting points, thus inducing a variable photocurrent $(i_N(t))$ [Val95, Mor96, Mor97]. Therefore the induced noise photocurrent is given by:

$$I_N = I_{Ndc} + i_N(t)\ . \qquad \textbf{(eq. 14)}$$

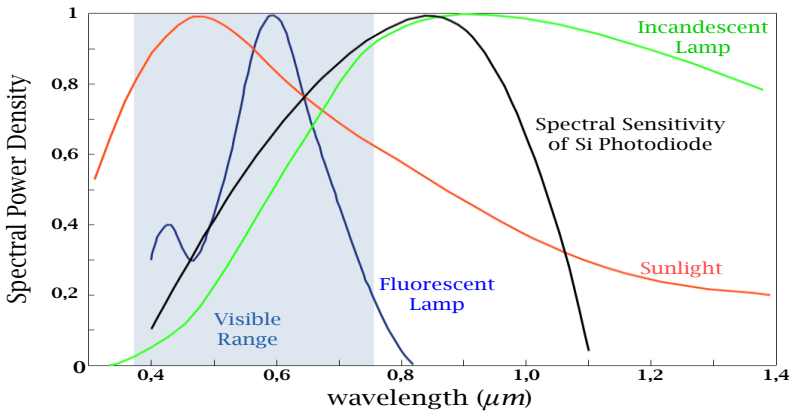

Figure 11: Normalized spectral power densities of common light sources [Tav99]

A usual simplification made to calculate the shot noise is to consider the average value of $i_N(t)$, thus I_N becomes the average current in the photodiode due to shot noise, making the optical channel an additive white Gaussian noise. The variance of the shot noise is proportional to this current and is defined by [Val95]:

$$\sigma_N{}^2 = 2.q.I_N.B, \quad \textbf{(eq. 15)}$$

where q is the electronic charge, and B is the equivalent noise bandwidth factor.

The average current in the photodiode (I_S) can be related to the optical power density (optical power per unit of surface area), also known as irradiance (H) through:

$$I_S = R.H.A_{eff}\ , \quad \textbf{(eq. 16)}$$

where R is the responsivity of the photodiode, and A_{eff} the effective signal-collection area. With the results of equations 15 and 16 it is now possible to specify the Signal-to-Noise Ratio (SNR) of an optical connection in free-space with dominating shot noise:

$$SNR = \frac{I_S}{\sigma_N} = \frac{R \cdot H_S \cdot A_{eff}}{\sqrt{2 \cdot q \cdot I_N \cdot B}} = \frac{\sqrt{R} \cdot H_S \cdot \sqrt{A_{eff}}}{\sqrt{2 \cdot q \cdot H_N \cdot B}}\ , \quad \textbf{(eq. 17)}$$

where H_S and H_N are the signal and noise irradiance respectively. From this expression, is possible to understand that the A_{eff} value is very important in order to achieve a high SNR [Val95].

Optical excess noise presents a spectral density concentrated in the low frequency range. Its effect can be considered as random fluctuations with a magnitude one hundred times higher to that of the detected data signal [Kum09]. In a VIDAS application scenario, a headlight of another vehicle circulating in the opposite lane, or even a street lamp, could cause an excess of optical signal in the receiver's photodiode.

Typical background noise is associated to shot noise, which can be reduced by controlling the amount of background radiation collected. In a free-space optical receiver the FOV and optical bandwidth determine the amount of radiation collected, therefore using a narrower FOV and an optical IR cut-off filter is a desirable solution.

Figure 12 represents the typical response of an IR-cut-off filter [EOweb]. Using this filter would reduce in approximately 5% the perceived input signal. However, the considerable attenuation provided to any IR component can significantly improve the receiver immunity to the IR component of optical noise sources. In order to better characterize the optical filter, the transmission coefficient can be defined as the sum of several parcels, one for each different light contribution [Mor96]:

$$T_{filter} = T_s + T_i + T_a + T_n\ , \quad \textbf{(eq. 18)}$$

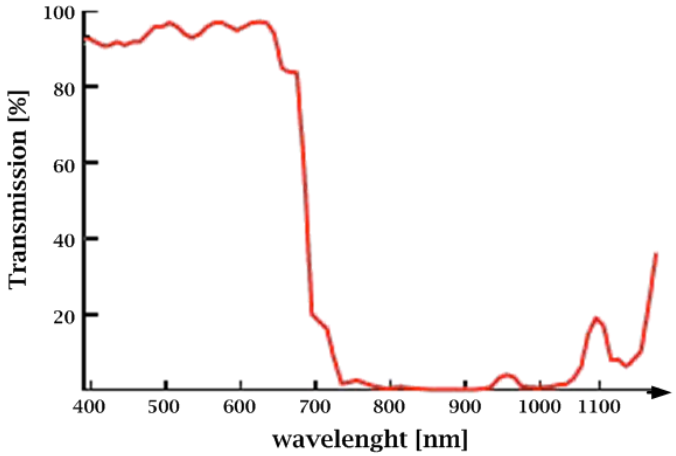

Figure 12: Transmission coefficient of typical IR cut-off filter [EOweb]

where T_s, T_i, T_a and T_n are the transmission coefficients for the transmitted signal, time varying artificial light, average artificial light and natural sunlight, respectively.

Although an optical filter might seem as an excellent solution for reducing noise interference, the price of such component is considerably high, especially when trying to build a cost effective solution. For example, an IR cut-off filter with 12,5mm of diameter costs at about 40€ [EOweb]. Another possible solution would be to use a photodiode that already includes an IR cut-off filter. These devices are made with a special coating over the photosensitive area that blocks IR light from reaching it. They are intended for visible light applications and usually have a smaller responsivity due to that same coating.

Other sources of noise in outdoor VLC systems, VIDAS in particular, are the unpredictable weather conditions. These can seriously limit the range or even the availability of a data link. The optical signal is subject to absorption due to the presence, in the atmosphere, of water and carbon dioxide particles. Also, by deflecting light, fog, haze, rain or snow cause scattering, which can be minimized by increasing the receiver's FOV. This can be achieved by using a concentrating lens or increasing the number of receiver cells, although the second solution is not practical in VIDAS or any other ADAS application, and in any case increasing the FOV has its disadvantages.

In conclusion…

VLC had a significant evolution over the last few years. Although the concept of using visible light is very old, it was only in recent years that it became a viable technology for a modern wireless optical communication system. Amongst the several factors that propelled VLC, the introduction of IR communications by Gfeller in [Gfe79] and the recent developments in solid-sate lighting are the most important.

HB-LED's have reached new performance standards that make them ideal for outdoor and indoor lighting. This opened the doors to a variety of application scenarios, where VLC can also be applied. One of these applications was proposed by project VIDAS and will be developed in this dissertation.

In order to better understand the behavior of the optical signals, receiver, emitter and propagation models were analyzed. Using the widespread knowledge available for IR communications, these models can easily be obtained. The emitter is characterized as having a typical Lambertian radiation pattern which is mostly defined by the half-power angle. The receiver is characterized by its effective signal collection area which is related to the FOV, physical area and the angle of the incident light. With these elements defined, the propagation model can be presented. Similar to many wireless optical communications, the VIDAS application relies on the LOS propagation model. One of the most important conclusions taken from this model is that the optical signal will decrease with the increase of the distance elevated to the square (equation 7).

Another important analysis to VLC systems is the presence and influence of optical noise sources. It is possible to conclude that artificial and natural light sources might create a significant interference to the receiver. Not only do they create a steady background noise, but fluorescent lights also have a transient component that might spread over several decades of frequency, thus causing a significant interference to the transmitted optical signal. Another important conclusion taken from the study of noise sources is that, in order to increase the SNR a device with a large active area should be used.

Chapter III

Emitter Design

A VLC emitter is an optic-electronic transducer device that transmits information using visible light waves as the transmission medium, usually with the resource to HB-LED's. VLC systems have become a more viable technology for the future of wireless data transmission, in large part due to the developments in the area of solid-state lighting. It becomes pertinent to study the light emitting devices and the different emitter topologies in order to obtain a better performance from a VLC emitter. The VIDAS application scenario presents its own specific obstacles and challenges to which the studied topologies were directed.

This chapter is organized in three subsections. Starting in III.i, the emitter device is defined by presenting the main building blocks. In subsection III.ii, HB-LED's are analyzed, electrical and optical characteristics are presented as well as some results previously obtained in the laboratory. In the final subsection, III.iii, the studied emitter topologies are presented and discussed.

III.i Emitter description

History has several examples of light emitting devices used to transmit messages. The shields of the ancients Greeks, the mirror in Alexander G. Bell's *photophone* [Bel81] and even flashlights, which are still used. This makes visible light a viable option as a transmission medium. A natural or artificial light source or a light reflector is the only device needed. However, an actual *"of-the-shelf"* VLC emitter is still some steps away.

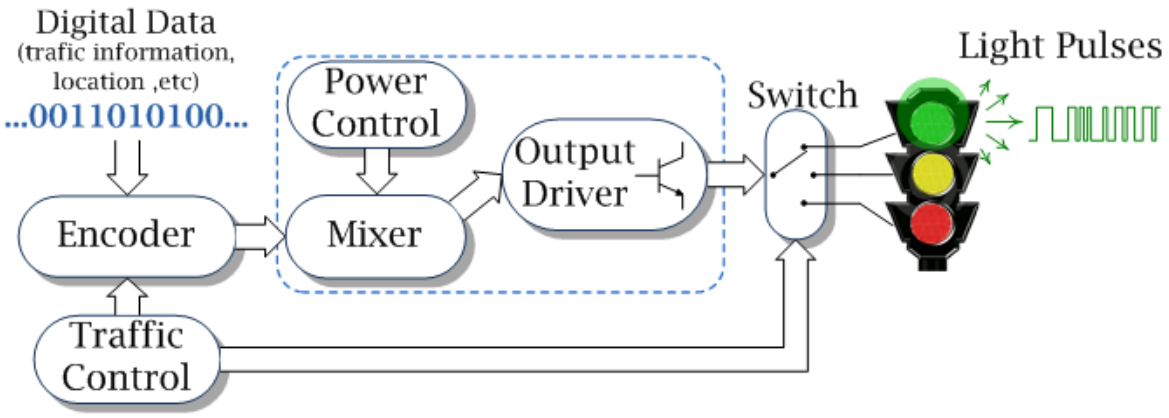

Figure 13: VLC emitter block diagram for a traffic light

Before comparing the desired VLC emitter to any commercially available emitter, it becomes necessary to describe and specify the device itself. The block diagram in figure 13 defines the basic building blocks for a VLC emitter in a traffic light. The digital data signal is passed to a data encoder that modulates the signal into the desired format, in this case a simple Non-Return to Zero (NRZ) encoding with an on-off keying (OOK) amplitude modulation. This block also receives information from the traffic control unit so that it can hold information while the light color changes, ensuring that there is no transmission in that brief interval. This signal is then passed to a mixer which will merge the data signal with the power supply from the power control block. The resulting signal is then used to control the switching of the LED through the output driver. To control which traffic light should be lit, the traffic control unit controls a switch that connects the correct color LED's with the output driver. Sometimes the electrical characteristics of the different color LED's, like the maximum forward current or the forward voltage, might imply the usage of an output driver with three distinct channels and a slightly different switch.

Considering the desired emitter as a full "o*f-the-shelf*" product, the encoder can be integrated, or the range of input signals specified. To build this block, a microprocessor is a relatively cost effective solution but upgrading it is not an easy process. Using a field-programmable gate array (FPGA) would be more expensive, but has better data processing capabilities, and it also makes upgrading easier. Such scenario, including an explanation on the concept of a wireless universal serial bus using a VLC system was addressed in [Kum08]. The current work addresses the problem of building the front-end electronics for VIDAS, therefore the encoder block falls somewhat out of range of the work's scope. The following subsections will therefore mainly address the issues that are found in designing the electronics of several emitter topologies.

In the front-end electronics, integrating the LED matrix is essential to specify power consumption, optical range, maximum operating frequency, etc. Next, in

subsection III.ii, the most important characteristics of commercially available LED's will be presented and compared. The power control and mixer blocks are also very important given that they control the LED's current levels, maintaining a steady average value.

Currently no such system is yet commercially available and even searching for the right components to build one is an arduous task. The currently available emitters are dedicated to the IR wavelengths, and their applications go from remote controllers, to digital imagery, IR optical communications, solid-state lasers, automotive sensors, and industrial process control.

III.ii Light Emitting Diodes for VLC

In subsection II.ii the advantages and the evolution of LED's in lighting systems were addressed. These devices have evolved significantly over the last few years, making them a perfect solution for future lighting systems. Being a semiconductor device, they also present fast switching capabilities which makes them, HB-LED's particularly, the perfect emitter for a VLC system.

Upon researching HB-LED's datasheets from several manufacturers, there are two sets of typical information available, one regarding electrical characteristics and the other regarding optical characteristics. Some manufacturers, like OSRAM or Philips LUMILEDS, supply very detailed information with tables and charts explaining parameters variation, and also simulation models for both electrical and optical simulation. Other manufacturers, like LUMEX present only the basic information tables. Nevertheless the typical information usually addresses:

- Optical characteristics:
  - → Manufacturing technology;
  - → Color range (peak wavelength or color temperature);
  - → Luminous flux (ϕ_L);
  - → Half-power-angle (hpa);
- Electrical characteristics:
  - → Typical forward voltage (V_F);
  - → Forward current (I_F);
  - → Operating temperature.

In table 3 there is a comparison between the optical characteristics of some of the most popular HB-LED's on the market. The information was taken from the datasheets available in the manufacturer's website. And in table 4 are the respective electrical characteristics.

Table 3: HB-LED's optical characteristics

Manufacturer	Model	Manufacturing Technology	Colour	Peak wavelength or Colour Temp.	Typical ϕ_L [lm] @ I_F [mA]	*hpa* [º]
LUMEX	SML-LX3939UWC	InGaN	White	6300 Kelvin	190,0 @ 350	65
	SML-LX2723UWC				31,0 @ 350	60
	SML-LX2723SIC	AlInGaP	Red	630 nm	31,0 @ 350	60
	SML-LX2723SYC	AlInGaP	Yellow	590 nm	31,0 @ 350	60
	SML-LX2723UPGC	InGaN	Green	525 nm	46,5 @ 350	60
	SML-LX2723USBC	InGaN	Blue	470 nm	9,0 @ 350	60
Philips LUMILEDS	LXML-PWC1-0100	InGaN	White	6500 Kelvin	180,0 @ 700	70
	LXK2-PW14-V00				140,0 @ 1500	70
	LXML-PD01-0040	AlInGaP	Red	627 nm	85,0 @ 700	70
	LXK2-PD12-S00				100,0 @ 700	70
	LXML-PL01-0030	AlInGaP	Amber	590 nm	65,0 @ 700	70
	LXK2-PL12-R00				75,0 @ 700	70
	LXML-PM01-0100	InGaN	Green	530 nm	180,0 @ 700	70
	LXK2-PM14-U00				130,0 @ 1500	70
	LXML-PB01-0030	InGaN	Blue	470 nm	58,0 @ 700	70
	LXK2-PB14-Q00				46,0 @ 1500	70
OSRAM	LUW W5SM	ThinGaN	White	6500 Kelvin	81,0 @ 350	60
	LUW W5AP				311,0 @ 1400	70
	LR W5SM	Thinfilm InGaAlP	Red	625 nm	49,0 @ 500	60
	LR W5AP				150,0 @ 1400	70
	LA W57B	InGaAlP	Amber	617 nm	17,6 @ 400	60
	LA W5AP	Thinfilm InGaAlP			185,0 @ 1400	70
	LY W57B	InGaAlP	Yellow	587 nm	17,6 @ 400	60
	LY W5AP	Thinfilm InGaAlP		590 nm	140,0 @ 1400	70
	LV W5SG	InGaN	Green	505 nm	35,0 @ 500	60
	LT W5AP	ThinGaN	True Green	528 nm	185,0 @ 1400	70
	LB W5SG	InGaN	Blue	470 nm	11,0 @ 500	60
	LB W5AP	ThinGaN			75,0 @ 1400	70

(For quick reference, the HB-LED's used in this project are grey shadowed)

A quick comparison of data shows that current HB-LED's have high luminous flux values, especially white and green colored ones. The blue LED's are the ones that show the smaller values of luminous flux, which is understandable given that these are the most recently discovered and development is still at an early stage. Given that HB-LED's are mainly used for lighting purposes, the half-power-angle values are very similar producing a uniform light radiation pattern instead of a directional pattern that is achieved with a smaller value. For further understanding of photometry units and definitions, please refer to [VIS04].

A comparison, of tables 3 and 4, shows that higher values of forward current usually mean higher values of luminous flux. Of course at such high currents, designing an LED driver is a dual challenge in power electronics and heat dissipation.

Table 4: HB-LED's electrical characteristics

Manufacturer	Model	Colour	Typical V_F [V] @ I_F [mA]	Max. I_F (DC) [mA]	Operating Temperature min. [ºC]	Operating Temperature max. [ºC]
LUMEX	SML-LX3939UWC	White	7,3 @350	700	-40	80
	SML-LX2723UWC		3,2 @ 350	350	-40	85
	SML-LX2723SIC	Red	2,0 @ 350	350	-40	85
	SML-LX2723SYC	Yellow	2,0 @ 350	350	-40	85
	SML-LX2723UPGC	Green	3,2 @ 350	350	-40	85
	SML-LX2723USBC	Blue	3,2 @ 350	350	-40	85
Philips LUMILEDS	LXML-PWC1-0100	White	3,4 @ 700	1000	-40	135
	LXK2-PW14-V00		3,9 @ 1500	1500	--	150
	LXML-PD01-0040	Red	3,6 @ 700	700	-40	120
	LXK2-PD12-S00		3,6 @ 700	700	--	150
	LXML-PL01-0030	Amber	3,6 @ 700	700	-40	120
	LXK2-PL12-R00		3,6 @ 700	700	--	150
	LXML-PM01-0100	Green	3,4 @ 700	1000	-40	135
	LXK2-PM14-U00		3,9 @ 1500	1500	--	185
	LXML-PB01-0030	Blue	3,4 @ 700	1000	-40	135
	LXK2-PB14-Q00		3,9 @ 1500	1500	--	185
OSRAM	LUW W5SM	White	3,2 @ 350	1000	-40	110
	LUW W5AP		3,5 @ 1400	2000	-40	150
	LR W5SM	Red	2,2 @ 400	1000	-40	110
	LR W5AP		2,5 @ 1400	2000	-40	150
	LA W57B	Amber	2,2 @ 400	400	-40	100
	LA W5AP		2,5 @ 1400	2000	-40	150
	LY W57B	Yellow	2,2 @ 400	400	-40	100
	LY W5AP		2,5 @ 1400	2000	-40	150
	LV W5SG	Green	3,8 @ 350	500	-40	100
	LT W5AP	True Green	3,5 @ 1400	2000	-40	150
	LB W5SG	Blue	3,8 @ 350	500	-40	100
	LB W5AP		3,5 @ 1400	2000	-40	150

(For quick reference, the HB-LED's used in this project are grey shadowed)

When designing an emitter, the maximum operating frequency is a key factor, as having a large bandwidth requires choosing the right design and the right components. For the power control, mixer and output driver blocks there are several alternatives available for components, with very extensive information on their electrical characteristics, but choosing an appropriate LED becomes hard work. Although manufacturers do not have a unique set of test conditions to characterize LED's, optical information is abundant, and comparison is not very difficult. Some manufactures even supply free software to help design lighting solutions, calculate power dissipation and color control. A problem arises when trying to determine the LED's switching capabilities.

In IR optical communications devices, rise and fall times are standard information in datasheets, but in visible light LED's such information does not appear in the component datasheet. After an intensive search the only set of information found on visible LED's switching behavior comes from VISHAY, in the document *"Physics of Optoelectronic Devices"* [VIS04], but these are reference values for the production technology in which the LED's are grouped by colors. The specific values for individual

LED's are not presented. Also the test conditions are for a forward current of 10mA, which raises the question of whether such information is for regular LED's, HB-LED's or both. In regard to simulation models, the scenario is basically the same. There is much information regarding optical simulation, but for electrical simulation the supplied PSpice models are only useful for steady-state analysis. A warning available at the OSRAM Opto-Semiconductors website states [OSweb]:

"Please read before using the OSRAM PSpice libraries!
- *Only the typical forward characteristic (Vf-If diagram) of each LED has been modeled.*
- *The typical forward characteristic can vary slightly in reality.*
- *All other PSpice parameters have not been modeled (e.g. reverse characteristic, transient behavior). ..."*

After analyzing this data and keeping the final application in mind, it is understandable that until the LED production industry becomes aware of such usage for their devices, it is necessary to do an individual characterization of several HB-LED's, and measure the maximum frequency at which information can be transmitted over a fixed distance in a controlled environment. In table 5 are some measured values of LED's switching speeds. These values were measured by Pereira at the Integrated Systems and Circuits laboratory of the Institute of Telecommunications of Aveiro, during the course of the work referred as [Per07]. This work is part of the VIDAS project.

From table 5 one thing is clear. One of the limitations for transmission data-rate will be the LED's maximum switching frequency. Although the amount of tested LED's is small, and not very diversified, it is safe to state that different building technologies, or color output, mean different behaviors. Even in LED's with the same color, the frequency values change, and comparing with the higher power LED's from OSRAM, it is clear that with higher currents the switching times are higher.

Table 5: LED's switching times measurements [Per07]

Manufacturer	Model	Colour	Frequency [MHz]	Switching [ns]	Max. I_F (DC) [mA]
OSRAM	LA W57B	Amber	3,1	114,5	400
	LY W57B	Yellow	4,1	85,3	400
	LV W5SG	Green	8,7	40,3	500
VISHAY	TLMK3100	Red	8,3	42,1	30
	TLCR5200		7,5	46,6	50
	TLCY5100	Yellow	5,9	59,4	50
	TLCY5200		8,0	43,5	50
	TLCTG5100	Green	6,5	53,5	30
	TLCTG5800		8,0	43,4	30
	TLCB5100	Blue	11,8	29,8	30
	TLCB5800		12,6	27,9	30
NICHIA	NSPW500BS	White	2,6	136,2	30

(For quick reference, the HB-LED's used in this project are grey shadowed)

III.iii Emitter topologies

There are several parameters that can influence the design topology of the emitter, but the basic principle consists on a digital signal that acts on the output driver, usually a power transistor, controlling the current flow through the array of HB-LED's. In the following subsections the emitter topologies are divided into three configuration groups according to the type of power supply or output driver used.

III.iii.i Alternating current topologies

When an alternating current (AC) power supply is used, the electrical connection of the HB-LED's greatly influences the optical efficiency of the emitter. Figure 14 shows the three possible configurations in which the HB-LED's can be connected, unilateral-AC, bilateral-AC and bilateral-AC with rectifying bridge. In these configurations, a modulated signal representing the digital information (V_{signal}) is used to enable current through the HB-LED's by controlling a power transistor like a digital switch [Per07].

The unilateral-AC configuration is easy to build, and the electrical grid can be used directly as the power supply. Nevertheless, it takes a high number of HB-LED's to achieve the voltage differential, and if a resistor is used, the power dissipation needs to be carefully calculated. Another disadvantage of this configuration is related to the electrical behavior of LED's, current will only flow through them on the half cycle when they are directly polarized, thus reducing the system's overall efficiency. Since data transmission requires a minimum level of voltage, the transmission window is even smaller than an half cycle, data packages need to be broken into these intervals which requires somewhat complex modulation and demodulation schemes. The bilateral-AC configuration can transmit in both of the voltage's half cycles, by using an array of HB-LED's and a transistor for each half cycle. Although it shows an increase in data-rate it also requires double the components. The bilateral-AC with bridge rectifier configuration uses the

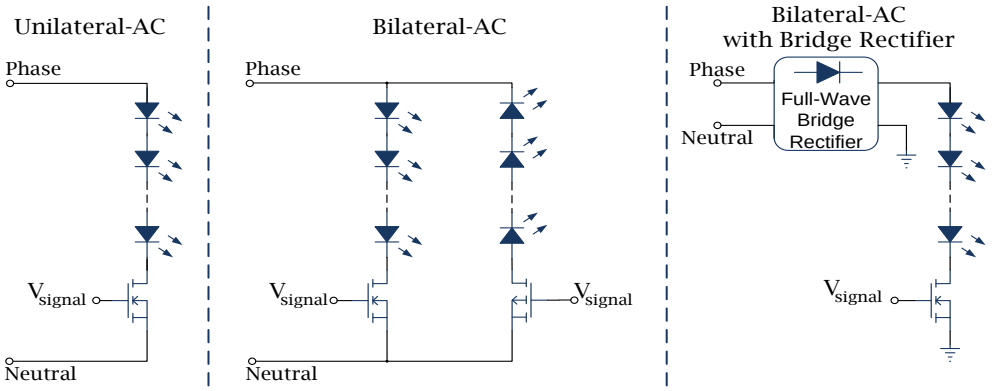

Figure 14: Emitter topologies for AC power supply

rectified voltage signal to directly polarize the HB-LED's in both of the half cycles. Therefore it only used a single array of HB-LED's and the respective transistor switch. By using the rectifier bridge the voltage peak value is decreased by about 1,4V.

III.iii.ii HB-LED driver topologies

After analyzing the previous configurations it seems clear that using direct current (DC) will result in higher efficiency with simpler modulation and demodulation schemes. It is not necessary to define transmission windows because the HB-LED's will always be directly polarized, and with the necessary current levels for data transmission. Also, by lowering the supply voltage the number of necessary HB-LED's to achieve the voltage differential is reduced. Therefore the main difference in DC topologies relies on the type of LED driver used. It is an obvious conclusion that these configurations require a dedicated DC power supply or an AC to DC converter. Given that there are plenty of commercially available and easy to implement solutions, it will be assumed that a DC power supply is available.

Recent development in HB-LED's has also led to the appearance of dedicated integrated circuits (IC's) for high-current HB-LED drivers. These devices are based in switching regulators which, on the contrary to linear regulators, can be configured in different arrangements providing voltage or current step-down (buck), step-up (boost) or both (buck-boost) functions. Switching regulators also improve the conversion efficiency, they interrupt the power flow while controlling the conversion duty-cycle to obtain the desired output voltage or current, but this causes a pulsating current that needs to be filtered by storage elements (capacitors and/or inductors). Another feature usually available in HB-LED's drivers is dimming capability and, although analogue dimming is easier to implement, digital dimming through pulse-width modulation (PWM) is used in most designs. This PWM signal is not to be confused with the PWM used in the DC to DC power conversion, and from now on will be referred to as on/off dimming.

The dimming capability emerges due to a fundamental characteristic of all LED's, the emitted light characteristics change with the drive current. With on/off dimming the drive current levels and the light characteristics can be maintained, and by varying the on/off dimming duty-cycle the light intensity output can be adjusted. For the human eye a small change in the correlated color temperature of white HB-LED's can easily be detect, as for monochromatic HB-LED's a change of a few nanometers is not so easily detected, and for any variation over 120Hz, the human eye averages the light output, not noticing any flickering from the on/off dimming [Nat09].

Although dimming techniques are used to control the output light levels, they might also be used for data transmission. Instead of a dimming control signal, a digital data signal with an OOK modulation can be used to control the light levels of the HB-LED, thus enabling data emission. However, using on/off diming would only work with very specific modulation techniques. Also, in order to keep the possibility of controlling the output light levels while transmitting data would require a much more complex device. For this work, only the data transmission capabilities are of interest. Therefore, the complexity of a device with both functions is unjustifiable at this early stage of development.

Standard switching regulators have soft-start and often a soft-shutdown in order to prevent sudden variations in start and shutdown currents, their design emphasizes low start and shutdown currents over response times. These protections work by creating a delay loop which increases the slew-up and slew-down times. On the contrary, HB-LED drivers with on/off dimming are built to minimize such delays by keeping their internal control circuits active even when the enable signal is set to disabled, also the regulator's topology is crucial to achieve higher dimming frequencies. The buck configuration is usually the fastest, this happens because it is the only one that delivers power to the output during the on-time of the power conversion cycle. By doing so it can be adapted to hysteretic control, which is faster than any of the best current-mode control loops. Also, the regulator's inductor is connected to the output during the entire power conversion cycle, ensuring a continuous output current, so the output capacitor can be eliminated making the buck regulator a true, high impedance current source, capable of slewing the output current very quickly. But even the fastest buck regulator without the output capacitor cannot achieve the on/off dimming frequencies that could be useful for data transmission in the VIDAS application. Limiting those frequencies are the delays present in turning the output current on and off, they appear from the propagation time in the regulator's IC and the physical properties of the output inductor. In order to bypass these delays, external circuitry is necessary [Nat09].

In figure 15 is represented a typical configuration of the LM3404 HB-LED driver, from National Semiconductor, capable of achieving high speed on/off dimming. Instead of using the dimming pin of the IC (Dim), a power switch is connected in parallel with the HB-LED array, in this case a field-effect transistor (FET) is used. In order to turn the HB-LED's off, the drive current is shunted through the switch while the regulator IC continues to operate and the inductor's current continue to flow. The main disadvantage is power waste when the HB-LED's are off, even though, in this interval, the output voltage drops to equal the current sense voltage at R_{sns}. Also, when dimming with a shunt FET,

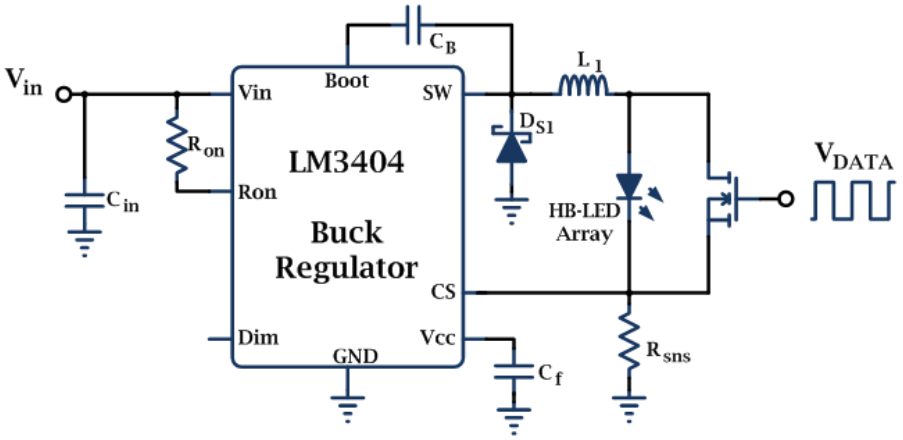

Figure 15: Buck regulator with shunt FET circuit

the output voltage will suffer rapid variations, to which the IC's control loop must respond even faster in order to keep a constant voltage output [Sar08].

After researching several HB-LED drivers, especially from National Semiconductor, one important aspect started to show. Although some of the IC's presented switching frequencies up to 8MHz (LM3519), the actual on/off dimming frequencies, which would enable data communication in a VIDAS application, never reached very convincing values. Devices with a power FET included have dimming frequencies around 25KHz, which leads to the conclusion that the best scenario will be achieved by using an external power FET. But in order to achieve up to 1MHz of dimming frequency, required for a 1Mbps signal with OOK modulation, would require even higher control switching frequencies in order to avoid aliasing in the conversion cycle and interference in the frequency range for data transmission. Additional filtering might also be necessary. All things considered, a VLC emitter with an HB-LED driver based in a switching regulator might become a viable solution when the requirements of such devices pull their performance up to higher frequencies. Also, if the IC's manufacturers where more aware to the VLC applications, an *"off-the-shelf"* device could easily be achieved, but for now a custom build discrete transistor solution is required.

III.iii.iii Discrete transistor topology

Discrete transistor topologies usually allow exploring faster switching frequencies, which is important to the current emitter application. Based in the work developed in [Per07] during the process of characterizing several LED's switching times, this topology achieves a higher transmission bandwidth in order to emit square pulses without distortion, the resulting circuit is represented in figure 16. Similar to the previous topologies, a digital signal (V_{data}) controls the equivalent Darlington transistor (Q) which enables or disables the current flow through the HB-LED. This was achieved by using a

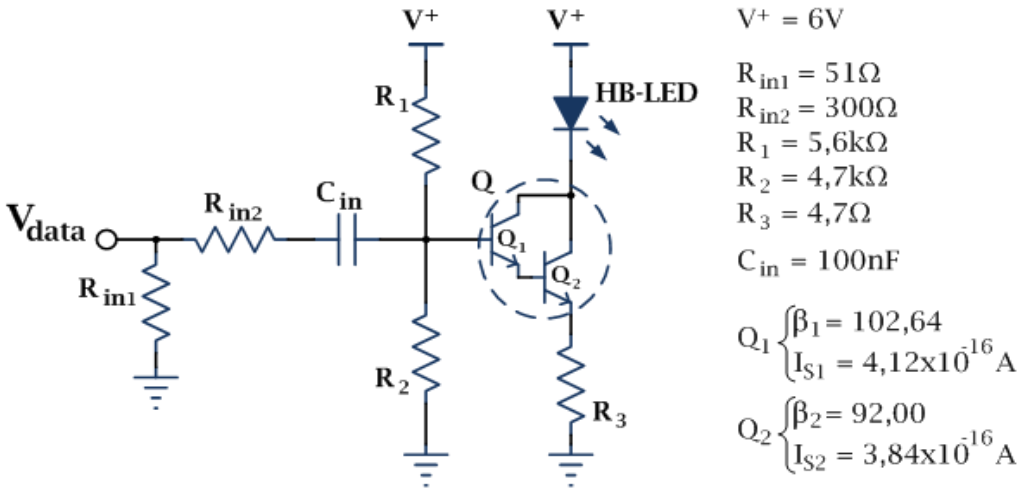

Figure 16: Discrete current-sink emitter topology

fast NPN transistor (Q_1 - BFR92A), followed by a power NPN transistor (Q_2 - BFG21W), in order to achieve a higher current gain with a large bandwidth. The resistors R_1 and R_2 set the operating point, R_{in1} and R_{in2} provide a matched input resistance of 50Ω and the input capacitor C_{in} provides DC signal blocking.

In a real VIDAS application scenario the traffic lights will need to work even if the data signal is disconnected, therefore setting the operating point of Q is very important. Considering the digital signal V_{data} varying between 0V and 3V, logic low and logic high respectively, the values for the current through the HB-LED (I_D) will switch between approximately 0A (cut-off region) and 400mA (active region). If V_{data} is disconnected the transistor will drive a steady current I_{Ddc}=200mA. These values were chosen in accordance with the HB-LED's maximum ratings, and although the color levels will be different, in a monochromatic HB-LED such difference is not easily noticed.

From the values taken from the devices datasheets, the base-emitter voltages (V_{BE}) can be calculated:

$$V_{BE1} = ln\left(\frac{\beta_1 \cdot I_{Ddc}}{(\beta_1+1)\cdot(\beta_2+1)\cdot I_{s1}}\right) \cdot V_T \; ; \qquad \textbf{(eq. 19)}$$

$$V_{BE2} = ln\left(\frac{\beta_2 \cdot I_{Ddc}}{(\beta_2+1)\cdot I_{s2}}\right) \cdot V_T ; \qquad \textbf{(eq. 20)}$$

$$V_{BE} = V_{BE1} + V_{BE2} \; . \qquad \textbf{(eq. 21)}$$

Replacing all known values gives, V_{BE1}=0,73V and V_{BE2}=0,73V, therefore V_{BE}=1,58V. With the value from equation 21, the base voltage of Q is given by:

$$V_B = V_{BE} + (I_{Ddc} \cdot R_3) \; , \qquad \textbf{(eq. 22)}$$

and in order to keep Q in the cut-off region when V_{data}=0V, the transistor's base-emitter junctions have to be reversely polarized, which means that V_B cannot go over 1,4V. The value of V_B, due to the effect of C_{in}, will have a DC component from the transistor's operating point in which the AC component from V_{data} will be centred. Neglecting the base current of Q and the effect of R_{in2}, when V_{data}=0V, V_B is approximately:

$$V_B = V_{CC} \cdot \frac{R_2}{R_1+R_2} - \frac{V_{data_{pp}}}{2}. \qquad \textbf{(eq. 23)}$$

Considering that this value has to be less than 1,4V and choosing R_1= 5,6KΩ, the value of R_2 has to be smaller than 5,2KΩ. As a safety margin to the approximations made, R_2= 4,7KΩ was selected. The remaining resistor R_3 can be obtained from equations 22 and 23 when V_{data} is disconnected:

$$V_{BE} + (I_{Ddc} \cdot R_3) = \left(V_{CC} \cdot \frac{R_2}{R_1+R_2}\right) - \frac{V_{data_{pp}}}{2}. \qquad \textbf{(eq. 24)}$$

In these conditions, replacing the previously obtained values results in R_3= 5,8Ω.

After some simulations and adjustments to the values of R_3 and R_{in2}, the simulation results presented in figure 17 and table 6, were obtained. The "a", "b" and "c" plots represent the current through the HB-LED for V_{data} frequencies of 100kHz, 1MHz and 10MHz respectively. Plot "d" represents the constant current that flows through the HB-LED when V_{data} is disconnected. The current values obtained are consistent with the projected values in a wide range of frequencies, without distortion. In figure 18 the frequency gain-phase response of the current amplifier (I_D/I_{Rin2}) is also presented, showing that the designed emitter has a large bandwidth, with a 3dB cut-off frequency of 84,92MHz and a steady gain of 52,45dB.

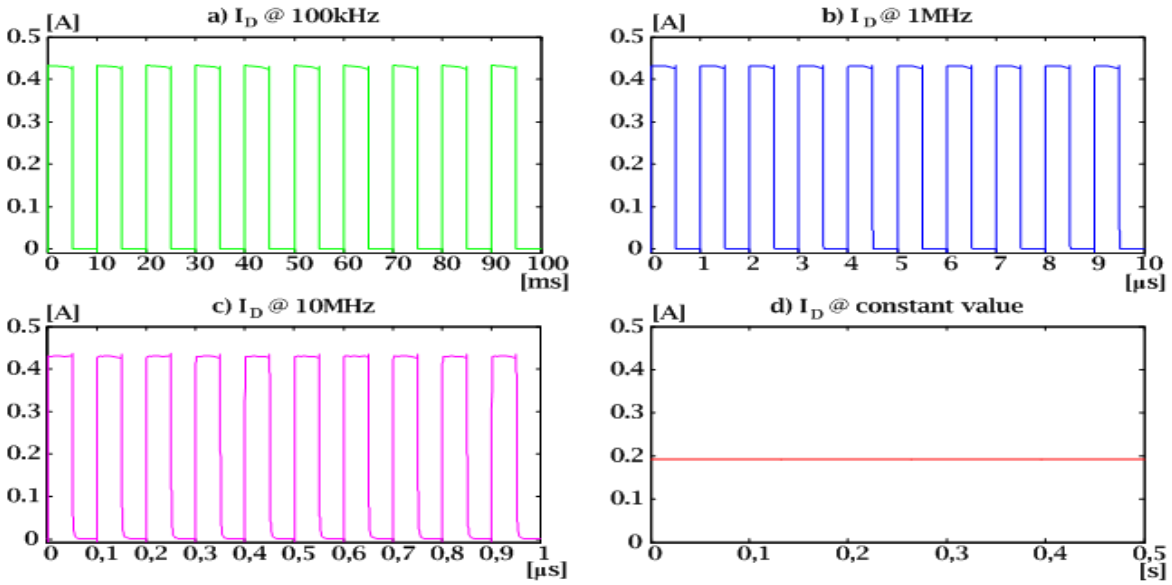

Figure 17: Emitter: time domain response at different frequencies

Table 6: Values of electrical current through the HB-LED

I_D @ f		a) @ 100kHz	b) @ 1MHz	c) @ 10MHz	d) constant value
V_{data}	logic high (3V)	433,1 mA	435,1 mA	437,8 mA	191,4 mA
	logic low (0V)	101,4 µA	124,6 µA	742,9 µA	

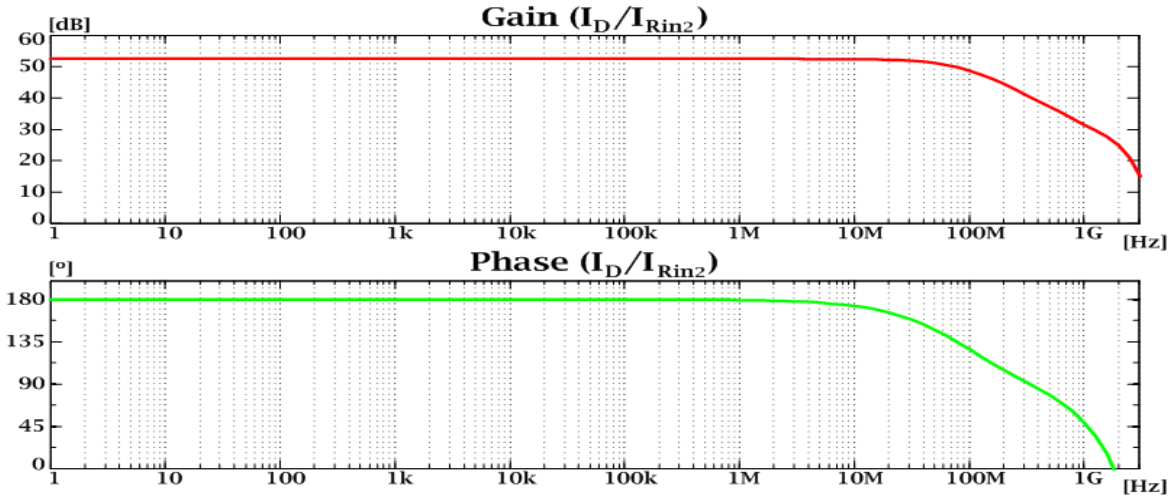

Figure 18: Emitter: gain/phase response (I_D/I_{Rin2})

The presented configuration is not very robust and even using a different color HB-LED may lead to adjustments in the circuit resistors. There is also no feedback controlling the output current, which makes it vulnerable to thermal runaway from the DC setting resistors, especially from resistor R_3. This component will have a particularly small value if a high current is to be achieved when using a small DC power supply voltage. Nevertheless, the topology from figure 13 is very easy to implement and allows for a wide range of adjustments. By selecting a current level under the maximum absolute rating of the HB-LED's, thermal runaway will not be a major source of problems. In the VIDAS application, small variations in the light characteristics will be acceptable, external noise sources such as weather conditions and other light sources will cause more interference in the perceived light characteristics than a variation in the forward current.

Another advantage of this configuration is the possibility of doing a partial simulation on PSpice, although the HB-LED's models only allow for steady-state simulations, the DC working point can be obtained. After obtaining the desired DC voltages, any change to the current sink can be simulated, transistors can be changed and a partial idea of the circuit behavior can be obtained, given that the models for the used transistors are available. This would not be possible if a commercial HB-LED driver was to be used, their models are not available and an equivalent would be hard to achieve, given that these are highly complex devices.

The studied configuration is simple and easy to implement, although it might need adjusting to a specific HB-LED, the process is relatively straightforward, making it a viable solution for studying the VLC emitters even further. In chapter V this study will be continued with the presentation of experimental values.

In order to measure the experimental values, an emitter prototype was necessary. It was built using surface mounted devices (SMD's) for their better performance at high frequencies. Stock resistors and capacitors were selected, and the OSRAM HB-LED's used were already available from previous works. As for the transistors a research had to be made. Given the required current levels, several Darlington transistors were considered, but the performance of the respective PSpice models showed a gain-bandwidth product (GBW) too small for the intended application. The alternative lied on using a Darlington configuration made from two independent transistors. For the input transistor a Phillips BFR92A NPN transistor was used, this is low-noise, 5GHz wideband transistor, suited for RF applications, and it can handle currents up to 25mA. It had already been used by the workgroup in previous prototypes with good results. For the second transistor a higher current handling was necessary, after some research the Philips BFG21W was chosen. The datasheet presents this component as a power transistor with an operating frequency up to 1,9GHz, high gain and a maximum current of 500mA, making it ideal for the second stage of the Darlington configuration, as previous simulation results confirmed.

Another characteristic of the emitter prototype was that the resistor R_3 was made from more than one resistor. An 1Ω resistor (R_4) was placed in series between R_3 and the ground connection. Thus, measuring the voltage drop at R_4 also gives in an indirect measurement of the current, which does not need any scale changing.

In the emitter prototype a ground plane was used on the bottom face along with several connection holes, also known as "vias", between the ground plane and ground islands on the top face. This technique ensures that a more reliable connection to the ground, or "0", voltage can be achieved, thus reducing noise interference in the circuit. This design also improves heat dissipation, and although the power transistor is not connected to the ground plane, the heat generated in such a small board will be easily transferred to the ground plane and islands. Also, several power-supply filtering capacitors were added to the prototype.

In conclusion…

There are several blocks that constitute the VLC emitter. However, this work is based on designing the power control, mixer and output driver. Another key component of the emitter is the LED. From the several devices researched, much information was found regarding optical and electrical characteristics. However, new information regarding switching behavior, which is of the most importance for this application, was hardly found. Therefore, the values presented in [Per07] served as a reference. From these values was clear to observe that HB-LED's have smaller switching frequencies than regular LED's. Even so, they are within the range for the required application.

As for the emitter topologies, several configurations can be used. AC topologies present, along with other implementation challenges, the necessity for complex modulation/demodulation schemes. On the other hand, DC topologies are easier to implement and do not require such complicated schemes. One of the possible solutions for implementing an emitter is to use one of the commercially available HB-LED drivers. However, these devices aren't intended for data transmission and using dimming techniques for data transmission is only possible with some modulation techniques, namely OOK. Therefore, the best solution to build the emitter is to use a discrete transistor topology. This can be roughly simulated in PSpice, thus helping the design process. The final solution found might not be very robust, but is easily adaptable and serves the required purposes.

Chapter IV

Receiver Design

The VLC receiver is an optic-electronic transducer that receives information, previously modulated in the visible light spectrum, and converts it into an electrical signal capable of being processed by a demodulator-decoder. The correct design of this device is crucial to ensure good performance of the overall VLC system. Among other concerning factors are the presence of low-level signals and high noise interference.

This chapter is organized into the following three subsections. In IV.i the receiver's basic definition is presented through its main building blocks. In subsection IV.ii the adequate photodiode devices are analyzed, and typical optical and electrical values presented. Finally, in subsection IV.iii the different modules of the receiver are analyzed and different preamplifier topologies presented and discussed.

IV.i Receiver description

Going back into the history of VLC, the system's receiver is usually the most complex. In his *photophone* Alexander G. Bell used a parabolic mirror in order to capture and concentrate the light beams into photoconductive selenium cells placed at the focal point, but the result of this configuration was only a faint signal [Bel81]. The ancient Greeks might have used a simple light reflector as an emitter, but in order to receive the information they had to use a very complex, and hard to replicate device, the human eye.

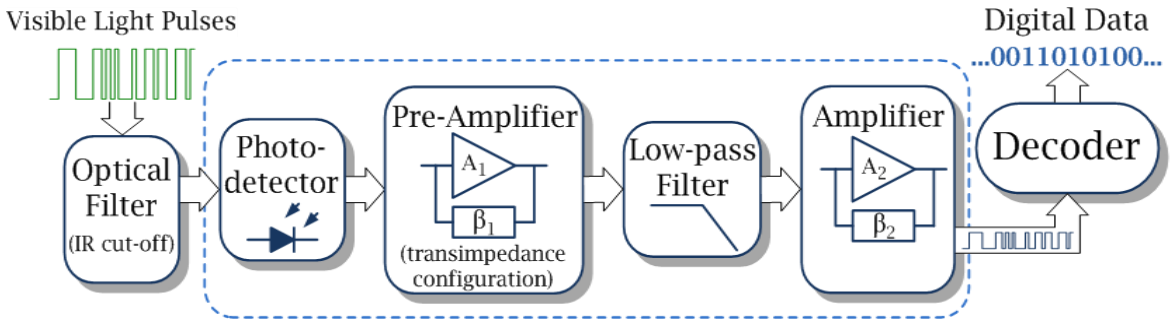

Figure 19: VLC receiver block diagram

In the VIDAS application, the receiver uses a photodiode in order to convert visible light into an electrical signal. Given the application scenario, this solution will be constantly subjected to several external noise sources as discussed in II.iv.i. Also, the typical signals generated at the photodiode are low-level currents, this leads to the necessity of several amplifying and filtering stages.

The main building blocks for a VLC receiver are represented in figure 19. The visible light pulses, originated at the system's emitter, are collected in the photo-detector, an optical IR cut-off filter is a viable solution for eliminating unwanted spectral content, but this is an optional component solution and will not be used in this project. Reversely biased the photodiode operates in the photoconductive mode generating a current proportional to the collected light. This current is of a small value and a preamplifier is used to convert it into a voltage. This preamplifier should have low distortion and a large GBW. The resulting voltage is then applied to a low-pass filter to remove any high-frequency noise. The resulting voltage signal is then further amplified in the final voltage amplifier stage. Also, DC signal filtering is applied at the input of the amplifying and filtering stages, which helps reduce the DC noise component of the captured signal as well as low-frequency components. The final voltage signal should correspond to the received light pulses which are then decoded in the final decoder block, thus extracting the digital data. This final block performs the inverse function of the emitter's encoder block, but it can also be implemented with a microprocessor or, even better, an FPGA.

As expected, similarly to what happens with the VLC emitter, there is no appropriate *"of-the-shelf"* solution that can be easily adapted to the VIDAS application. In fact, the design of the receiver presents several challenges that need to be addressed in order to achieve a better system performance. In subsection IV.ii the photodiode devices will be analyzed. Making the correct choice involves analyzing both the device's active area as well as the junction capacitance. Device simulation is also an issue as there are no available PSpice photodiode models for the commercially available devices.

The preamplifier block being probably the most critical in the entire receiver, a study on the effect of the photodiode's junction capacitance at the input of this stage will be addressed in subsection IV.iii.i. Also, three variations of the transimpedance feedback topology used will be compared. From this study the necessity for a low-pass filter appeared, and with the help of free software, a multiple feedback topology was dimensioned, and further simulated with PSpice. The final voltage amplifier was studied in a final stage of the design process in order to improve the overall performance of the VLC receiver.

IV.ii Photodiodes for VLC

A photodiode is a semiconductor junction diode that has been optimized for visible, ultraviolet or IR detection. In the most common mode of operation, and also the one used in this work, the diode is reverse-biased. In this case, and in the absence of light the current is very small (dark current). In a normal diode the photons from the incoming radiation cause hole-electron pairs to be formed and a current can flow, which can be shown to be proportional to radiation power [RP2web]. In order to increase the active volume for hole-electron pair production, a suitably doped layer can be added between the p+ and n- regions. This layer, if the doping is correct, can behave as an intrinsic (i. e., undoped) layer, giving rise to what is called a P-intrinsic-N diode, or PIN diode [Ham03, RP1web]. PIN photodiodes are extensively used for light-detection applications, as efficiency is increased and at the same time, due to the increase in thickness of the depletion layer, diode capacitance is reduced. This type of photodiode, when associated with a high-speed preamplifier, can achieve large bandwidth and lower noise, using only a small bias voltage [Ham03].

Photodiodes can also be operated in the photovoltaic mode, that is, in the forward-conducting region of operation. Normally the device is zero biased, and, similarly to what happens in a solar cell, when illuminated the photodiode generates a voltage at its terminals. This has a linear dependence on incident light. However both dynamic range and switching speed are severely limited, so photodiodes are not usually operated in this mode in communication applications. Due to the presence of the "intrinsic" layer, PIN diodes cannot be used in the photovoltaic mode [RP2web].

The photoconductive mode occurs if the device is reversely biased. When illuminated an electrical current (photocurrent) flows through it. This current has a linear dependence over several orders of magnitude on the incident light intensity. A PIN photodiode can maintain a linear response for an input light power of a few nanowatts up to tens of milliwatts. Although a higher reverse voltage does not influence the induced

photocurrent, it reduces the device's junction capacitance allowing for faster switching times [Ham03].

The dark current is the current that flows through the photodiode when operated in the photoconductive mode with no incident light. It represents an important source of noise for photoconductive applications, namely fiber-optic communications, and choosing a device with a small dark current is advisable [Ham03]. However, for free-space optical communications, the levels of the input signal and background lighting illumination easily overlap the effect of the dark current.

Similar to LED's, photodiode's characteristics can be divided into to two different groups, electrical characteristics and optical characteristics. Upon research of several datasheets, the most common are:

- Optical characteristics:
  - → Spectral sensitivity range:
    - Wavelength at which the sensitivity falls under 10% $(\lambda_{min}, \lambda_{max})$;
    - Wavelength of maximum sensitivity (λ_{peak});
  - → Active area (A_{PD});
  - → Half-Angle (φ_{PD});
- Electrical characteristics:
  - → Spectral sensitivity at λ_{peak} (S_λ);
  - → Dark current (I_{dark}) at a given reverse voltage (V_R);
  - → Junction capacitance (C_{PD}) at a given reverse voltage (V_R);
  - → Photocurrent switching times (t_{sw} or f_{sw}).

From the different types of materials used to manufacture PIN photodiodes, Si presents the most adequate spectral sensitivity with a range that goes from 190nm up to 1100nm. This range gives manufacturers the ability to adapt their devices spectral sensitivity within the visible plus near-IR interval of the electromagnetic spectrum. By using a filtering coat over the photosensitive cell the resulting spectral sensitivity can be shaped to any desired interval. Two examples of this technique are the Hamamatsu S3204-09 and the Sharp BS100C. These Si photodiodes have a λ_{max} of 730nm and 750nm respectively, thus cutting the undesired near-IR radiation. Although they might be a possible low-cost alternative to an optical filter, they also present a high junction capacitance and dark current which does not makes them that a good solution for the desired application. These results as well as the optical and electrical characteristics of several Si photodiodes analyzed are presented in tables 7 and 8.

Table 7: Si photodiodes optical characteristics

Manufacturer	Model	Spectral Sensitivity Range λ_{min} [nm]	λ_{max} [nm]	λ_{peak} [nm]	A_{PD}	[mm^2]	φ_{PD} [º]
EG&G VACTEC	VTH2091	400	1100	960	9,2x9,2 =	84,64	--
HAMAMATSU	S1133	320	730	560	2,8x2,4 =	6,7	--
	S3204-09	320	1100	960	18x18 =	324,0	--
KODENSHI	SP-101	450	1050	880	π x(3/2)^2 =	7,1	50
	SP-1CL3	450	1050	900	π x(3/2)^2 =	7,1	50
	SP-1KL	450	1050	900	π x(4,65/2)^2 =	17,0	15
OSRAM	BP 104S	400	1100	850	2,2x2,2 =	4,8	60
	BPW 34B	350	1100	850	2,7x2,7 =	7,3	60
	BPW 34S	400	1100	850	2,7x2,7 =	7,3	60
SHARP	BS100C	400	750	560	2,9x4,3 =	12,5	--

(For quick reference, the photodiodes used in this project are grey shadowed)

Table 8: Si photodiodes electrical characteristics

Manufacturer	Model	S_λ @ λ_{peak} [A/W]	I_{dark} @ V_R [pA]	C_{PD} @ V_R [pF]	t_{SW} [µs]	f_{SW} [MHz]
EG&G VACTEC	VTH2091	0,60	5.000 @ 30V	120 @ 12V	15.000	-
HAMAMATSU	S1133	0,30	10 @ 1V	700 @ 0V	2,5	-
	S3204-09	0,66	6.000 @ 70V	130 @70V	-	20
KODENSHI	SP-101	-	500.000 @ 5V	17 @ 0V	-	-
	SP-1CL3	-	500.000 @ 5V	50@ 0V	-	-
	SP-1KL	-	100.000 @ 5V	50@ 0V	-	-
OSRAM	BP 104S	0,62	2,00 @10V	48 @ 0V	20.000	-
	BPW 34B	0,20	2,00 @10V	72 @ 0V	25.000	-
	BPW 34S	0,62	2,00 @10V	72 @ 0V	20.000	-
SHARP	BS100C	-	3 @ 1V	500 @0V	200	-

(For quick reference, the photodiodes used in this project are grey shadowed)

Upon analyzing these results it is clear that, except for the filtered photodiodes, the spectral sensitivity range is very similar. Also, a higher active area, which is important to achieve a higher SNR, does not mean a better solution. Keeping in mind that the junction capacitance (C_{PD}) decreases with the increase of the reverse voltage applied (V_R) it is necessary to find a balance between a large active area and a small C_{PD} capacitance. Another consideration to be made is the value of the dark current (I_{dark}), a smaller value comes at the cost of a smaller active area. Given that a reverse voltage is to be used in order to decrease the junction capacitance (C_{PD}), the variation of I_{dark} with V_R must be taken into account in order to keep the associated noise to a minimum. All factors considered, the EG&G Vactec VTH2091 and the OSRAM BPW34S are two balanced solutions, with the first having a larger active area and the second a smaller junction capacitance, with small dark currents.

After choosing an appropriate photodiode, it would be productive if they could be integrated into the PSpice simulations, but the PSpice models for photodiodes are not

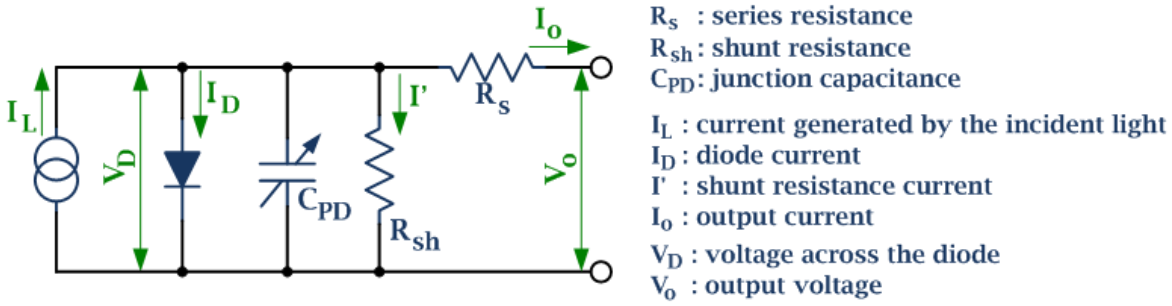

Figure 20: Photodiode electrical equivalent model [Ham03]

defined and the equivalents are not provided by manufacturers. It is then necessary to create an electrical equivalent model of the photodiodes from the available parameters. In the technical document from Hamamatsu [Ham03], the equivalent model shown in figure 20 is presented.

From the same source, a simplification to the currents relations can be obtained. The output current is given by:

$$I_o = I_L - I_D - I'. \qquad \textbf{(eq. 25)}$$

The resistor R_s is usually just a couple of ohms as R_{sh} reaches from 10^7 up to 10^{11} ohms, which makes them negligible over a width range. Neglecting the current through the diode, the input photodiode can be modeled by a current source with a capacitor in parallel [Ham03]. Although the result is not a very accurate model, it suffices in analyzing the effect of C_{PD} on the input preamplifier, during the linear range of the photodiode.

IV.iii Receiver modules

In this subsection the different modules that make the receiver are analyzed, although they are analyzed independently, the design is oriented towards the final application, in which the several modules are integrated in a single device. From the datasheets analyzed in IV.ii, the capacitance values for the two chosen photodiodes at a reverse voltage of approximately 6V are:

- EG&G Vactec – VTH 2091: $\boldsymbol{C_{PD}}$**= 180pF @** $\boldsymbol{V_R}$ **= 6V**;
- OSRAM – BPW34S: $\boldsymbol{C_{PD}}$**= 22pF @** $\boldsymbol{V_R}$**= 6V**

IV.iii.i Pre-Amplifier behavior

The preamplifier module is of critical importance to the receiver overall performance. Therefore, choosing a correct amplifier topology is essential. The biggest challenge in a front-end amplifier design is to achieve a high-gain, stable configuration

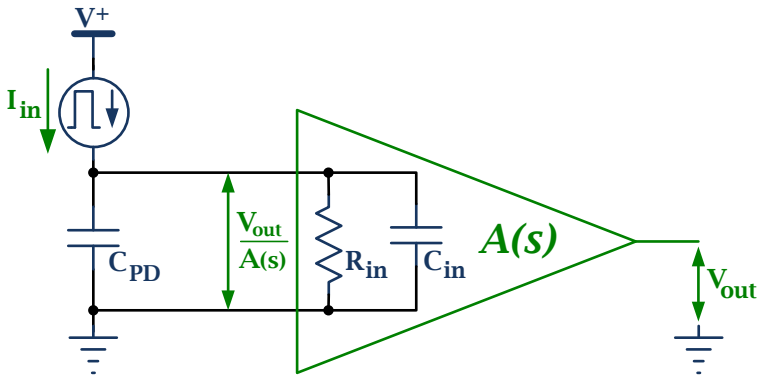

Figure 21: Simplified small signal input stage

with a large bandwidth. These conditions become hard to achieve mostly due to limitations imposed on the GBW by the input circuitry.

Figure 21 shows a simplified small signal equivalent model of the front-end input stage. Although the photodiode is more complex than the one illustrated, in a design perspective it can be represented by a current source (I_{in} – converted photocurrent) and a capacitance (C_{PD} – photodiode junction capacitance). As for the amplifier, and for demonstration purposes, a first order parallel association of a resistance (R_{in}) and a capacitance (C_{in}) is considered. Also, an ideal amplifier output resistance of 0 ohms is considered.

Considering only the amplifier, its gain response is given by:

$$A(s) = \frac{A_0}{1+\frac{s}{\omega_0}}, \text{ and } (\, s = j \cdot \omega \,) \qquad \textbf{(eq. 26)}$$

where, ω_0 is the cut-off frequency imposed by the time constant ($1/\, R_i \cdot C_i$), and A_0 is the gain of the amplifier.

The asymptotical gain response of the amplifier is represented in figure 22. From the GBW relation, the unitary gain frequency ω_t is equal to ($\omega_0 \times A_0$). This result can be obtained from equation 26 by replacing "s" with "$j \cdot \omega$", $A(s)$ with the value 1 and solving in order to "ω".

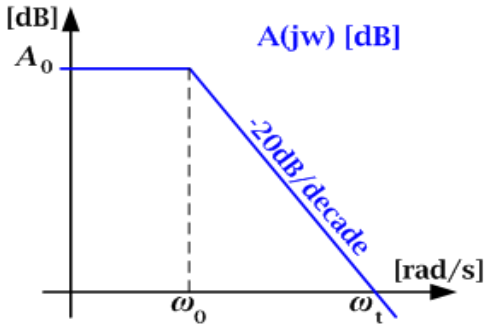

Figure 22: Bode asymptotical gain plot for a first order amplifier

In figure 21, the input capacitances are placed in parallel and can be represented as a single capacitance (C_t):

$$C_t = C_{PD} + C_{in} \ . \qquad \textbf{(eq. 27)}$$

This way, the pole contribution of the input circuitry is determined by the time constant ($1/ R_i \cdot C_t$). Assuming that the amplifier can be designed so that the other poles have much smaller associated time constants, the input circuitry will impose the dominant time constant [Alv08]. Therefore, and in order to achieve a high bandwidth, the input time constant should be minimized. There are two possibilities to achieve this, reducing the input capacitance or reducing the front-end input impedance. The first possibility is achieved by reducing the intrinsic photodiode capacitance, but usually means using a smaller area photodiode which is not always suitable for the required application. Therefore the second possibility is usually preferred. By using a correct amplifier configuration, the input impedance can be reduced without having a significant effect on the global device performance. The transimpedance amplifier better suits the intended application. It presents the required current to voltage transfer characteristic and can be achieved by using a feedback configuration. In the overall, transimpedance amplifiers represent the best compromise between gain and bandwidth [Alv08].

From figure 21, the transimpedance gain is given by:

$$\frac{V_{out}}{A(s)} = I_{in}.Z_{in}(s) \ , \qquad \textbf{(eq. 28)}$$

where Z_{in} is the equivalent parallel impedance of resistor R_{in} and capacitance C_t. It is given by the following equation:

$$Z_{in}(s) = \frac{R_{in}}{1+s\cdot R_{in}\cdot C_t} \ . \qquad \textbf{(eq. 29)}$$

Replacing equations 26 and 29 in equation 30 results in:

$$\frac{V_{out}}{I_{in}}(s) = A_T(s) = \frac{A_0\cdot R_{in}}{\left(1+\frac{s}{\omega_0}\right)\cdot(1+s\cdot R_{in}\cdot C_t)} \ . \qquad \textbf{(eq. 30)}$$

This equation represents a two pole transfer function, and assuming that $\omega_0 \gg (1 \ / \ R_{in} \cdot C_t)$, the respective Bode asymptotic gain/phase response is represented in figure 23.

Established feedback theory has it that if the phase delay of the amplifier is less than π at the frequency where the loop gain, $A(s)$, is equal to unity, the amplifier is stable. In practice, some phase margin, e. g. 45º, must be guaranteed.

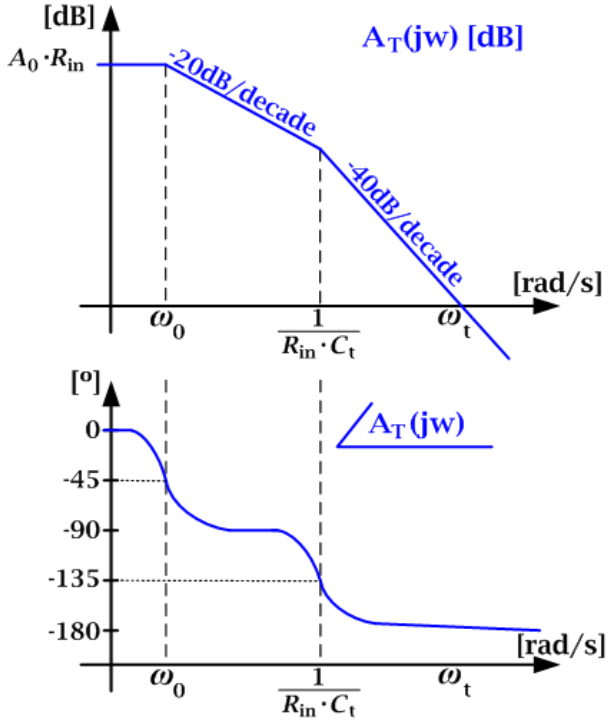

Figure 23: Bode asymptotical gain/phase plot of a second order amplifier

The usual choice for stability design is the Bode criterion. It states that, when the $A(s)$ and the $1/\beta(s)$ curves are drawn on the same (logarithmic) graph, at the point of intersection where $A(s) \times \beta(s) = 1$, or $A(s) = 1/\beta(s)$, the difference in the slopes of the two curves must be at most 20dB/decade. This has been amply justified in the literature and studied over the years.

In this case, a transimpedance configuration in the shunt-shunt feedback topology, represented in figure 24, is used. The feedback impedance (Z_F) is composed of a resistor (R_F) in parallel with a capacitor (C_F).

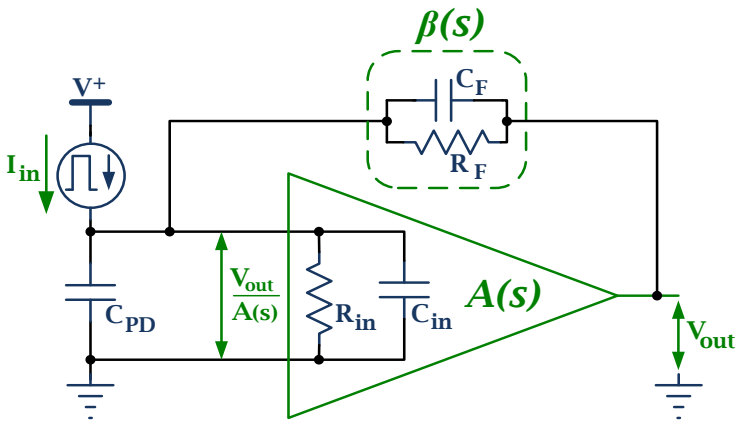

Figure 24: Transimpedance amplifier in a shunt-shunt feedback topology

The open loop gain is, in this case, the transimpedance of the proper amplifier, which is $A_T(s)$. As for $1/\beta(s)$:

$$\frac{1}{\beta(s)} = \frac{R_F}{1+s \cdot R_F \cdot C_F} . \qquad \textbf{(eq. 31)}$$

When the curves of $A_T(s)$ and $1/\beta(s)$ are drawn on the same coordinates, the graphic from figure is obtained.

One can see at once that in order for the preamplifier to be stable for any value of R_F, the knee frequency of $1/\beta(s)$ must be less or equal than the highest frequency pole of the amplifier. Therefore the following condition should be met:

$$R_F \cdot C_F \leq R_{in} \cdot C_t . \qquad \textbf{(eq. 32)}$$

An approximation to the transimpedance gain of the amplifier can be obtained from analyzing the circuit from figure 24. For the medium-frequency range, if the effect of R_{in} can be neglected, the steady transimpedance gain will be approximately the value of R_F.

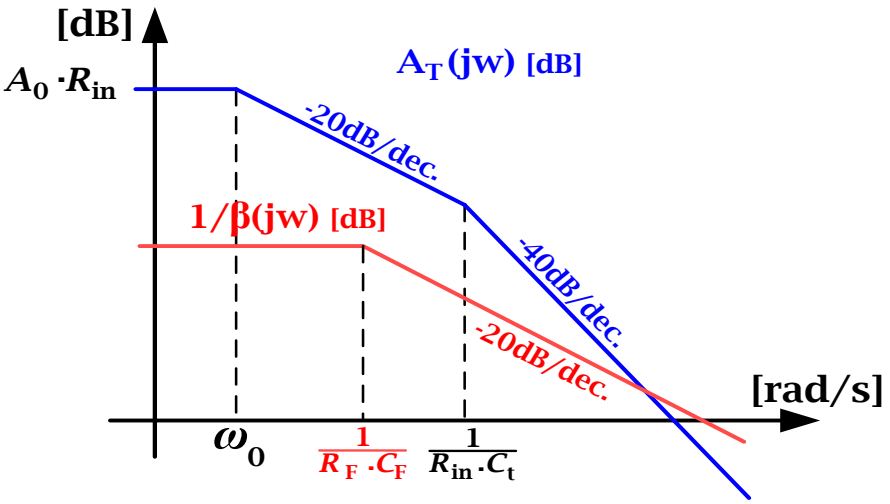

Figure 25: Bode plot with the intersection of the $A_T(s)$ and $1/\beta(s)$ curves

IV.iii.ii Pre-Amplifier configurations

Upon analyzing the expected general behavior of the preamplifier and the recommended configurations, three variations of the implemented transimpedance topology are presented. The configuration used is a discrete topology that has been tested for many years, yet it is adaptable to a wide range of applications.

The simulations of all three variations of the preamplifier topologies were made with the prototyping and experimental characterization process in mind. In order to correctly characterize the devices a 50Ω matched input resistance is required. Also, the input signal will be a voltage source that needs to be converted into a current. These conditions were satisfied by placing a 51Ω resistor in parallel with the input while a 10kΩ is placed in series, similar to what was done in the emitter's simulation.

Given the influence of the photodiode's junction capacitance on the preamplifier gain/phase response, an equivalent capacitor will be used in the following configurations. The equivalent capacitance of the OSRAM BPW34S photodiode will be used. For a 6V reverse voltage it is expected to be 22pF.

Figure 26 presents the first version of the preamplifier topology implemented, like what was said before, the resistor R_{in1} and R_{in2} provide a 50Ω adapted input, and conversion of the source voltage (V_S) into a current. The photodiode's junction capacitance (C_{PD}) is placed at the input of the preamplifier just before the coupling capacitor (C_{coup}) and the biasing resistor (R_{bias}) . By setting the correct operation points of transistors Q_1 and Q_2 they will operate similar to a current mirror. When the base voltage of the NPN Q_1 transistor (BFR92A) rises or falls, the transistor will sink more or less

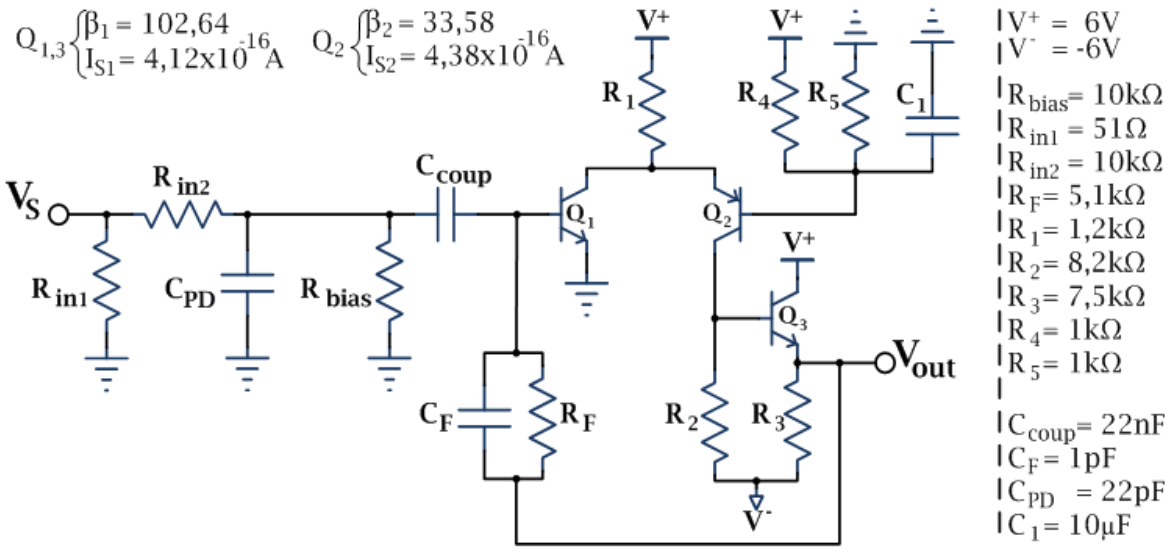

Figure 26: Preamplifier version 1

current, decreasing or increasing the current flow through the PNP Q_2 transistor (BFT92), choosing balanced transistors is important to ensure a symmetric current flow. Resistor R_1 sets the total current that flows through both transistors, which should be equally divided in order to get a better response from this first stage. Resistors R_4 and R_5 polarize transistor Q_2 while the C_1 capacitance ensures a virtual ground at the base of Q_2. The second stage of the preamplifier is made by transistor Q_3 whose operation point is set by the R_2 and R_3 resistors. Resistor R_2 also sets the value of steady current through Q_2. The R_F resistor and the C_F capacitor make the feedback loop. In this transimpedance configuration, the value of transimpedance gain is approximately the same of R_F. In order to compensate some overshoot in the preamplifier's gain/phase response, a low value C_F capacitor is used.

Considering an equal current of 1mA to polarize both Q_1 and Q_2 transistors, the current through R_1 will be 2mA. From Kirchhoff's laws the following equations are obtained:

$$V_{C1} = V^+ - R_1 \cdot I_{R1}, \quad \textbf{(eq. 33)}$$

$$\frac{V_{B2}}{R_5} = \frac{V^+ - V_{B2}}{R_4} + I_{B2}. \quad \textbf{(eq. 34)}$$

From the current relations in Q_2, the base current I_{B2} is given by:

$$I_{B2} = \frac{I_{E2}}{\beta_2 + 1}, \quad \textbf{(eq. 35)}$$

replacing the value I_{E2} and β_2 by 1mA and 33,58 respectively, the base current is I_{B2} = 28,92µA. Neglecting this small current value in equation 34 and setting V_2 in 3V, the resistors R_4 and R_5 become equal, and R_4=R_5=1kΩ was chosen.

The (V_{EB2}) voltage can be expressed by two equations:

$$V_{EB2} = ln\left(\frac{I_{E2} \cdot \beta_2}{I_{S2} \cdot (\beta_2 + 1)}\right), \text{ and} \quad \textbf{(eq. 36)}$$

$$V_{EB2} = V^+ - R_1 \cdot I_{R1} - \left(\frac{V^+ \cdot R_5 + I_{E2} \cdot (R_4 \cdot R_5)}{R_4 + R_5}\right). \quad \textbf{(eq. 37)}$$

Combining equations 36 and 37, and replacing all known values, the resistor R_1 is 1,14kΩ, approximating to the closest available value R_1=1,2kΩ.

The remainder of resistors will be dependent on the feedback loop, which influences the circuit behavior keeping the transistors in their active region. Given that the feedback current is the base current of Q_1 and has a negligible value, the output voltage will be approximately the base-emitter voltage of Q_1. This can be approximated by

0,7V, such as the base-emitter voltage of Q_3. Therefore an approximation to the value of R_2 is given by:

$$R_2 = \left(\frac{(2 \cdot V_{BE}) - V^-}{I_{E2}}\right), \quad \textbf{(eq. 38)}$$

resulting in R_2=7,4kΩ, a value that was adjusted through simulation. Finally, if a similar current of 1mA is used to polarize the Q_3 transistor, the value of the R_3 resistor is also set at a few kilo-ohms. Through simulation, a value of 7,5kΩ was achieved.

Upon adjusting the remaining biasing resistors that led to the circuit values of figure 26 and with a photodiode capacitance of 22pF, the effect of the R_F resistor on the GBW of the preamplifier was tested. The low (f_L) and high (f_H) cut-off frequencies as well as the steady gain are registered in table 9. Figure 27 contains the corresponding plots of the gain/phase responses.

For the desired application a 1MHz signal frequency is required. In order to guarantee a proper response of the implemented topologies a minimum of 10MHz should be considered for the high cut-off frequency. Parasitic components not taken into account in the simulation, but present in the prototypes may reduce significantly the available bandwidth, so with a higher value projected it is expected that the preamplifier will still be able to operate correctly at the frequencies of the received signals.

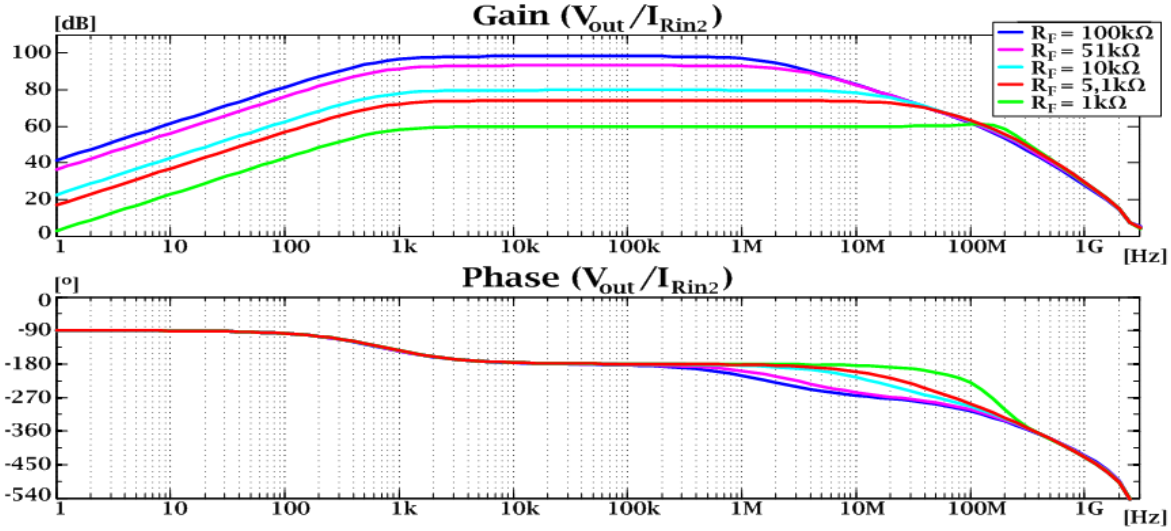

Figure 27: Preamplifier version 1: gain/phase response (V_{out}/I_{Rin2}) for different R_F values

Table 9: Preamplifier version 1: gain/phase results (V_{out}/I_{Rin2}) for different R_F values

R_F [kΩ]	f_L [Hz]	f_H [MHz]	Gain [dB]
1	992,44	205,15	59,93
5,1	731,92	33,21	74,01
10	730,53	15,70	79,78
51	719,00	3,11	93,23
100	705,28	1,71	98,29

The gain/phase response of R_F =5,1kΩ is adequate to the desired application. With a low cut-off frequency of 731,92Hz the effect of low-frequency noise from external light sources is minimized, also, it has a high cut-off frequency of 33,21MHz, and steady gain of 74,01dB, which corresponds to the expected transimpedance of 5,02kΩ.

With this study, the values of the preamplifier's components are set. It is now possible to observe the effect of the input capacitor C_{PD} by observing the gain/phase response of the preamplifier for different capacitances. Figure 28 and table 10 show the simulation results.

As expected, from subsection IV.iii.i, increasing the photodiode's junction capacitance reduces the available bandwidth, while the gain maintains a relatively stable value. This supports the claim that the photodiode's junction capacitance creates a pole that, although not having a dominant effect, greatly influences the high cut-off frequency. This way it can become a major limitation for exploring higher frequencies [Agu99, Alv08]. Also from these results, it is safe to say that the preamplifier will have a satisfactory response even with photodiode's with capacitances nearing, but under, the 1000pF. This result is particularly important in order to attain an idea as to which photodiode to use.

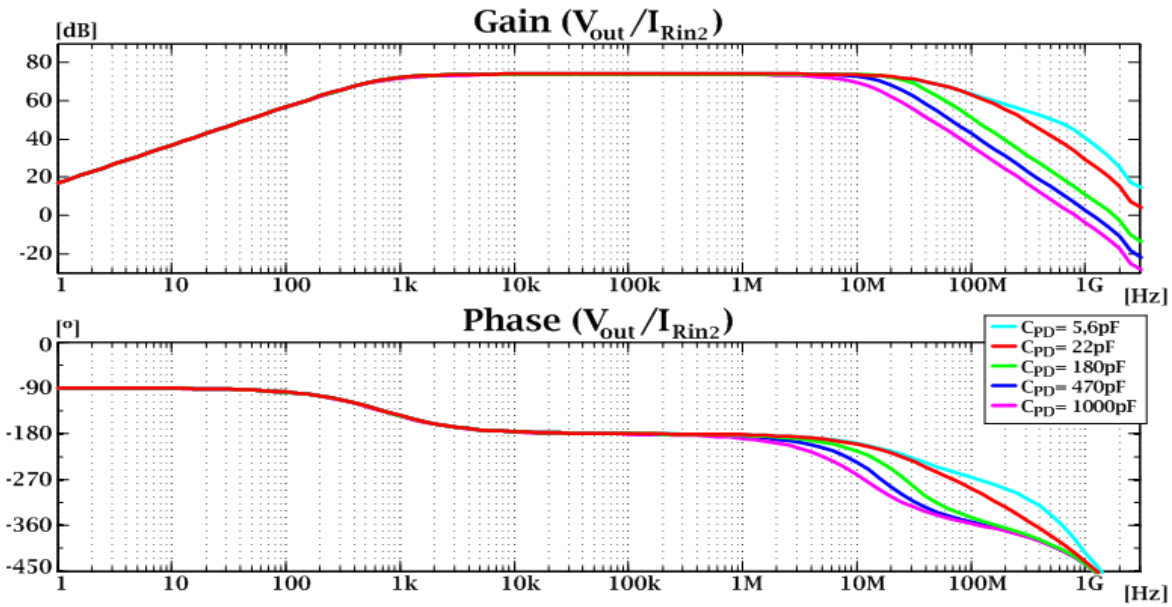

Figure 28: Preamplifier version 1: gain/phase response (V_{out}/I_{Rin2}) for different C_{PD} values

Table 10: Preamplifier version 1: gain/phase results (V_{out}/I_{Rin2}) for different C_{PD} values

C_{PD} [pF]	f_L [Hz]	f_H [MHz]	Gain @ 100kHz [dB]
5,6	732,43	31,80	74,02
22,0	731,92	33,21	74,01
180,0	726,95	25,61	73,95
470,0	717,92	15,19	73,84
1000,0	701,26	8,44	73,64

As was shown previously, in subsection IV.ii, photodiodes with larger active areas have higher capacitances. However, these devices also capture and convert more optical power into photocurrent, which means that the output signal is increased. Therefore, by choosing a photodiode with a large active area and a junction capacitance under 400pF, just to have a safety margin, the overall system performance can be improved.

The gain/phase response from figure 28 also shows that for frequencies above the hundreds of megahertz, there is still a positive gain, which could lead to high-frequency noise components to be amplified, and it would be convenient to reduce the attenuation at such frequencies. It is therefore advisable the study of a low-pass filter to be placed after the preamplifier.

For a quick practical reference, the red and green plots, of the 22pF and 180pF respectively, correspond to the junction capacitances of the OSRAM BPW34S and the EG&G Vactec VTH2091 with a reverse voltage of 6V.

There were two more configurations of the preamplifier topology which were analyzed. The second version, represented in figure 29, uses a *bootstrap* capacitor breaking resistor R_2 resistor and creating a feedback loop on the second stage of the preamplifier at transistor Q_3. The gain/phase response is shown in figure 30.

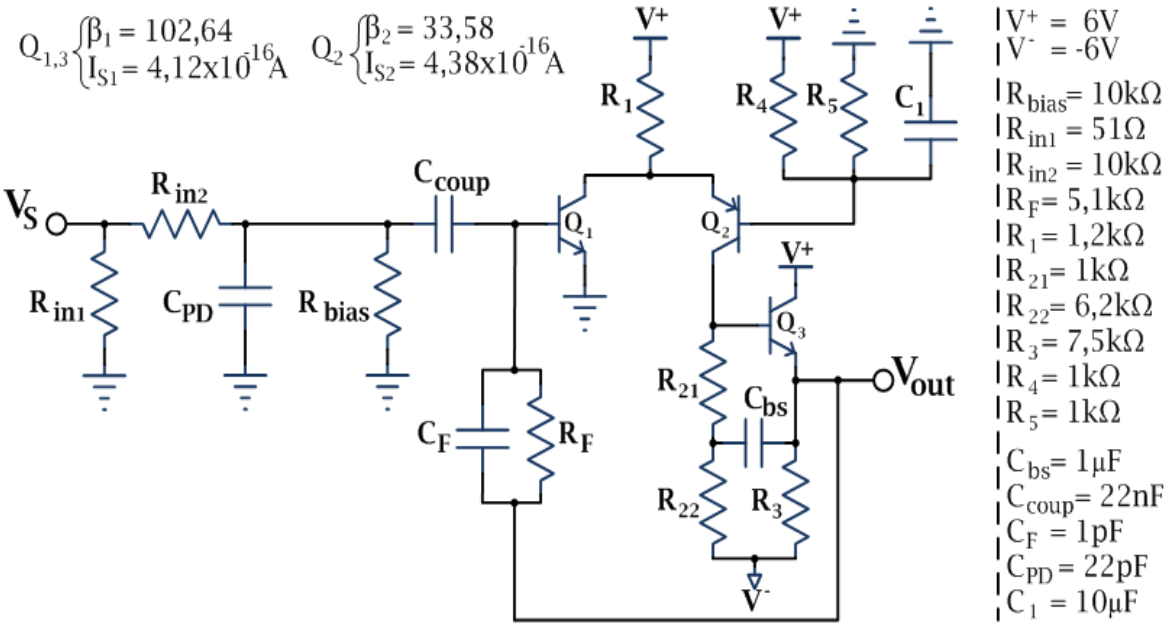

Figure 29: Preamplifier version 2

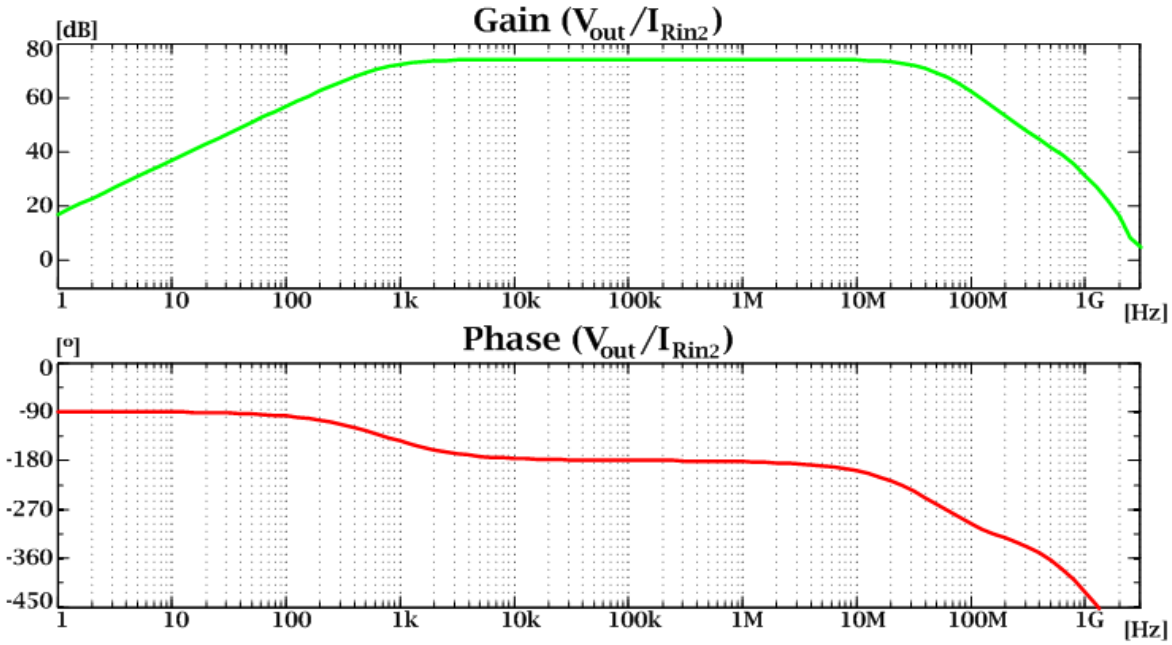

Figure 30: Preamplifier version 2: gain/phase response (V_{out}/I_{Rin2})

The third configuration, represented in figure 31, uses a current source to bias transistor Q_2. By using a transistor, a more stable and reliable current can be guaranteed. Neglecting the base current in transistor Q_3, the collector currents I_{C2} and I_{C4} both have the same value of 1mA. Therefore, the values of resistors R_{B1}, and R_{B2} are easily obtained from the current relations in transistor Q_4. The gain/phase response of this preamplifier is represented in figure 32.

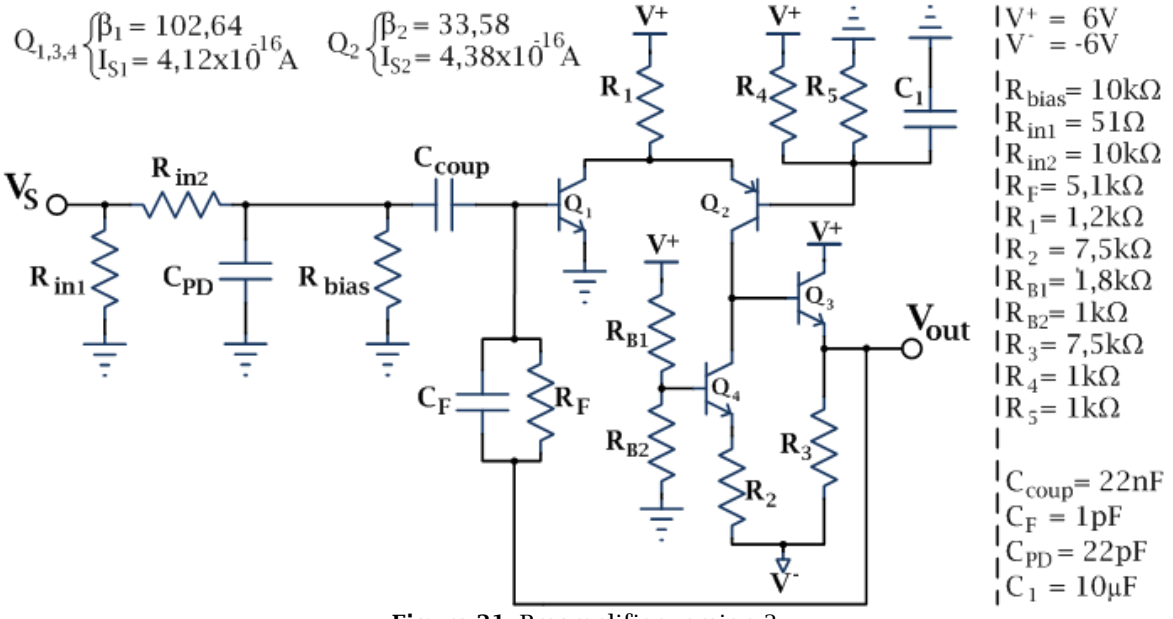

Figure 31: Preamplifier version 3

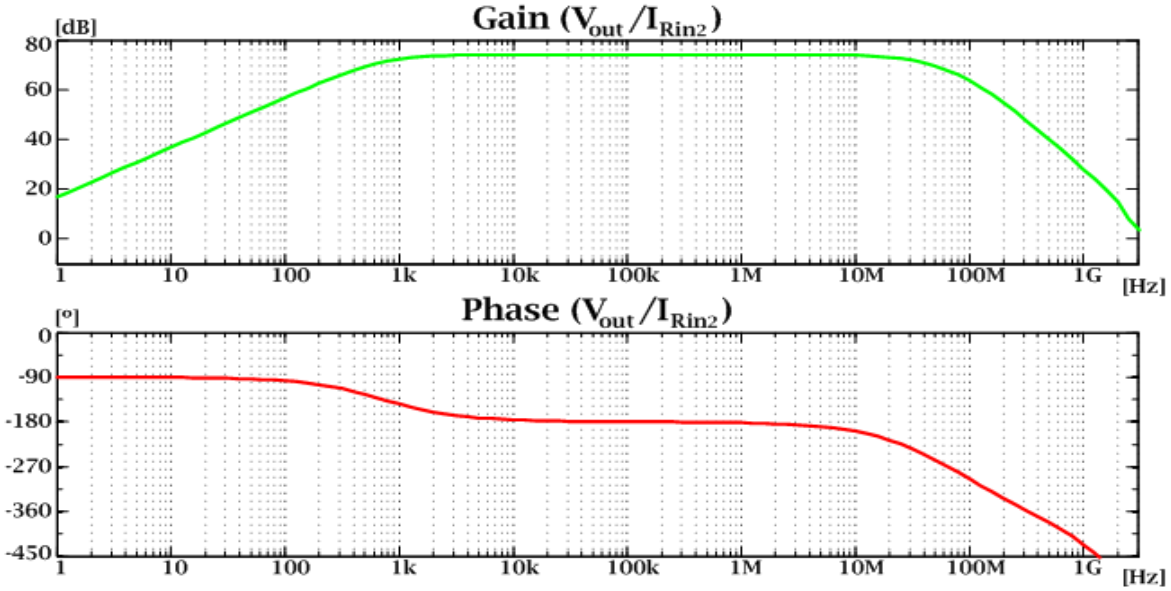

Figure 32: Preamplifier version 3: gain/phase response (V_{out}/I_{Rin2})

Table 11: Results of the gain/phase response (V_{out} /I_{Rin2}) of the preamplifier configurations

Pre-Amplifier	f_L [Hz]	f_H [MHz]	Gain @ 100kHz [dB]
Version 1	731,92	33,21	74,06
Version 2	734,55	37,66	74,12
Version 3	733,16	37,39	74,12

Versions 2 and 3 of the preamplifier where studied as possible improvements to the initially proposed configuration. The primary intent was to obtain a more stable frequency response with a larger bandwidth. However, the results shown in table 11 indicate that all three configurations have a very similar behavior. Although, there is an increase in the high cut-off frequency and gain, of versions 2 and 3, the results are almost insignificant. Given that PSpice simulations are not as accurate as an experimental characterization, before producing the final receiver, prototypes of the three configurations were built. This way, an experimental characterization can be performed, and a better set of results obtained. Given the simplicity the version 1 of the preamplifier, it is most likely the best solution.

In regard to the stability of these configurations, the Bode stability criterion is expected to be met. As was shown in subsection IV.iii.i, the condition $R_F \cdot C_F \leq R_{in} \cdot C_t$ is required. Given that both R_F and the R_{in} resistors are in the order of a few kilo-ohms, the decisive factor will be the value of the capacitors. And C_t is at least ten times larger than C_F. Therefore, the preamplifier is expected to be stable.

IV.iii.iii Low-Pass filter

The low-pass filter implemented was designed with the help of free software from Texas Instruments, the Filter Pro™ v2 [Texweb]. This program is simple to use and offers several options, such as filter type, circuit type, available resistor and capacitor series, along with the common filter defining parameters.

In order to reduce signal noise and achieve a linear response in the pass-band, a Butterworth response is the most adequate. This filter type presents a practically flat response in the pass-band, with almost no ripple. At the projected cut-off frequency the attenuation is 3dB and, for higher frequencies, it decreases with a steep 20dB per decade per pole ratio. A multiple-feedback (MFB) configuration was chosen due to its low sensitivity to component variations and gain accuracy.

After selecting the necessary filter and circuit types, a 50MHz low-pass, unity-gain filter with 2 poles was chosen. The E24 series resistors and E12 series capacitors were selected and optional entries adjusted. The resulting circuit was then simulated in PSpice with a TEXAS OPA820ID operational amplifier. Also, a buffer was added between the preamplifier and the low-pass filter in order to increase the input impedance of the filter stage, thus not causing any effect on the preamplifier. Figure 33 represents the low-pass filter design with an input buffer, and figure 34 shows simulation results for the gain/phase response of (V_{out}/V_{in}). In figure 35 is the comparative response of the preamplifier, with and without the low-pass filter. In table 12 are the low (f_L) and high (f_H) cut-off frequencies along with the stable gain values.

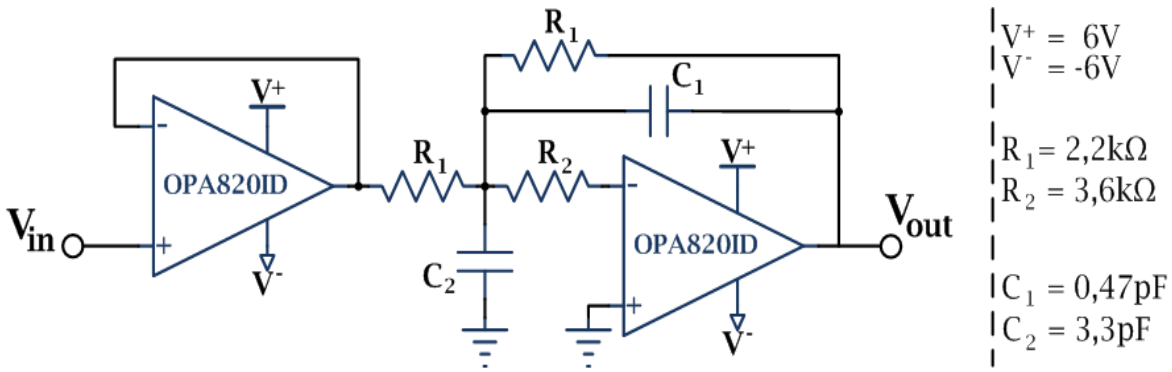

Figure 33: Low-pass filter with an input buffer

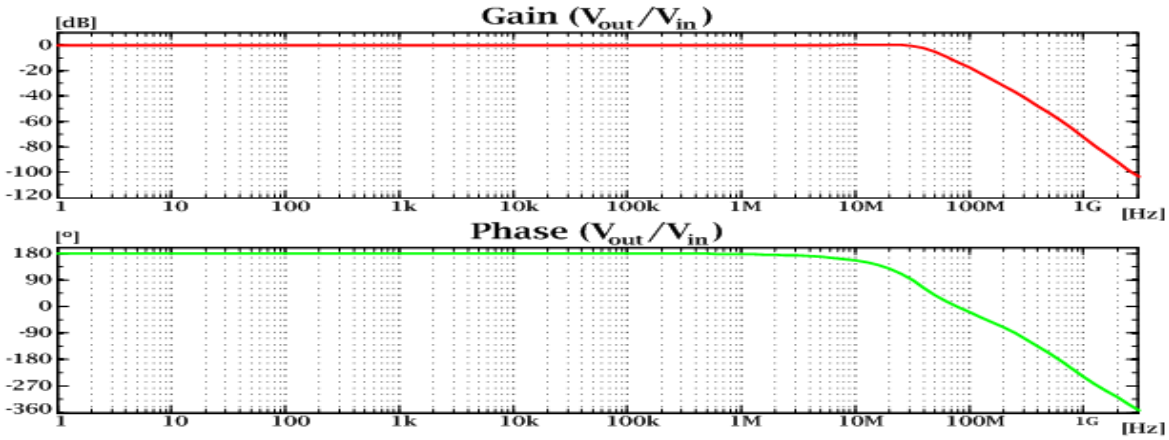

Figure 34: Low-pass filter: gain/phase response of (V_{out}/V_{in})

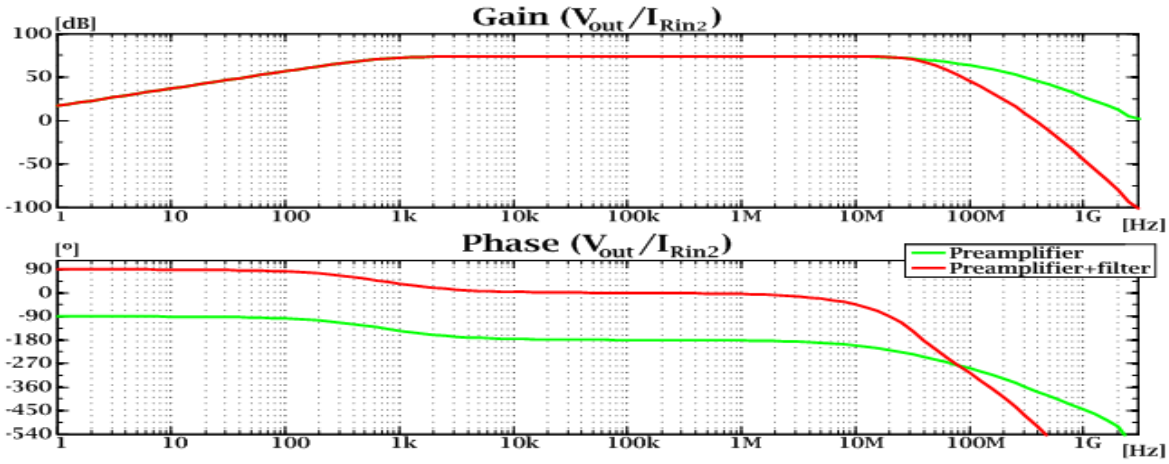

Figure 35: Filter's effect on the receiver: gain/phase response of (V_{out}/I_{Rin2})

Table 12: Gain/phase results of the filter's effect on the receiver

Circuit	f_L [Hz]	f_H [MHz]	Gain [dB]
Low-pass filter	---------	41,00	0
Preamplifier	731,92	33,41	74,01
Preamplifier + filter	731,93	30,59	74,01

The low-pass filter shows a stable response with a high cut-off frequency of 41MHz, a 40dB per decade attenuation at higher frequencies and a 180º phase shift in the pass-band. Combining the filter with the preamplifier, results in a much more adequate gain response. The low cut-off frequency is almost identical and the high cut-off frequency decreases slightly. For higher frequencies the level of gain reduction reaches a considerable 100dB per decade slope, this way improving cut-off response to any unwanted high frequency component. Also, the combined phase shift response is now set around 0º in the pass-band, which means that the output data signal is no longer inverted.

IV.iii.iv Voltage amplifier

The voltage amplifier module is designed to increase the voltage levels of the data signal before it is delivered to a decoder. Although this is not an essential element in the receiver's design, it may, at least in theory, increase the range of the optical receiver. Therefore, a simple voltage amplifier configuration is presented, along with the respective PSpice simulation results.

Considering an optical channel without noise, the incident power collected at the receiver's photodiode has a reversely proportional reason to the square of the distance between receiver and emitter, as was shown in equation 7, page 21. This relation means that, in the linear region of the preamplifier plus filter gain/phase response, the output voltage will also decrease with the square of the distance. When the levels of the output voltage fall below the minimum required for a correct detection in the signal decoder, data transmission will be lost. By using a voltage amplifier, the output levels can be increased so that a correct detection is made, thus increasing the available service area. The flaw with this analysis occurs when noise sources are considered. As explained before, in the current application noise levels are not negligible, and, for increasing distances, the incident optical power may contain a noise component that would make impossible to guarantee correct signal detection, even with an output voltage amplifier.

The proposed voltage amplifier configuration, shown in figure 36, uses a two stage voltage amplifier with an input capacitor, which filters the DC component and centers the voltage value on 0V. Each amplifying stage is made from an operational amplifier LM6723 in an inverting configuration, with a moderate gain and a large bandwidth. This way, the resulting two stage amplifier will present a non-inverting response with a large bandwidth and a gain equal to the product of the individual gains:

$$A_v = \left(-\frac{R_{12}}{R_{11}}\right) \times \left(-\frac{R_{22}}{R_{21}}\right) = \frac{R_{12} \cdot R_{22}}{R_{11} \cdot R_{21}}. \qquad \textbf{(eq. 39)}$$

Figure 37 shows the gain/phase response (V_{out}/V_{in}) of the voltage amplifier, followed by the comparison of its effect on the gain/phase response (V_{out}/I_{Rin2}) on the receiver (preamplifier and filter), in figure 38. The respective low (f_L) and high (f_H) cut-off frequencies along with the stable gain values are presented in table 13.

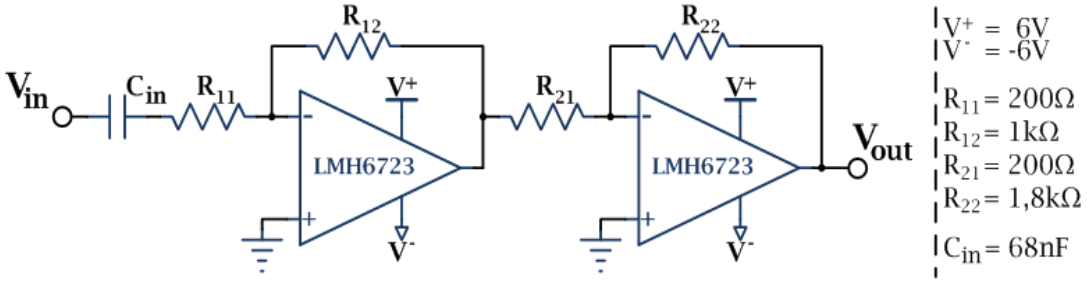

Figure 36: Two stage voltage amplifier

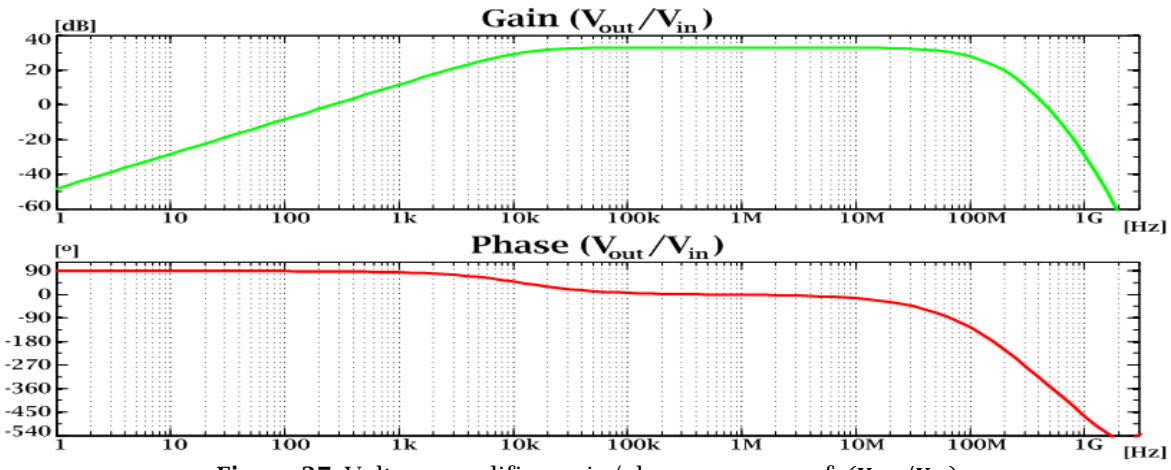

Figure 37: Voltage amplifier: gain/phase response of (V_{out}/V_{in})

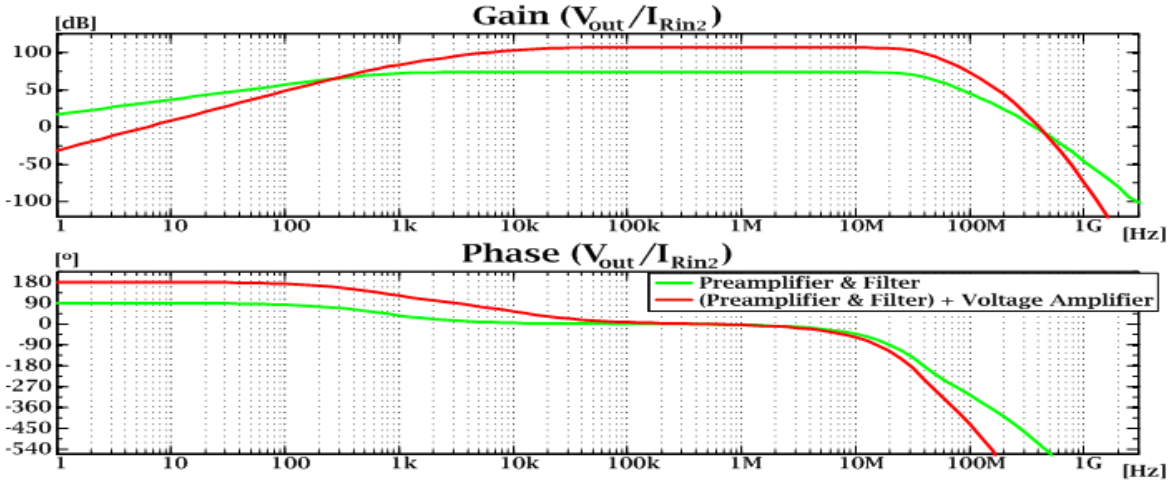

Figure 38: Voltage amplifier's effect on the receiver: gain/phase response of (V_{out}/I_{Rin2})

Table 13: Gain/phase results of the voltage amplifier's effect on the receiver

Circuit	f_L [Hz]	f_H [MHz]	Gain [dB]
Voltage amplifier	11.782,00	69,82	30,03
Preamplifier+filter	728,89	29,84	74,01
Preamplifier+filter + voltage amplifier	11.822,00	27,56	107,04

The voltage amplifier shows a 30,03dB gain which is close to the expected voltage gain of 45V/V. The low cut-off frequency, due to the input capacitor, is higher than previously obtained values, but still in an acceptable range. As for the high cut-off frequency, the 69,82MHz are sure to guarantee a stable amplification through the receiver's pass-band, without causing a significant reduction on the overall high cut-off frequency. The final receiver configuration shows a steady response, with a gain of 107,04dB in the pass-band, a high cut-off frequency of 27,56MHz, well over the 1MHz expected working frequency, and a low cut-off frequency of 11,82kHz which is helpful in reducing low-frequency noise from artificial light sources, without affecting the system's performance. The phase response shows that the input current has a 0º phase shift with the output voltage in the approximated interval of 10kHz to 10MHz. Such results allow for a relatively stable and effective receiver to be expected, with the main concerns relying on the noise effects and optical power available.

In order to conclude the receiver's analysis, the relation between the input current and the output voltage was measured. Knowing that the typical photocurrent varies from hundreds of microamperes to tenths of milliamperes, a DC sweep from -5mA to 5mA was performed. The resulting $V_{out}(I_{in})$ curve is presented in figure 39. In order to obtain these results the input circuitry was replaced with a current source, and the input capacitor of the voltage amplifier stage was removed.

The measured values show that the receiver, as expected, easily saturates between approximately +5V and -5V. This is mostly due to the output voltage amplifier. From the detail graphic, on the right, it is also clear to see that there is a constant ratio between the output voltage and the input current in the interval between the two saturation stages. In this interval the output voltage varies 9,956V and the input current 42,540µA. In order to confirm the reliability of this simulation, the steady gain can be compared. Using the

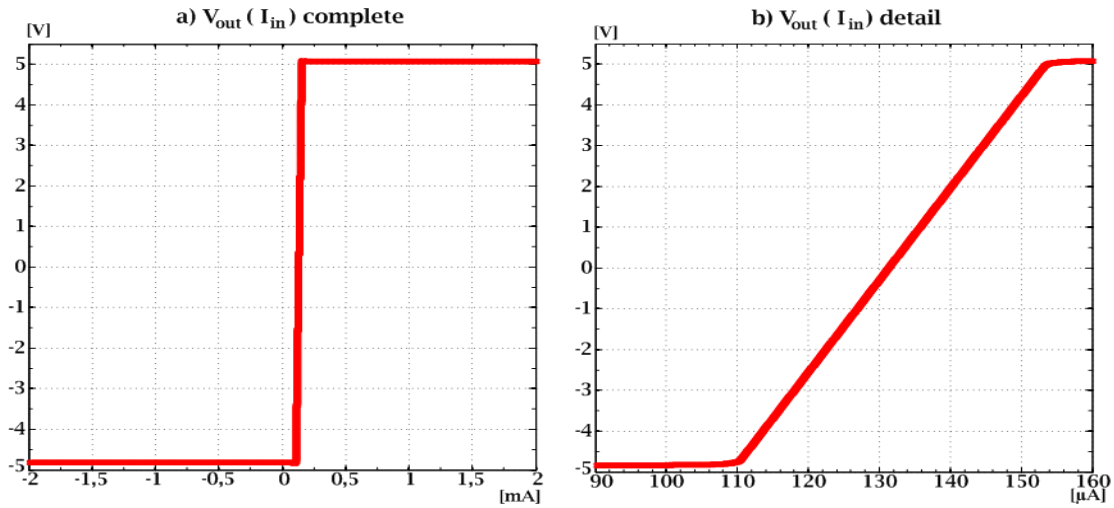

Figure 39: Receiver: DC sweep $V_{out}(I_{in})$ response

following relation:

$$\frac{V_{out}}{I_{in}} = 20 \times log\left(\frac{\Delta V_{out}}{\Delta I_{in}}\right) [dB]. \quad \textbf{(eq. 40)}$$

Replacing the voltage and current values results in a gain of 107,40dB, which is almost identical as the one presented in table 13. From figure 39 it is also possible to observe that the $V_{out}(I_{in})$ curve is not centred in 0A. This is to be expected given the complexity of the circuit. A current of approximately 134µA is necessary to achieve the positive saturation point, and for currents under 110µA the output is in the negative saturation point.

These results are also helpful in order to understand the effect of the dark current on the receiver. From table 8, the dark current values of the researched photodiodes are all under 500nA. Therefore the designed receiver should be indifferent to its effect. Also, in a real application scenario the levels of the incident light, either from a signal or noise source, are much higher than that of the dark current.

Regarding ambient noise, the result might be a lot different, ambient noise generates photocurrents that might go from a couple of microamperes up to a couple of milliamperes [Mor96, Mor97, Tav97], and although only the AC noise from artificial light sources would be amplified, it still has a considerable magnitude. Therefore implementing the voltage amplifier in the receiver's design might not be completely necessary, or even adequate to the intended application. As an alternative, a high sensitivity decoder could be used.

The influence of noise components cannot be accurately measured through simulation, therefore prototyping and experimental characterization of the different modules is required before a final device is built. Starting with the preamplifier, prototypes were built for the three proposed configurations in subsection IV.iii.ii. Given the importance of this module, different layout configurations were also tested. The experimental results showed a necessity for a low-pass filter, of which an analysis is presented in subsection IV.iii.iii. After prototyping and testing of the filter, an acceptable receiver configuration was achieved and the final receiver prototype was built.

In order to perform the experimental characterization, prototypes were built only for the preamplifier versions and the low-pass filter. The electrical circuits of these devices include several additional filtering capacitors. Similar to the receiver, SMD's were used. The chosen transistors were the Philips BFR92A NPN and its matched PNP equivalent, the Philips BFT92. In the filtering stage, the Texas OPA820ID was selected. This is a unity-gain stable, low-noise operational amplifier with a high bandwidth, ideal for the filtering stage.

In conclusion…

There are several blocks that constitute the front-end of the VLC receiver. From these blocks, the preamplifier is the most critical. As was discussed in subsection II.iv.i, the most of the optical noise effects will be shown on the photodiode. Therefore it is important to choose a proper device. However, this is not an easy choice. In order to capture the most of the emitted signal, a large area is necessary, but this comes at the price of a high junction capacitance. According to the analysis presented in IV.iii.i, this capacity will have an effect on the available bandwidth, reducing it significantly. With these conclusions in mind, two photodiodes were selected, one with a small junction capacitance and a small active area, and another with a larger active area and a bigger junction capacitance.

Given the importance of the preamplifier, three configurations of a well known transimpedance amplifier were presented and studied. From the simulation results they appear to have a good performance for the desired application. However, and given that simulation results usually vary from practical results, prototypes for each version of the preamplifier were built and characterized. Also, from the simulation results, the necessity for a low-pass filter emerged. Resourcing to the Filter Pro™ v2 [Texweb] software, a simple yet robust filter configuration was tested and built.

Although a voltage amplifier was studied, it is not completely necessary for the experimental characterization. Also, its implementation and behaviour are very straightforward. Therefore the experimental characterization will focus only on the most important devices, namely the preamplifier and the low-pass filter.

Chapter V

Optoelectronic Transceiver

The optoelectronic transceiver is a device that converts a signal from an electrical medium to an optical one, and vice-versa. In order to build an effective VLC transceiver for project VIDAS, designs for the emitter optical driver and the receiver front-end were presented in previous chapters. In order to assess their capabilities, experimental results were obtained by building prototypes of the designed solutions. These results are essential to assess the viability of the optoelectronic transceiver in a practical scenario.

The current chapter is divided into three subsections in which the experimental results of the implemented transceiver are addressed. Subsection V.i gives an introduction to the design guidelines and the development aspects of the optoelectronic transceiver. In subsection V.ii the measurement setups, with which the experimental results were obtained, are described. Finally, in subsection V.iii, the experimental results are presented and discussed.

V.i Design guidelines

From the VIDAS applications, vehicle-to-traffic light communications was considered as the primary application scenario for the designed transceiver. In this scenario the VLC emitter and receiver are placed in a LOS configuration. With the present work being a study on system design, a small scale model was built. In this model a single HB-LED emitter and a single photodiode receiver were used. Nevertheless, the presented devices can be adapted to a full scale scenario.

Following previous considerations, an emitter made from a discrete transistor topology in a current-sink configuration is used to drive the HB-LED. A digital voltage signal is modulated into the output light intensity by controlling the current that flows through the device. The optical receiver was also made from a discrete configuration and, at first, only a photodiode followed by a transimpedance amplifier was considered. Further developments led to the usage of an additional low-pass filter. Although an output voltage amplifier design was presented, it was never practically implemented. This module has a straightforward implementation, and isn't critical to the system performance. Therefore, and in order to better assess the behavior of the preamplifier, the receiver consists only on a photodiode followed by the preamplifier and an output low-pass filter.

The optoelectronic transceiver was developed in the Integrated Circuits and Systems laboratory, where several prototypes of the main modules of the optoelectronic transceiver were built and characterized. In a first stage the OrCAD Capture v16.0 software package and the PSpice simulator in particular, were used to simulate the front-end electronics. Although the optical signals behavior could not be included in the simulation, the workgroup previous experience and results provided a guideline to the initial design. After an acceptable simulation result, a printed circuit board (PCB) prototype would be drawn, with the help of the OrCAD Layout software, and built. The experimental results sometimes led to new designs, layout changes or even additional modules to be considered.

V.ii Measurement setups

V.ii.i Optical emitter

The optical emitter characterization consists on several measurements of the current through the HB-LED at different frequencies of the input digital signal. As was indicated earlier, a 1Ω resistor was added to the circuit in order aid in the process of measuring the current through the HB-LED. This way, the voltage waveforms measured at this resistor are a good approximation to the desired current.

Figure 40 represents the measurement setup used to make the different measurements. An HP E3631A power supply was used to provide a stable DC voltage of 6V. Using the equipment capabilities, a maximum average current of 400mA was chosen in order to protect the HB-LED from a possible overcharge. With a DS 435 function generator, a square wave with amplitude of 2,5V and an offset of 1,25V was selected. For the different measurements the frequency values were adjusted to the desired values, and

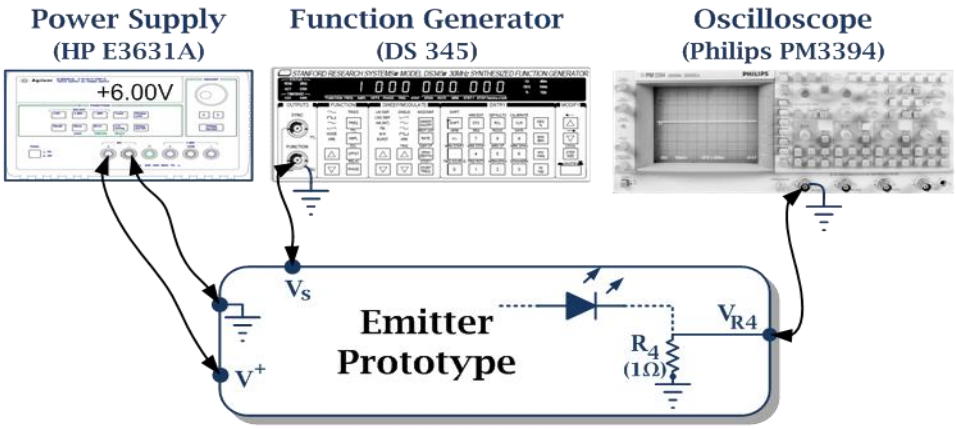

Figure 40: Emitter characterization: measurement setup

in the final measurement the connection cable was removed. With the Philips PM3394 oscilloscope, the resulting voltage waveforms at the output resistor were observed. For each measurement the time/division scale was corrected in order to observe a reasonable number of output pulses. Also, the voltage/division scale was also adjusted. In order to correctly measure the DC level of the output voltage, a DC coupling was chosen at all time.

V.ii.ii Optical receiver

The characterization of the receiver and its modules was made using an HP 4195A network/spectrum analyzer. Several gain/phase measurements of the different preamplifier configurations, as well as the filter were made. Also, a spectrum analysis of the implemented receiver in an isolated environment was performed.

Figure 41 shows the setup used for the several gain/phase experimental measurements. In this configuration, an HP E3631A provides a symmetrical power supply of ±6V DC. In order to execute the required measurements, an HP 41952A transmission/reflection test set is necessary to generate a power split. Also, an HP 41800A active probe is used to measure the output voltage, given that the output impedance is not matched to the 50Ω of the network analyzer ports.

In the network/spectrum analyzer the “Network” option under the configuration menu was selected, followed by correct port configuration of “T2/R1”. The frequency range was defined by setting the start frequency at 10Hz and the stop frequency at 500MHZ, also, a resolution bandwidth of 3Hz was chosen. With these initial settings, a direct connection was made between the output of the power splitter and the input of the active probe. In the calibration menu, a “THROUGH” calibration was made, and the calibration points were activated. This removes any effect of the measurement setup from

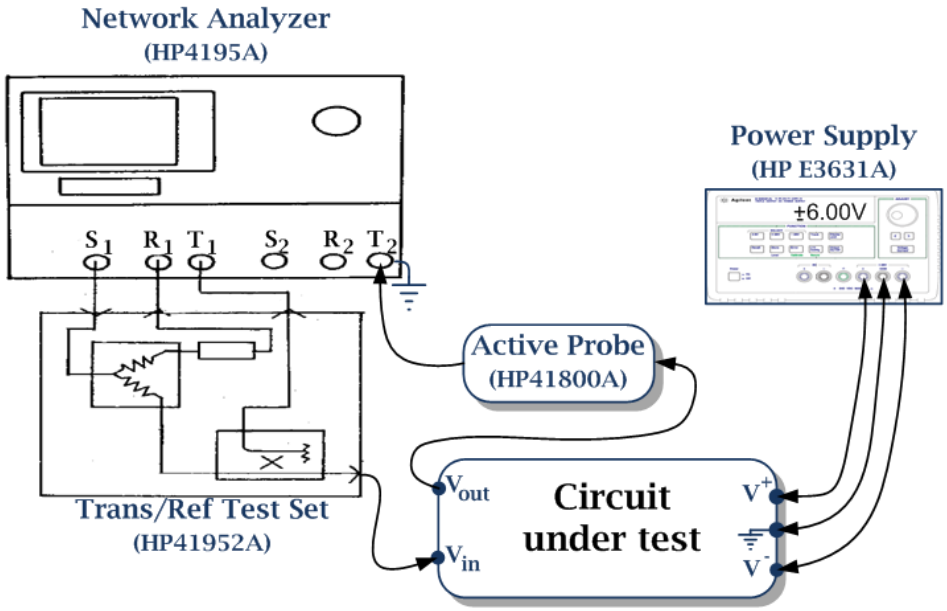

Figure 41: Receiver characterization: measurement setup for network analysis

the response of the circuit under test. With these configurations selected, a frequency sweep was performed and the results were saved in a floppy disk for future reference.

The spectrum measurements were made with the spectrum analysis capabilities of the HP4195A network/spectrum analyzer. In this case, the receiver was placed inside a shielded box, built in a similar fashion to a Faraday cage. This cage was made from several layers of aluminum foil, which also covered the power supply cables. These layers were in contact with each other and were connected to the earth ground reference available in the power supply. This cage was made to prevent electromagnetic interference and to isolate the receiver photodiode from external light sources. Therefore, the natural noise response of the receiver could be obtained. The experimental setup is shown in figure 42. The DC power supply is provided by the HP E3631A, and the output signal is measured directly by the spectrum analyzer.

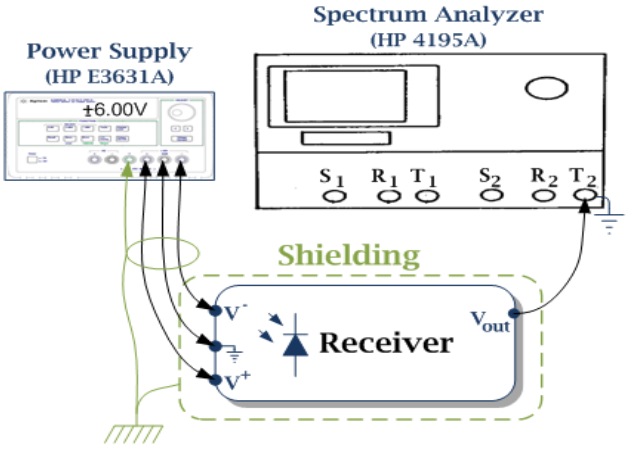

Figure 42: Receiver characterization: measurement setup for spectrum analysis

In the network/spectrum analyzer the “Spectrum” option under the configuration menu was selected, also the respective input port was defined. Given that the spectrum mode takes a significant amount of time, especially at high frequencies with a low resolution bandwidth, the measurement was divided into several intervals with different ranges and resolution bandwidths. Also the stop frequency was reduced to 40MHz. This is only slightly higher than the receiver high cut-off frequency, but it is still enough to assess the noise behavior.

V.ii.iii Optoelectronic transceiver

The final characterization measurements were done in order to assess the performance of the optoelectronic transceiver over distance, frequency and different light conditions. The measurement setup is presented in figure 43. It shows a HP E3631A power supply with a symmetrical output voltage of ±6V DC that is delivered to the receiver, and a single 6V DC voltage supply that is delivered to the emitter. The DS 345 signal generator provides a square wave to the input of the emitter. As was used earlier, the square wave had a 2,5V of amplitude with a 1,25V offset. The frequency value was adjusted as required. In order to measure the output voltage of the receiver, a Philips PM3394 oscilloscope was used. For each measurement voltage/division and time/division scales were adjusted to perform a correct observation of the output signals. Also, a DC coupling was maintained in all measurements.

During these measurements the emitter and the receiver prototypes were kept aligned, with the HB-LED pointed directly at the photodiode. The receiver was fixed at the base of the measurement setup, while the emitter was placed at the different heights required. A shielding box, that covered the emitter and receiver, was also used to block external light sources when the measurement would require it.

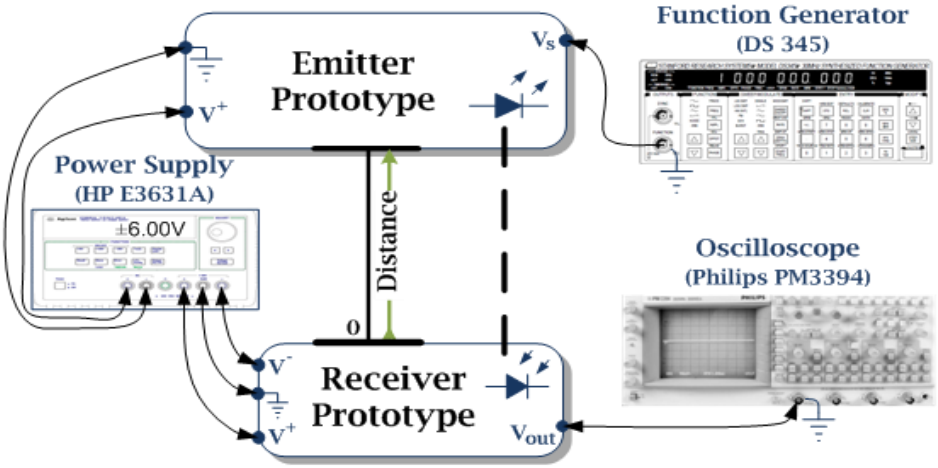

Figure 43: Transceiver characterization: measurement setup

V.iii Experimental results

V.iii.i Optical emitter

The optical emitter's characterization consists on several measurements of the current through the HB-LED at several frequencies. Using an oscilloscope, the voltage at the 1Ω resistor (R_4) was measured. This way a good approximation of the current through the HB-LED can be obtained, without significantly altering the circuit. Also, voltage and current waveforms are equal.

During the experimental characterization, square pulses with a 50% duty-cycle were used. By testing the emitter, and eventually the receiver, with a square pulse a more accurate result is obtained. As is known, a square pulse with a frequency of, for example, 1MHz has a spectral distribution that includes significant components at higher frequencies. If a sinusoidal signal was to be used to characterize the devices, it would not be so easy to guarantee a correct performance with a square pulse of the same frequency. Therefore, and given that an OOK amplitude modulation is typically used in these applications, the square pulse is the best signal to use during the system characterization.

Figure 44 and table 14 show the approximate HB-LED electrical current signals (I_D), and respective values. These were measured for an input signal (V_{data}) of 100kHz, 500kHz, 1MHz, 2MHz and 5MHz. Also, a measurement was made with the input signal disconnected which corresponds to a constant output value. As was explained in subsection III.iii.iii, the receiver's behavior can easily be corrected by changing the resistors values. However, in an experimental scenario, there is also the possibility of adjusting the input voltage. In order to achieve the transition of the Darlington transistor between the linear and the cut-off mode, the input signal amplitude was reduced to 2,5V.

Table 14: Experimental values of electrical current through the HB-LED

I_D @ f		a) @ 100kHz	b) @ 500kHz	c) @ 1MHz	d) @ 2MHz	e) @ 5MHz	f) constant value
V_{data}	logic high (2,5V)	310 mA	300 mA	300 mA	295 mA	280 mA	140 mA
	logic low (2,5V)	10 mA	10 mA	10 mA	10 mA	15 mA	

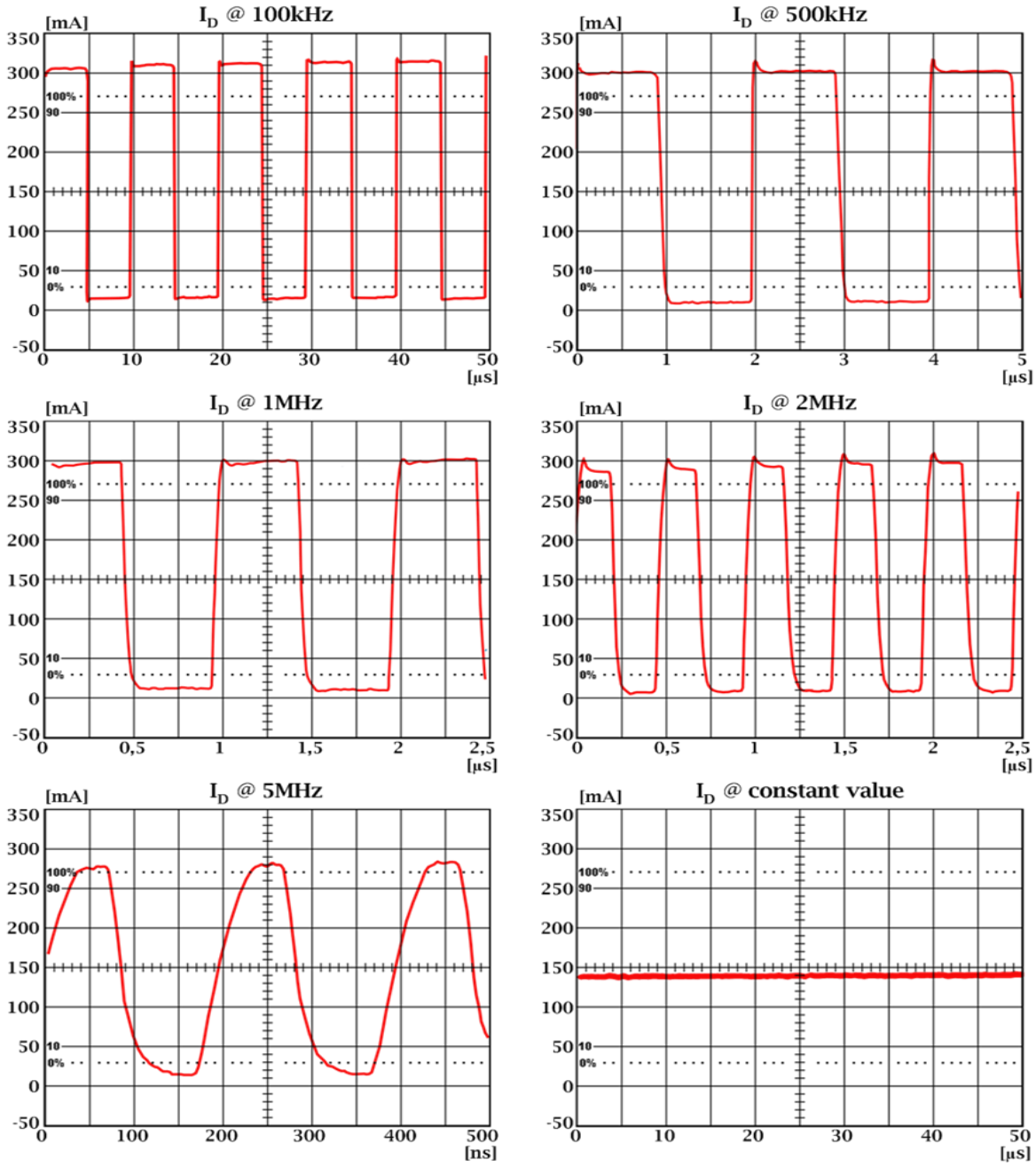

Figure 44: Emitter: LED current measurements at different frequencies

In a first analysis to the experimental measurements, it is clear to observe that the receiver has a correct response with current pulses up to 2MHz, which is still under the HB-LED's cut-off frequency and enough for the required application. For higher frequencies signal distortion and attenuation is obvious, and a correct square pulse transmission is not possible. When the digital signal is disconnected a constant current is obtained, and the HB-LED can be used as a regular light source, as was projected. The overall current values are well within the HB-LED's maximum ratings, and although they are under the simulation results, such was expected due to the reduction in the input

signal amplitude. If the original amplitude is used and the resistors values adjusted, higher currents can easily be achieved. However, for the intended application, these values are acceptable, such as the overall emitter performance.

V.iii.ii Optical receiver

Several tests were made to characterize the performance of the optical receiver. In order to test the gain/phase response of the built prototypes, in particular the preamplifier, the HP 4195A network/spectrum analyzer was used. This device measures the gain ratio between the output and the input voltages (V_{out}/V_{in}). This is used to characterize the filter, but in order to measure the gain ratio between the output voltage and the input current (V_{out}/I_{in}), it is necessary to do a correction to the measured values. In the preamplifier, an adapted input impedance of 50Ω was made by the R_{in1} and the R_{in2} resistors. The relation between the input current and the input voltage is given by:

$$\frac{I_{in}}{V_{in}} = \frac{R_{in1}}{R_{in1}+R_{in2}} \times \frac{R_{in1}+R_{in2}}{R_{in1}\cdot R_{in2}} = \frac{R_{in1}}{R_{in1}\cdot R_{in2}}\text{, or} \qquad \textbf{(eq. 41)}$$

$$\frac{I_{in}}{V_{in}} = 20 \times log\left(\frac{R_{in1}}{R_{in1}\cdot R_{in2}}\right) = -80dB\ . \qquad \textbf{(eq. 42)}$$

This result shows that the measured voltage gain values for the preamplifier configurations will have a negative 80dB difference to the transimpedance gain (V_{out}/I_{in}), and will corrected for better analysis.

For the three proposed preamplifier configurations two prototypes were built for each one. They will be referred to as preamplifier version “a”.”b”, where “a” corresponds to the configuration version (1,2 or 3) and “b” corresponds to the version of the PCB layout (0 for the first version, and 1 for the second).

The first PCB versions showed an irregular gain response for frequencies above 50MHz, as shown in figures 45, 46 and 47. Instead of decreasing, the gain curve shoots to values even higher than the gain obtained in the pass-band, this was observed in all preamplifier versions.

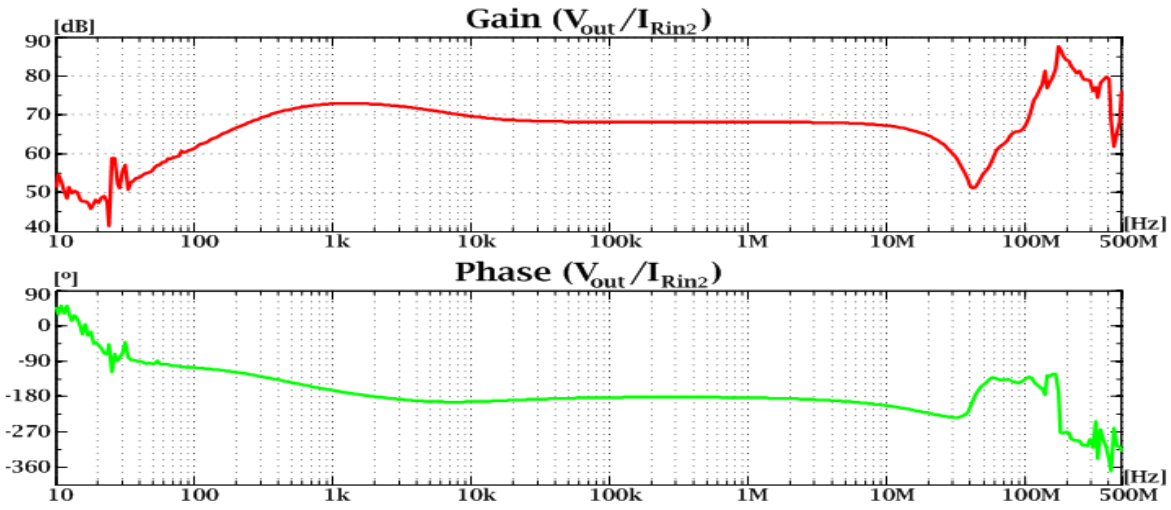

Figure 45: Preamplifier version 1.0: gain/phase (V_{out}/I_{Rin2}) measurements

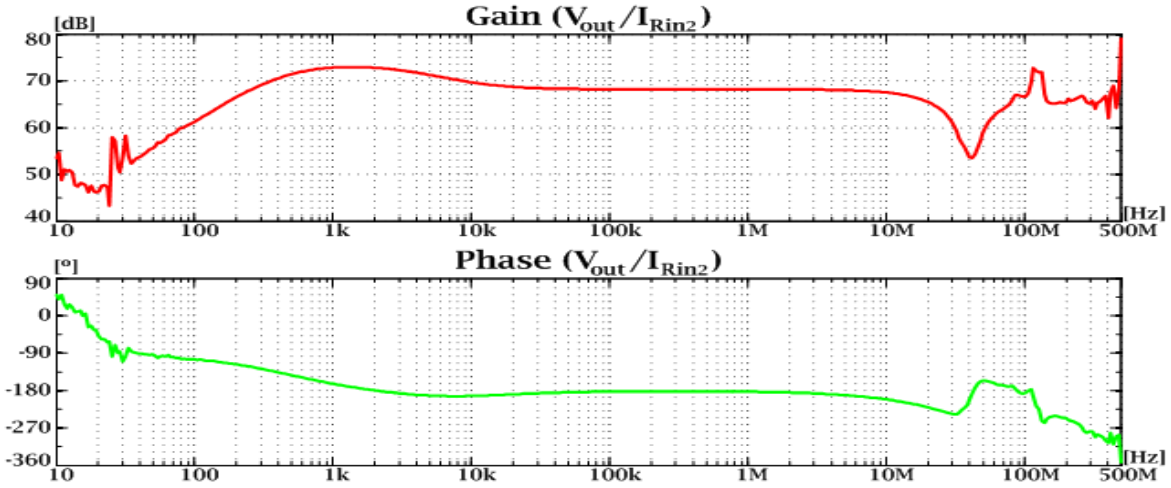

Figure 46: Preamplifier version 2.0: gain/phase (V_{out}/I_{Rin2}) measurements

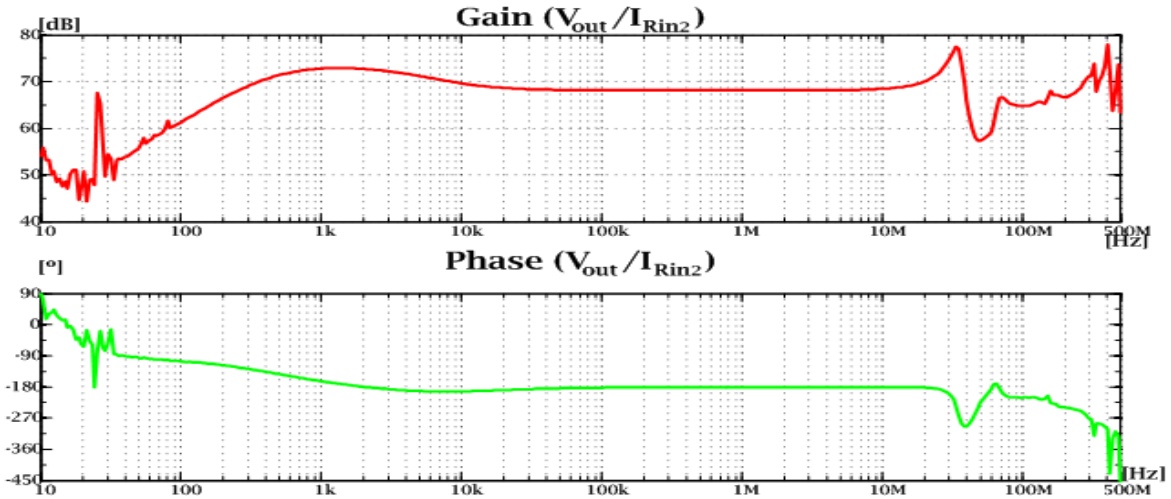

Figure 47: Preamplifier version 3.0: gain/phase (V_{out}/I_{Rin2}) measurements

Given that these effects were most likely due to the layout configurations, a redesign was made in which several layout considerations were taken into account. A special attention was given to the distance between tracks and their design. The primary signal track and the feedback signal track were built to be as short and straight as possible. Also, the distance between them and any other neighboring track was of at least twice the wide of the signal's track. This suggestion intended to avoid the effect of parasitic capacitors created between tracks. The other solution considered to improve the gain/phase responses was to build a low-pass filter. In figure 48 the gain/phase response of the filter is presented. The responses of the new layout versions of the preamplifier connected to the filter are presented in figures 49, 50 and 51. Table 15 shows a summary of the cut-off frequencies and stable gain measurements.

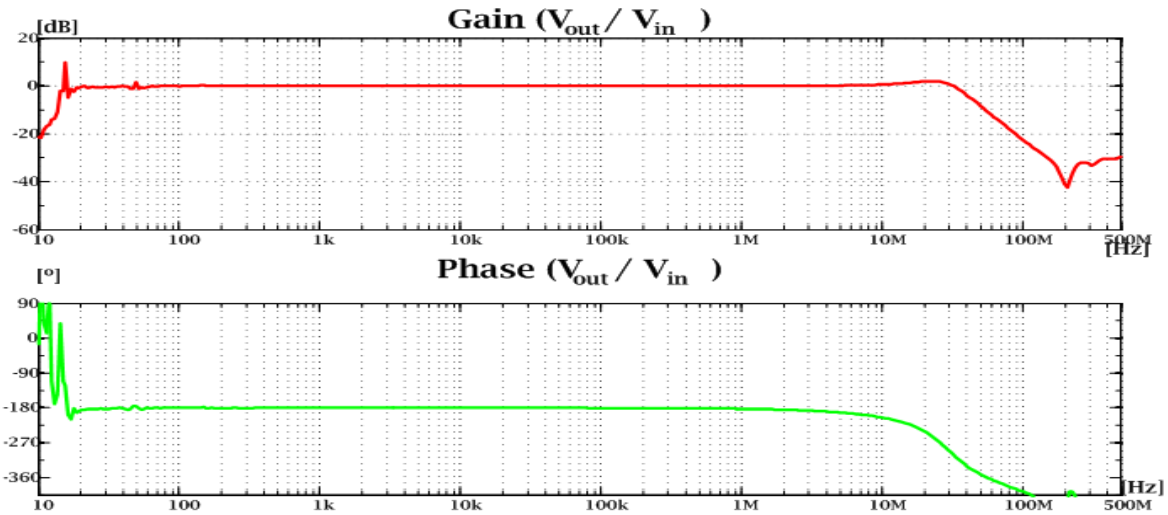

Figure 48: Low-pass filter: gain/phase (V_{out}/V_{in}) measurements

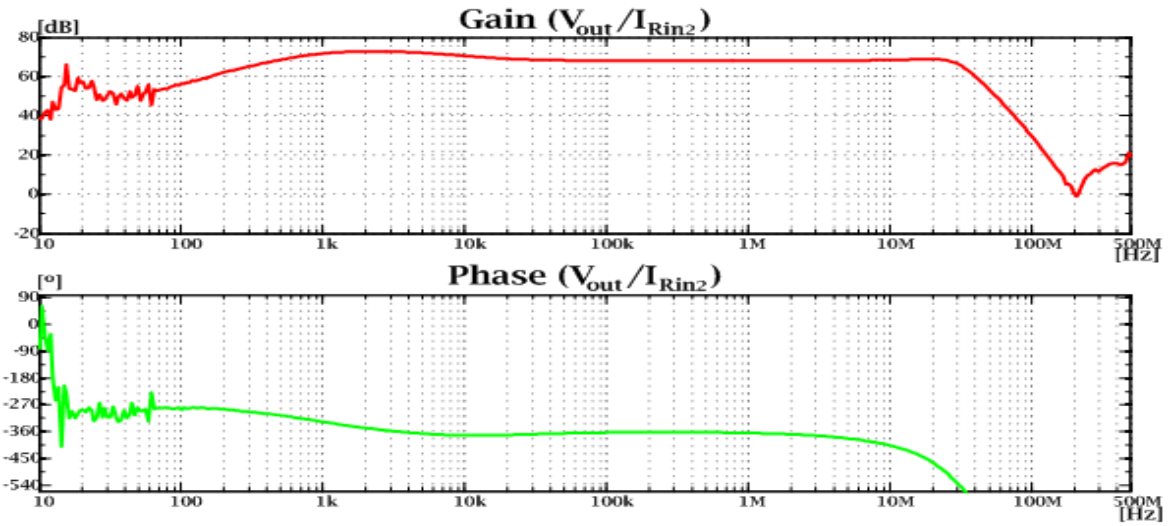

Figure 49: Preamplifier v1.1 and low-pass filter: gain/phase (V_{out}/I_{Rin2}) measurements

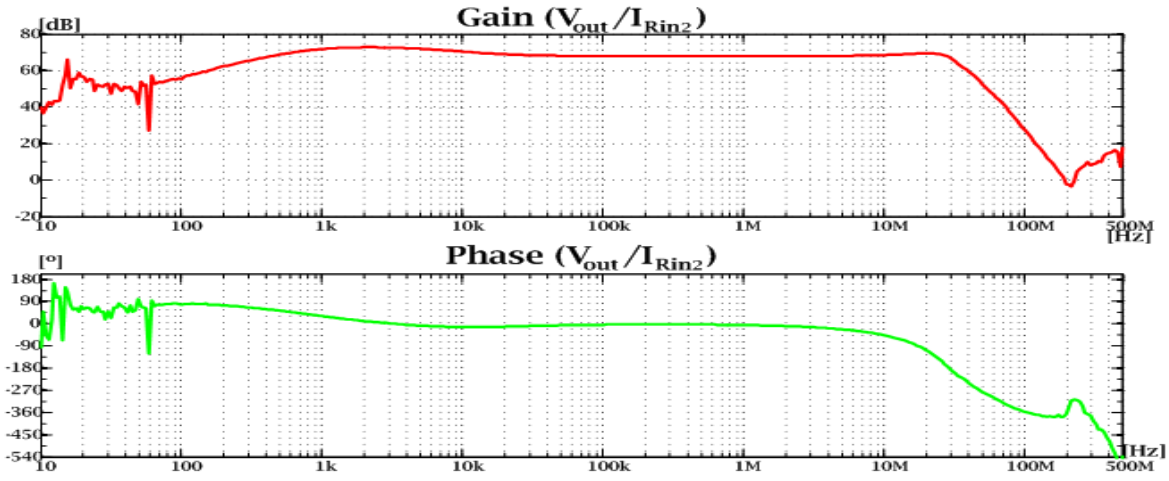

Figure 50: Preamplifier v2.1 and low-pass filter: gain/phase (V_{out}/I_{Rin2}) measurements

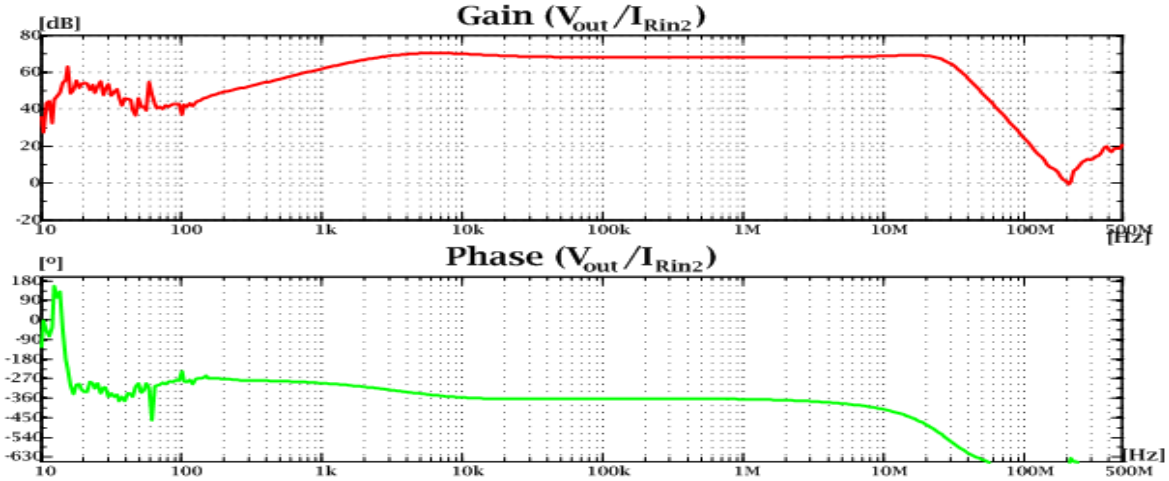

Figure 51: Preamplifier v3.1 and low-pass filter: gain/phase (V_{out}/I_{Rin2}) measurements

Table 15: Measurements of the gain/phase responses of the different prototypes

Circuit	f_L [Hz]	f_H [MHz]	Gain [dB]
Preamplifier version 1.0	163,10	18,82	68,16
Preamplifier version 2.0	170,50	21,50	68,20
Preamplifier version 3.0	163,10	39,98	68,14
Low-pass filter	---------	38,25	-0,02
Preamplifier version 1.1 + filter	303,40	32,04	68,03
Preamplifier version 2.1 + filter	290,30	32,04	67,97
Preamplifier version 3.1 + filter	1.496,00	29,32	67,99

(Note: close values may be equal do to the resolution of the measurement device)

These results show that the receiver made from a preamplifier and a low-pass filter is a good solution. All three presented configurations have a steady gain, and a phase response of 360º, which means that the output signal is not inverted. Given the implementation simplicity, version 1 of the preamplifier, followed by a low-pass filter is the best solution for a VLC receiver.

Although the voltage amplifier would help increase even further the output signals, it is more accurate to measure the effect of different light sources with only the two first modules. Also, the output voltage amplifier does not have a linear response, and therefore, characterization would become much harder.

The spectrum response of the receiver with photodiode connected, but isolated from external light sources is presented in figure 52. The value floats around -105dB, with peaks reaching -80dB. These peaks occur close to 50Hz, which means that their mostly interference in the power grid. From this analysis it is possible to conclude that the receiver generates small noise level due to its own components and layout.

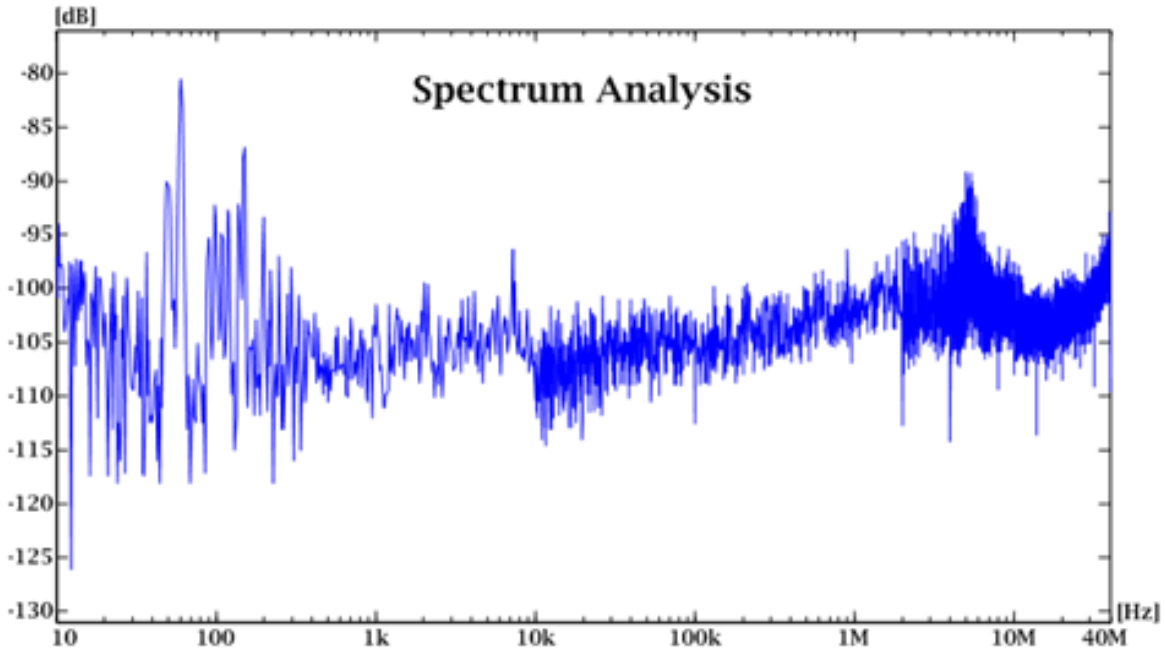

Figure 52: Receiver: spectrum analysis measurement

V.iii.iii Optoelectronic transceiver

The first test was done in a dark environment, isolated from external light sources. It represents the behavior of the transceiver over for different frequencies. For this test the HB-LED was aligned with the photodiode at a fixed distance of 100mm. The previously characterized emitter was used to drive the HB-LED at different frequencies. The results are presented in figure 53, and show that, despite a little noise, up to 1MHz, signal detection is possible and has low distortion, for frequencies above that value, in the high to low transition in particular, there is a considerable signal distortion that would cause inter-symbol interference.

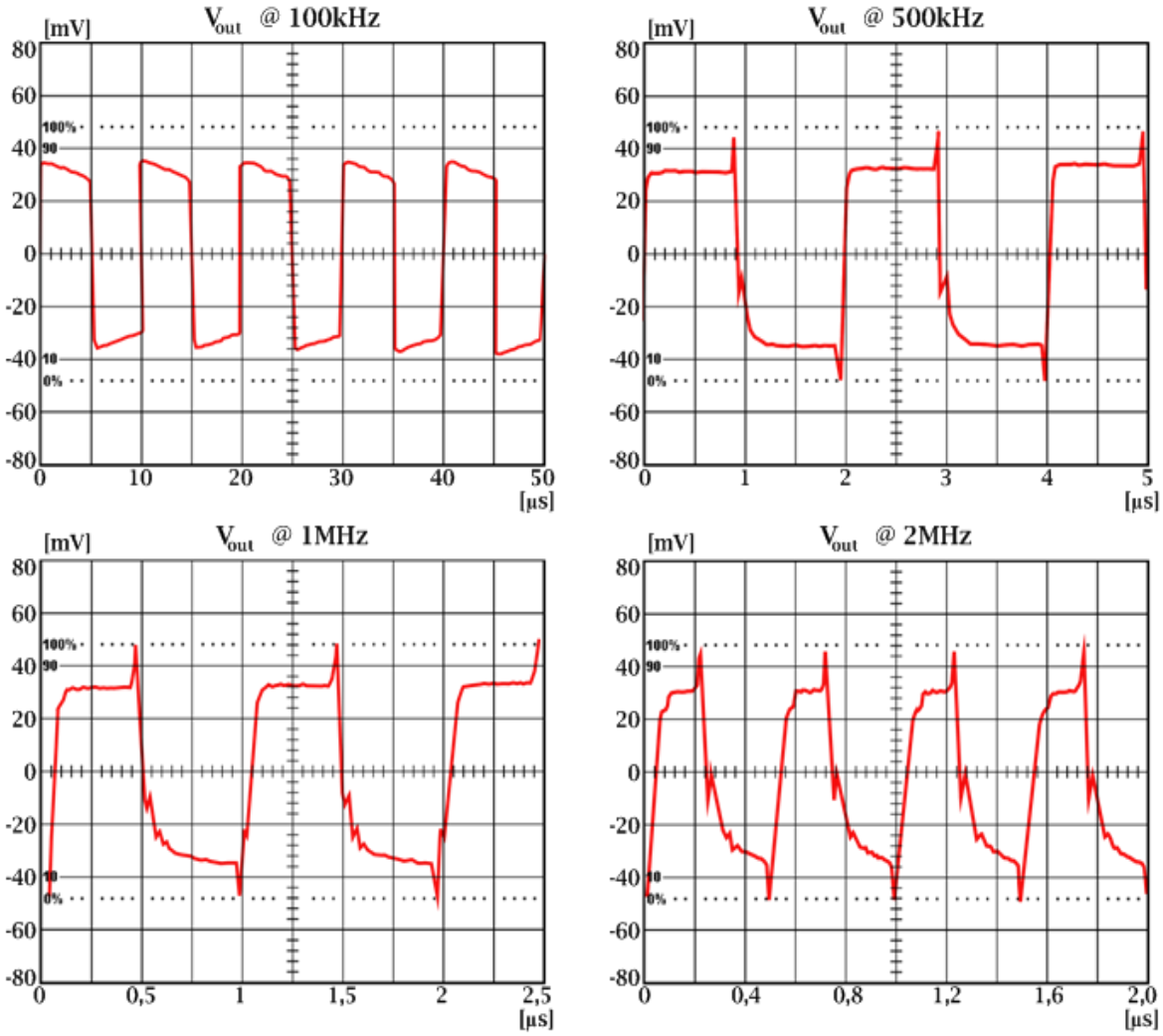

Figure 53: Transceiver in a dark environment: measurements for different frequencies

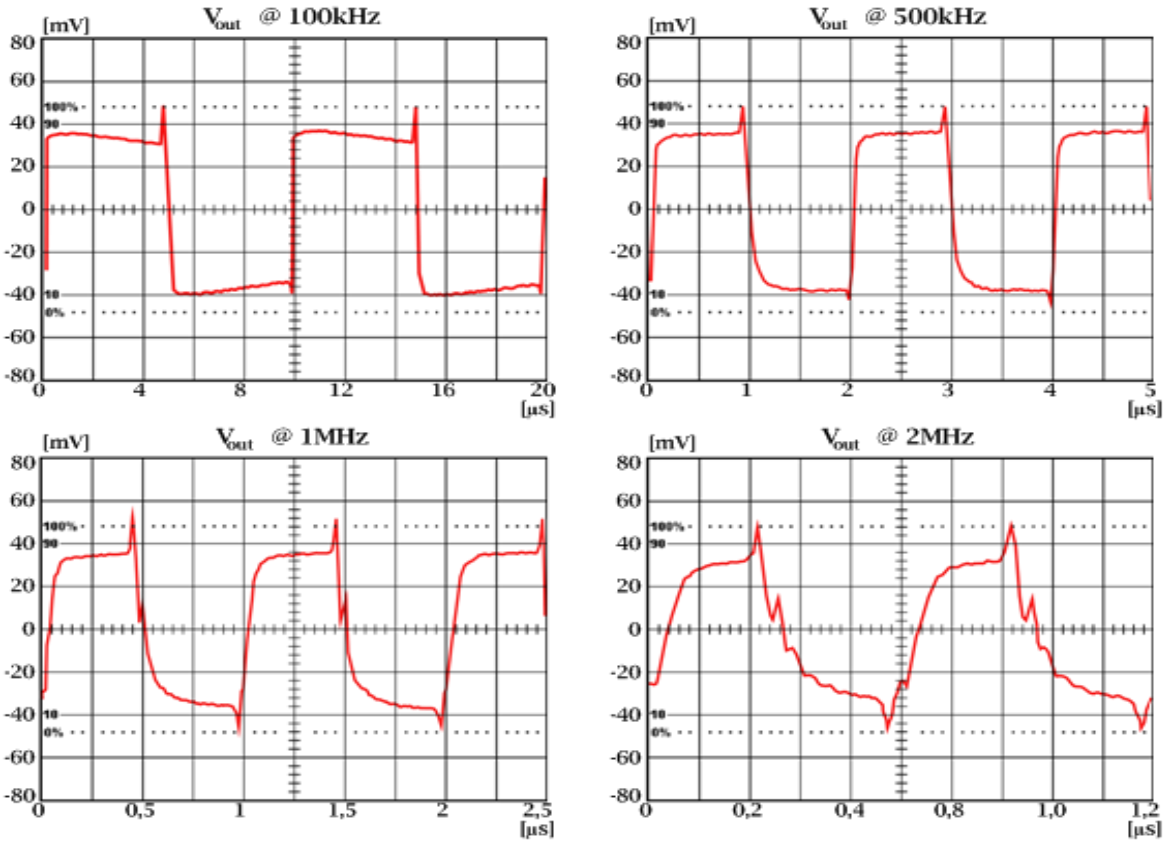

Figure 54: Transceiver at ambience light: measurements for different frequencies

In a similar test, the receiver was subjected to an indoor ambience light, which was composed of several fluorescent lamps placed in the ceiling at approximately two meters from the receiver. With the same HB-LED configuration and placement at 100mm, the results from figure 54 were obtained. Although the DC effect of external light sources is not shown due to the output capacitor, it is clear to see that there is some fluctuation due to the transient components in fluorescent lights output. However, the resulting response is quite reliable even in the presence of moderate ambience light.

In order to further visualize the influence of an external light source on the receiver, a fluorescent lamp with electronic ballast was placed at approximately 300mm, with an inclination to the receiver's normal of 30º. The results obtained at 100kHz and 1MHz, shown in figure 55, clearly represent two aspects of external noise sources. In both graphics, a transient component from the fluorescent light is noticeable, with oscillations in the orders of the hundreds of kilo-hertz being present in the receiver's output voltage. This is expected given that fluorescent lights can show significant harmonics up to 1MHz [Mor96, Mor97, Tav97]. The other aspect of external light interference is only noticed on the response at 100kHz, the output saturates for a high input signal. This is not seen at 1MHz, mostly due to a small amplitude variation for different input signals. Most of this noise interference could be minimized if an IR cut-off filter was used, given that sunlight

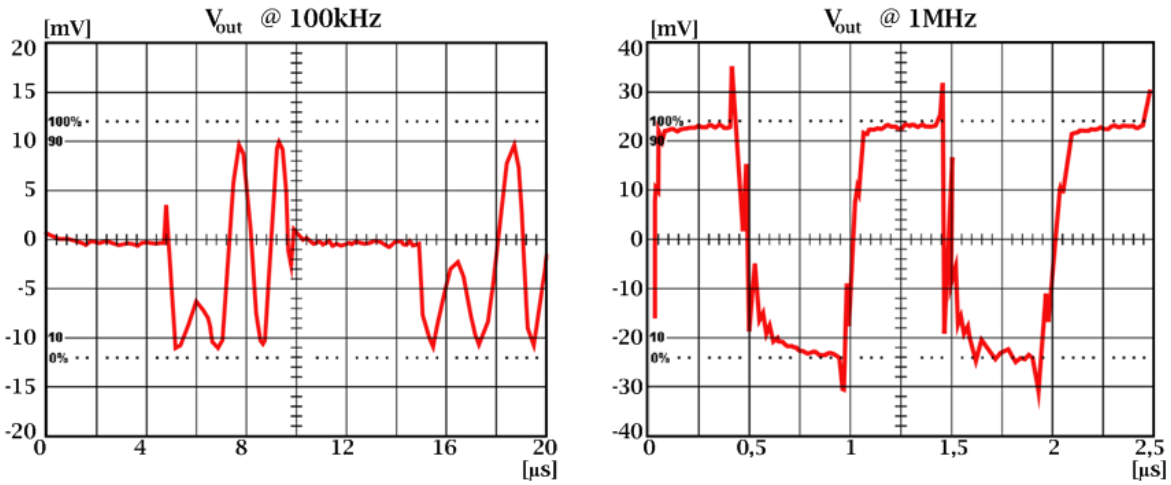

Figure 55: Transceiver with a close noise source: measurements for different frequencies

and conventional light sources have a significant IR component, which is captured in the unfiltered Si photodiode.

In conclusion, the optical receiver is very stable for frequencies up to the projected frequency value of 1MHz. Also, it can be used for several environments with a relative indifference to external light sources, when placed at some distance from them.

To perceive the the output signal variation with the increasing distance, several measurements were made with a fixed 1MHz signal from the emitter, in a dark environment at different distances. The resulting output peak-to-peak voltage over distance is plotted in figure 56. The curve shows the expected behavior, for a close distance, the input signal is so great that the preamplifier saturates and the output voltage is almost zero (blue dots). When the critical value is crossed, at approximately 40mm, the output reaches its maximum value and decreases in an approximately quadratic relation with the distance (red trace).

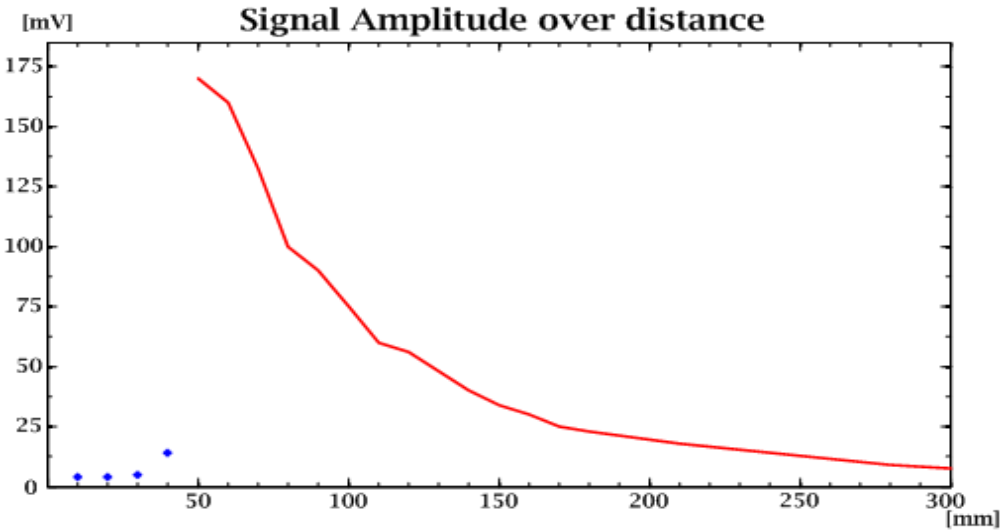

Figure 56: Transceiver behaviour over distance ($\boldsymbol{V_{out}(distance)}$)

In conclusion…

Doing an experimental characterization of such devices is a complex task. From the building of the prototypes, to the measurement of the experimental results, there are many things to consider. However, if time is dedicated to properly design the devices, the experimental results will usually be within the expected.

Considering the obtained results, they clearly support the design simulation results as well as some of the optical behavior predicted in previous chapters. Although there is still some room for improvement, the optoelectronic transceiver implemented seems to have a generally good performance. Both the emitter and the receiver, show that they can be used in the VIDAS application. However, there is still space for many improvements, mostly regarding optical filtering.

With these devices, it is now possible to do some field measurements that support some of the current mathematical models being developed for VIDAS. Also, they serve as a good base reference for the final VLC transceiver.

Chapter VI

Conclusions

Upon the conclusion of the work that served as the basis for the current text, several conclusions need to be registered. Starting with the research made on VLC systems, it appears to be a viable technology and has a good opportunity towards becoming a widespread technology in the future of optical wireless communications. This is also supported with the results obtained. However, there are still many things that need to be more thoroughly studied and analyzed.

An important constraint to VLC and this work as well, is the fact that manufacturers have not realized the potential in this type of applications. They can provide, in a near future, a new range of applications for their products. But in order for this commercial growth to happen, manufacturers need to release more information about their products. Although optical characteristics are well specified, in most datasheets the electrical transient behavior of the devices is not provided. This happens particularly in LED's datasheet, making research of devices for a VLC transceiver a hard task.

Another important conclusion comes from the practical implementation of the designed devices. Although the experimental results of the projected devices are within the range of the simulations, it was left clear that prototyping is important. The behavior of the optoelectronic components cannot be fully translated into the simulations. Therefore, the best way to completely characterize the implemented devices is by prototyping, which becomes essential towards assessing their real behavior.

From the prototype designing and building, became clear that the effect of the layout used cannot be overlooked. It is important to design solutions that minimize the circuit footprint, and improve connectivity. And although the noise generated by the components cannot be removed, a correct layout and assembly can help reduce it.

As for the obtained results, the proposed application seems viable. In this small scale design, the experimental results were satisfactory. Although more could be done, the implemented configurations are stable and work for a frequency range well within the required for the VIDAS application. However, it is also clear from the measured gain/phase and transient responses, that there is significant reduction in the available frequency ranges due to the optical components used.

VI.i Future work proposed

In order to improve the optoelectronic transceiver for the VIDAS application, several considerations can on implementation issues can be made, as well as guidelines for future development and improvement.

Regarding the receiver, upon looking to the obtained results, it is clear that external light sources will have a strong influence. This could seriously compromise the overall performance of the transceiver. As it was addressed during this dissertation, optical filtering is an expensive solution. However it should be tested. If a simple IR cut-off filter is used, a large spectrum of the interfering signals could be removed. Should this solution be implemented, choosing a correct filter is very important. Not only it needs to cut-off the IR component, but it cannot have a considerable influence on the visible light. Another line of thought, that should be pursued in the future, is how to implement a multiple receiver system. Instead of using a single receiver cell, like the one developed, solutions on how to integrate several photodiodes, or even several integrated receivers, should be studied and developed. In this scenario, the background knowledge obtained by the workgroup in IR wireless systems will prove to be extremely helpful, and previous designs should be used as guidelines.

The implemented emitter was designed to pulse a HB-LED in order to simulate a traffic light. However, if a real life solution is to be implemented, the commercially available HB-LED traffic lights should be analyzed. A study on whether it is possible or not to adapt those devices to the VIDAS application should be made. Also, solutions to integrate the transmission modules with the traffic control need to be studied.

Upon developing the different devices that make the optoelectronic transceiver, it is now possible to use them in order to characterize different light conditions and environments. Given the simplicity of the proposed designs, a group of receivers could be

built and integrated into an environment characterization setup. This setup would become a practical tool to make field measurements, which can support some of the current mathematical models being developed for VIDAS.

References

[802web] – **IEEE 802.11 Workgroup** website, available at: http://www.ieee802.org/11/index.shtml

[Agu99] – **Aguiar, R. L.**; A. Tavares; J. L. Cura; E. de Vasconcelos; L. N. Alves; R. Valadas; D. M. Santos; "Considerations on the design of transceivers for wireless optical LANs", IEE Colloquium on Optical Wireless Communications (Ref. No. 1999/128), June 1999, pp. 2/1-231

[Aka01] - **Akanegawa**, M.; Y. Tanaka; M. Nakagawa; "Basic Study on Traffic Information System Using LED Traffic Lights", IEEE Transactions on Intelligent Transportation Systems, Vol. 2, No. 4, Dec 2001, pp. 197-203

[Alv08] – **Alves, L. N.**; "High gain and bandwidth current-mode amplifiers: study and implementation", Thesis presented at the Universidade de Aveiro for the degree of Ph.D. in Electronics Engineering, 2008, pp.2-6

[Bel80] – **Bell**, **A.** and C. Tainter; "Drawing by Alexander Graham Bell and Charles Sumner Tainter, April 1880", The Alexander Graham Bell Family Papers, available at: http://memory.loc.gov/mss/magbell/252/25200104/0001.jpg

[Bel81] – **Bell, A.**; "Upon the Production of Sound by Radiant Energy", Paper read before the National Academy of Sciences, April 21st, 1881, available at: http://www.archive.org/details/uponproductionof00bellrich

[Cra95] – **Craford, M. G.**; "LEDs Challenge the Incandescents", IEEE Circuits and Devices Magazine, Vol. 8, No 5, Sept. 1995, pp. 24-29

[EOweb] – **Edmund Optics**; IR Cut-off Filters products website, available at: http://www.edmundoptics.com/onlinecatalog/displayproduct.cfm?productID=1328

[Gfe79] – **Gfeller, F. R.** and U. Bapst; "Wireless In-House Data Communication via Diffuse Infrared Radiation", Proceedings of the IEEE Vol. 67, No. 11, Nov. 1979, pp. 1474-1486

[Hai99] – **Haitz, R.**; F. Kish; J. Tsao; J. Nelson; "The Case for a National Research Program on Semiconductor Lighting", Optoelectronics Industry Development Association (OIDA 1999), Washington, Oct. 1999, available at: http://lighting.sandia.gov/lightingdocs/hpsnl_long.pdf

[Ham03] – **Hamamatsu**; "Photodiode Technical Information", Feb. 2003, available at: http://sales.hamamatsu.com/assets/applications/SSD/photodiode_technical_information.pdf

[Har08] – **Haruyama, Shinichiro**; "Japan's Visible Light Communications Consortium and Its Standardization Activities", Jan. 2008, available at: https://mentor.ieee.org/802.15/file/08/15-08-0061-01-0vlc-japan-s-visible-light-communications-consortium-and-its.pdf

[Hra05] – **Hranilovic, S.**; "Wireless Optical Communication Systems", New York, 2005 Springer Science + Business Media, Inc., 2005, Chapter I

[IEweb] – **IEEE 802.15 WPAN Task Group 7** website, available at: http://www.ieee802.org/15/pub/TG7.html

[Kah97] – **Kahn, J. M.** and J. R. Barry; "Wireless Infrared Communications", Proceedings of the IEEE Vol. 85, No. 2, Feb. 1997, pp.265-298

[Kom03] – **Komine, T.** and M. Nakagawa; "Integrated Systems of White LED Visible-Light Communications and Power-Line Communications", IEEE Transactions on Consumer Electronics, Vol. 49, No. 1, Feb. 2003, pp. 71-79

[Kra02] – **Krames, M. R.**; H. Amano; J. J. Brown; P. L. Heremans; "Introduction to the Issue on High-Efficiency Light-Emitting Diodes", IEEE Journal on Selected Topics in Quantum Electronics, Vol. 8, No. 2, March 2002, pp. 185-188

[Kra07] – **Krames, M. R.**; O. B. Shchekin; R. Mueller-Mach; G. O. Mueller; Zhou Ling; G. Harbers; M. G. Craford; "Status and Future of High-Power Light-Emitting Diodes for Solid-State Lighting", Journal of Display Technology, Vol. 3, No. 2, June 2007, pp. 160-175

[Kum08] – **Kumar, N.**; N. Lourenco; M. Spiez; R. L. Aguiar; "Visible Light Communication Systems Conception and VIDAS", IETE Technical Review, Vol. 25, Issue 6, 2008, pp. 359-367

[Kum09] – **Kumar, N.**; L. N. Alves; R. L. Aguiar; "Design and Analysis of the Basic Parameters for Traffic Information Transmission Using VLC", 1st International Conference on Wireless Communication, Vehicular Technology, Information Theory and Aerospace & Electronic Systems Technology (Wireless VITAE 2009), May 2009, pp. 798-802

[Mor96] – **Moreira, A.**; R. Valadas; A. De Oliveira Duarte; "Reducing the Effects of Artificial Light Interference in Wireless Infrared Transmission Systems", IEE Colloquium on Optical Free Space Communication Links, Feb. 1996, pp. 5/1 – 510

[Mor97] - **Moreira, A.**; R. Valadas; A. De Oliveira Duarte; "Optical Interference Produced by Artificial Light", Wireless Networks, Vol. 3, Issue 2, May 1997, pp. 131-140

[Nat09] - **National Semiconductor**; "LED Drivers for High-Brightness Lighting", Solutions Guide, Vol. 2, 2009, available at:
http://www.national.com/vcm/NSC_Content/Files/Documents/national_lighting_solutions.pdf

[OSweb] – **OSRAM** PSpice LED's Library Warning, available at:
http://catalog.osram-os.com/applications//Electrical_Simulation/LED/ReadMe%20-%20Warning.txt

[Pan99] – **Pang, G.**; Ka-Lim Ho; T. Kwan; E. Yang; "Visible Light Communication for Audio Systems", IEEE Transactions on Consumer Electronics, Vol. 45, No. 6, Nov. 1999, pp. 1112-1118

[Pan02] – **Pang, G.**; T. Kwan; H. Liu; Chi-Ho Chan; "LED Wireless", IEEE Industry Applications Magazine, Vol. 8, No. 1, Jan. 2002, pp. 21-28

[Per07] – **Pereira, J.**; "Projecto Luz Comunicante", Final year project report for the 5 years-long Engineering Degree in Electronics and Telecommunications at the Universidade de Aveiro, Jul. 2007

[Perr03] – **Perry, T. S.**; "Red Hot [light emitting diodes]", IEEE Spectrum, Vol. 40, No. 6, June 2003, pp. 26–29

[Rio07] – **Riordan, M.**; "Books: Tales of Nakamura [review of Brilliant! Shuji Nakamura and the Revolution in Lighting Technology (Johnstone, B.; 2007)]", IEEE Spectrum, Vol. 44, No. 5, May 2007, pp. 56-58

[RP1web] - **RP Photonics**; "p-i-n Photodiodes", Encyclopedia of Laser Physics and Technology, available at:
http://www.rp-photonics.com/p_i_n_photodiodes.html

[RP2web] – **RP Photonics**; "Photodiodes", Encyclopedia of Laser Physics and Technology, available at:
http://www.rp-photonics.com/photodiodes.html

[Sar08] - **Sarhan, S.** and C. Richardson; “A matter of light, Part 4 – PWM dimming”, Power Management DesignLine, June 2008, available at:
http://www.powermanagementdesignline.com/howto/showArticle.jhtml;jsessionid=N3UDLKEXH11LEQSNDLPSKH0CJUNN2JVN?articleID=208402471

[Shu05] – **Shur, M. S.** and R. Zukauskas; “Solid-State Lighting: Toward Superior Illumination”, Proceedings of the IEEE, Vol. 93, No. 10, Oct. 2005, pp. 1691-1703

[Tav97] – **Tavares, A.** and R. Valadas; “IRWLAN Deliverable 1.1 – Signal and Noise Propagation in Indoor Envoirenments”, IRWLAN Project (PRAXIS 2/2.1/TIT/1578/95), Nov. 1997

[Tav99] – **Tavares, A.** and R. Valadas; “IRWLAN Deliverable 1.3 - Signal-to-Noise-Ratio estimation and combining techniques”, IRWLAN Project (PRAXIS 2/2.1/TIT/1578/95), May 1999

[Texweb] – **Texas Instruments**; “Filter Pro website”, available at:
http://focus.ti.com/docs/toolsw/folders/print/filterpro.html

[Val95] – **Valadas, R.**; “Redes de Comunicações de Área Local Não-Cabladas por Raios Infravermelhos”, Thesis presented at the Universidade de Aveiro for the degree of Ph.D. in Electronics Engineering, Nov. 1995

[VIDweb] – **VIDAS Project Summary**, available at:
http://www.fct.mctes.pt/projectos/pub/2006/Painel_Result/vglobal_projecto.asp?idProjecto=75217&idElemConcurso=894

[VIS04] – **VISHAY**; “Physics of Optoelectronic Devices”, Technical Note, Rev. 1.2, July 2004, available at:
http://www.vishay.com/docs/80097/physics.pdf

[VLweb] - **Visible Light Communications Consortium** website, available at:
http://www.vlcc.net

[Zhe07] – **Zheludev, N.**; "The life and times of the LED — a 100-year history", Nature Photonics, Vol. 1, Apr. 2007, pp. 189–192, available at:
http://www.nanophotonics.org.uk/niz/publications/zheludev-2007-ltl.pdf

Annexes

- Emitter prototype: electrical circuit

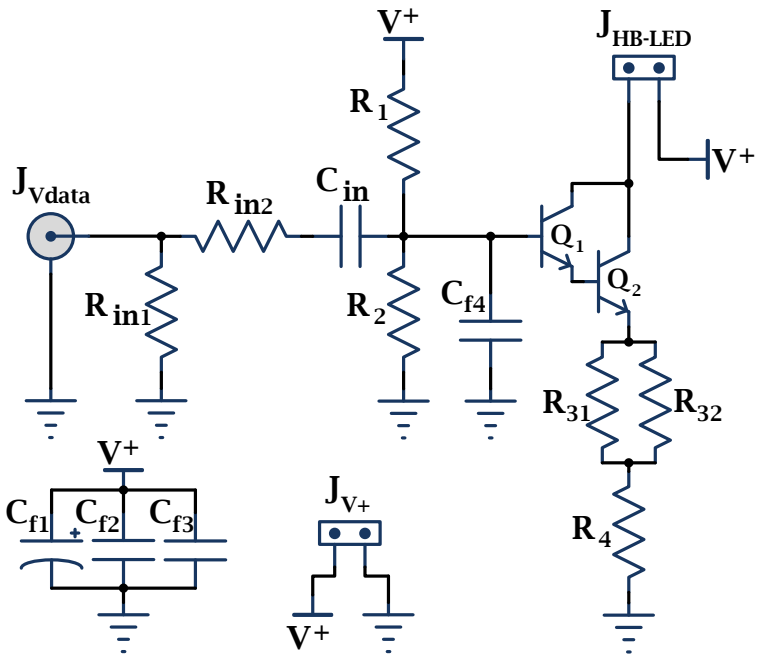

V^+ = 6V

R_{in1} = 51Ω
R_{in2} = 300Ω
R_1 = 5,6kΩ
R_2 = 3kΩ
R_{31} = 6,8Ω
R_{32} = 10Ω
R_4 = 1Ω

C_{in} = 22nF
C_{f1} = 10µF
C_{f2} = 10nF
C_{f3} = 1pF
C_{f4} = 1pF

Q_1 - BFR92A
Q_2 - BFG21W

J_x - connector

- Emitter prototype: PCB

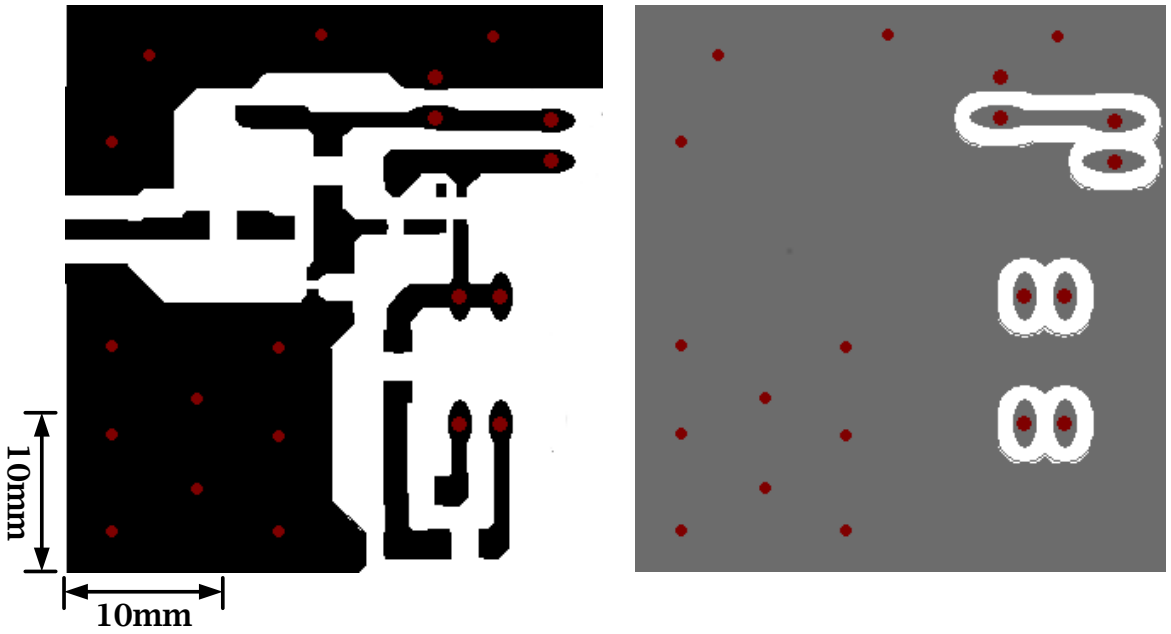

- Receiver prototype: electrical circuit

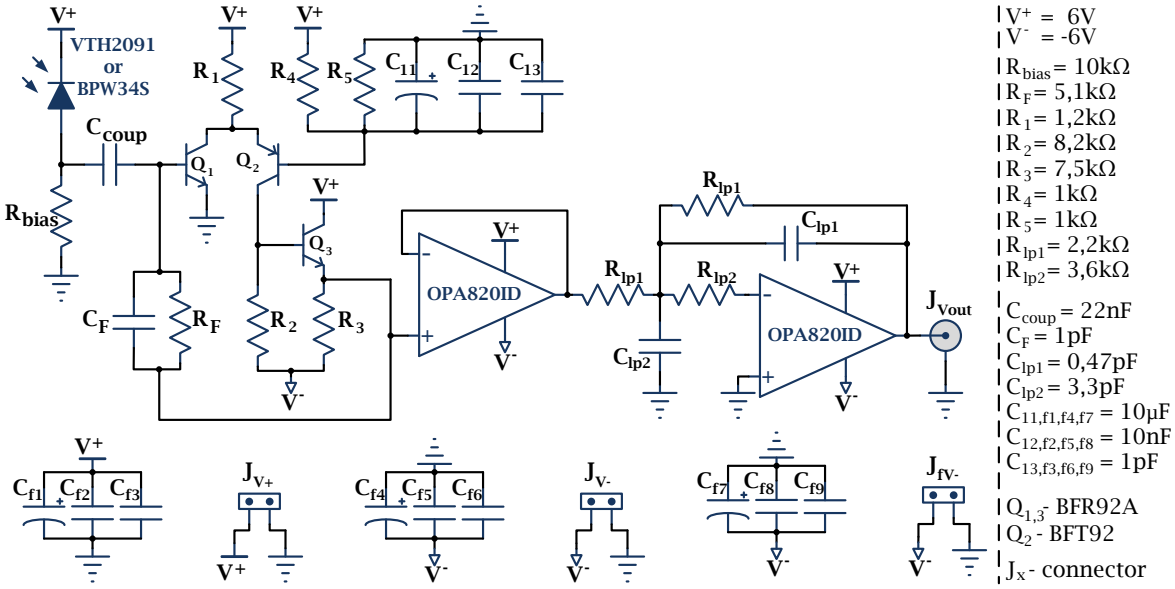

- Receiver prototype: PCB